NORTHWESTERN UNIVERSITY

Techniques for Assessing the Material Properties of Muscle and its Constituents

A DISSERTATION

SUBMITTED TO THE GRADUATE SCHOOL

IN PARTIAL FULFILLMENT OF THE REQUIREMENTS

for the degree

DOCTOR OF PHILOSOPHY

Biomedical Engineering

By

William Eric Reyna

EVANSTON, ILLINOIS

December 2020

ABSTRACT

We rely on the properties of our skeletal muscles to traverse our world, interact with objects, and complete everyday tasks. The macroscopic properties of muscles that endow us with these abilities arise from the material properties of muscle fibers and the surrounding extracellular matrix (ECM), as well as how they are arranged in muscles with different architectures. Consequently, changes in these primary constituents of muscle can contribute to some of the pathological conditions that arise from injury, disease, or aging. Unfortunately, we lack the knowledge of muscle's material properties necessary to better understand how changes influence function. While we know the Young's modulus of whole muscle, this fails to distinguish the independent contributions from muscle fibers and ECM. Furthermore, Young's modulus is not sufficient to characterize the mechanical properties of muscle as it does not allow for estimation of shear, a property important for force transfer. The objective of this dissertation was to fill these two gaps by quantifying and evaluating techniques for assessing the material properties of muscle and its constituents.

This objective was pursued in three parts. First, I quantified the three-dimensional (3D) shear modulus of whole muscle in muscles of differing architectures. I found no significant difference in shear moduli between muscles with different architectures. Muscle, when subjected to shear deformations, had a linearly increasing shear modulus with increasing strain. Further, shear modulus, when sheared perpendicular to muscle fibers was greater than any other direction. At the maximum predicted physiological strain (0.4), the shear modulus was 7 ±1 (mean ±CI), 6 ±1, and 4 ±1 kPa when measured perpendicular, parallel, and across muscle fibers, respectively. Second, I evaluated the efficiency and effect of three decellularization methods on isolating the ECM for direct testing. I found latrunculin B with osmotic shock was the most efficient method

for removing cells compared to two other commonly used methods. Latrunculin B decellularization reduced DNA content to less than 10% of controls and substantially reduced the myosin and actin content to 15% and 23%, respectively. Additionally, following latrunculin B decellularization, the Young's modulus of the remaining ECM was approximately half of the total passive stiffness. This result suggest that ECM carries approximately half of the passive load in muscle. Third, I discuss our understanding of how muscle structure may influence the measures from shear wave elastography (SWE), a noninvasive tool that has the potential to measure changes in the material properties of muscle's constituents. Despite a plethora of studies using SWE, I found a lack of work that validated the assumptions of SWE in muscle against directly-measured material properties. There are a great deal of studies showing correlation between muscular diseases and shear wave speed, but none that have established how the underlying structural changes in muscle influence shear wave propagation. This unknown influence is partly due to the fact that we lack quantitative measures of the material properties of muscle at a level of detail on par with the shear waves we are inducing. Overall, this dissertation provides novel measures of muscle's anisotropic shear moduli, a method to isolate ECM for mechanical testing, and future steps towards validating the measures of ultrasound elastography. These results provide insight into the anisotropic nature of muscle and parameters that can be used in muscle models to simulate 3D deformations.

ACKNOWLEDGEMENTS

First, I would like to thank my wife, Tara, for her amazing support through the ups and downs of this adventure. Thank you for being my rock, the constant in what was sometimes an uncertain time.

To my advisor, Dr. Eric Perreault, who believed in me even when I was doubting myself. Thank you for being patient and making me into a better researcher. I have learned a great deal from you, and for that I am incredibly grateful. Thank you for welcoming me into your lab, guiding me through this journey, and preparing me for the future.

To my committee members, Drs. Wendy Murray, Sabrina Lee, and Thomas Sandercock, thank you all for the great insight and help you have provided throughout the years to get me here. Thank you for all your words of wisdom and encouragement.

To the members of the Neuromuscular Control Laboratory, thank you all for the feedback on presentations and writing, which has no doubt improved my scientific communication skills. Thank you for all your support over the years, it was an honor to learn and grow alongside you. Thank you to Daniel for sharing your knowledge on statistics and answering all my questions. And to Tim Haswell for making sure I didn't lose any fingers and helping me in the machine shop.

To the Biologicals Lab, my home away from home. Thank you Raji, Nicole, and Ben for teaching me how to conduct biological assays. And for being there when I just needed a break to talk. Thank you all for a perspective I couldn't have gotten anywhere else.

To my Mom and Dad, thank you for instilling in me the value of an education. For the moral support and pushing me to achieve my best. Thank you for distracting me when I was down and celebrating all that I have achieved. You all have made me into the man I am today.

LIST OF ABBREVIATIONS

3D: Three-dimensional

AFM: Atomic Force Microscopy

ECM: Extracellular Matrix

EDL: Extensor Digitorum Longus

FEA: Finite Element Analysis

SDS: Sodium Dodecyl Sulfate

SWE: Shear Wave Elastography

TA: Tibialis Anterior

DEDICATION

To my loving grandparents

TABLE OF CONTENTS

LIST OF FIGURES

Chapter 1: Introduction

Skeletal muscles are instrumental in our ability to traverse the world around us. Through the generation of force, muscles move our limbs and allow us to perform a variety of complex tasks and behaviors. Our muscles enable us to complete activities like get out of bed, walk, and lift weights. Our function is greatly influenced by the material properties of muscle, which are dictated by the structural arrangement and composition of the muscle fibers and extracellular matrix (ECM). For simplicity, the scale of muscle fibers and extracellular matrix will be referred to as microstructure in the remainder of this dissertation. Consequently, changes to these primary constituents of skeletal muscle can contribute to pathology and influence muscle function. These changes can be positive or negative. For example, strength training can increase force production and endurance (Holviala et al., 2014; Narici et al., 1989), while aging, injury, or disease can lead to weakness and immobility (Bemben et al., 1991; Brooks and Faulkner, 1994; Frontera et al., 2008; Ingber, 2003; Kragstrup et al., 2011). These maladaptive microstructural changes can arise from increases in collagenous ECM, infiltration of fat, or degradation of muscle fibers (Kragstrup et al., 2011; Lexell, 1995; Lexell et al., 1988; Trappe, 2009). Often, these changes result in pain and reduced range of motion, which culminates in clinical visits (Woolf and Pfleger, 2003; Woolf and Akesson, 2001; Yelin et al., 2016). Currently, the diagnosis of stiffness-related muscle conditions with palpation is unspecific in identifying the source of any changes in stiffness from the microstructure and incapable of examining deep muscles. This limited method in turn diminishes clinicians' ability to track, manage, and promote rehabilitation in people with musculoskeletal impairments. One promising tool that may identify changes to the stiffness of muscle constituents is ultrasound shear wave elastography (SWE) (Brandenburg et al., 2014; Drakonaki et al., 2012). This method has been used to identify hardened masses (tumors) in

homogeneous materials by measuring the speed of shear wave propagation (Berg et al., 2012; Cosgrove et al., 2012; Frulio and Trillaud, 2013). Unfortunately, we lack the knowledge of muscle's material properties necessary to better understand how changes in microstructure influence shear wave propagation or muscle function. While we know the Young's modulus of whole muscle, this fails to distinguish the contributions from muscle fibers and ECM. Furthermore, Young's modulus is not sufficient to characterize mechanical properties in muscle as it does not allow for estimation of shear, a property important for force transfer. The objective of this dissertation was to fill this gap by quantifying and evaluating techniques for assessing the material properties of muscle and its constituents. We accomplished this objective by quantifying the anisotropic shear modulus of skeletal muscle to provide properties necessary for understanding shear deformations and shear wave modelling in three-dimensions (3D). We also critically evaluated chemical isolation techniques used to separate ECM from muscle to establish a method to determine the material properties of the ECM. The measures and methods provided in this dissertation present a novel assessment of muscle material properties which are useful not only in the basic understanding of muscle, but also for the future validation of shear wave elastography.

In the remainder of this chapter, I introduce muscle architecture and the influence of microstructural arrangement on the macroscopic material properties of muscle. I identify gaps in our current understanding of muscle's material properties at both a macroscopic and microscopic level. I describe the current clinical approach through which muscle stiffness changes are identified and monitored. I introduce the utility of SWE and briefly discuss the caveats of its use and the potential influence of microstructure that complicate its diagnostic capabilities. Finally, I summarize the aim of this dissertation is to better understand muscle mechanics and provide

material properties that can be used to gain better insight into muscle function, impairments, and SWE.

Prevalence of Musculoskeletal Impairment

We rely on the health and performance of our skeletal muscles to complete all the movements of our body. Whether it's getting out of bed in the morning or running in a marathon, we constantly depend on the mechanics of our muscles to move. Unfortunately, changes in muscle function due to aging, injury, or disease can result in pain, reduced range of motion, and difficulty in completing everyday tasks (Alnaqeeb et al., 1984; Handorf et al., 2015; Lieber et al., 2003; Woolf and Pfleger, 2003). Across the world, one in four adults report some level of musculoskeletal impairment (White and Harth, 1999; Woolf and Akesson, 2001), with a disproportionate amount (65 – 80%) occurring in people over the age of 65 (Ansari, 2019). This loss in muscle function not only has a physical effect, but also a psychological one. In some cases, individuals lose their independence, relying on a caregiver's assistance to bathe, dress, and eat (Brooks and Faulkner, 1994; Sansone et al., 2012). These functional losses not only impact an individual's quality of life, but also financially strains the individual and the health care system. In 2011 in the United States, the estimated cost of musculoskeletal conditions was $796.3 billion – approximately 5.2% of the Gross National Product (Weinstein and Yelin, 2014). Musculoskeletal conditions, and their associated costs, continue to rise (Woolf and Pfleger, 2003; Yelin, 2003; Yelin and Callahan, 1995; Yelin et al., 2019). The United Nations and World Health Organization have recognized this worldwide burden, by endorsing 2000-2010 as the Bone and Joint Decade (Tsou and Chng, 2002).

Skeletal Muscle Architecture and Composition

Muscles depend on their structural properties and complex varied architecture to fulfill a diverse set of functional demands (Gans, 1982; Lieber and Friden, 2000). Muscle architecture is the orientation of muscle fibers relative to the axis of force generation (Lieber and Friden, 2000). The fiber orientation describes how pennate or parallel a muscle is. A muscle with parallel fibers has a pennation angle of zero. An idealized muscle with parallel fibers will have fibers that act purely in translation, while pennate fibers will rotate (Gans, 1982). This variation in fiber orientation contributes to the differences in muscles and their function (Huijing, 1999; Lieber and Friden, 2000). At higher pennation angles, muscles and fibers will experience higher shear strains and higher shear resistance (Huijing, 1999). Knowing the shear modulus, a measure of shear resistance, is important to understanding shear deformation in architectural distinct muscles. Unfortunately, shear modulus has not been measured, or compared, in muscles with different architectures. In Chapter 2, we address this gap by quantifying the shear modulus in three muscles with different pennation angles.

Muscle is composed of many mechanically important parts of varying scale. Two major components of muscle microstructure are the ECM and muscle fibers. The ECM and fibers are arranged with each other to formulate the macroscopic properties of muscle. The ECM is further composed of three hierarchal layers –the endomysium, perimysium, and epimysium –which scale in size from smallest to largest (Purslow, 2002; Purslow and Trotter, 1994; Trotter and Purslow, 1992). The endomysium surrounds individual muscle fibers, which bundle together to form fascicles. Fascicles are surrounded by the perimysium, which also bundle to make whole muscle. Finally, the whole muscle is surrounded by the epimysium (Wisdom et al., 2015). The ratio, health,

and size of these parts facilitate cellular growth, mobility, homeostasis, and disease progression (Handorf et al., 2015).

Each layer of ECM is composed of many wavy collagen fibers, which provide mechanical support for the nerves, blood vessels, and fibers that run through muscle (Purslow, 2002). Purslow and Trotter (1994; 1992) have obtained iconic images of ECM's structure detailing the collagen fiber arrangement. Within the subdivided structure of ECM, the collagen fibers of the epimysium and perimysium are oriented at approximately ±55 degrees with respect to muscle fibers (Purslow and Trotter, 1994). On the contrary, in the endomysium, the collagen fibers are oriented randomly (Trotter and Purslow, 1992). These images by Purslow and Trotter have been used throughout muscle research to describe the ECM and organized packing of muscle fibers. Work by Gillies et al. (2017; 2011) expanded upon these images by imaging the individual collagen fibers within the endomysium and perimysium. They showed the collagen fibers were kinked and wrapped around each other with few terminating on the muscle fiber. These images have resulted in increased speculation of the ECM's role in the nonlinear mechanics and contribution to macroscopic stiffness of muscle (Lieber and Friden, 2019).

The muscle fibers, much like the ECM, are comprised of many smaller elements. The contractile unit of muscle fibers are the sarcomeres, which consist of three types of myofilaments (Squire et al., 2017): the thick filament containing myosin, the thin filament containing actin, and the third myofilament containing titin (Wang et al., 1984). The thick and thin filament form the myosin-actin cross-bridge (Huxley, 1957). This cross-bridge is where muscle generates force (Huxley, 1969). Myosin converts chemical energy, in the form of adenosine triphosphate, into mechanical energy by binding and moving along the actin filaments. Titin, termed the molecular spring, is a giant protein (~3000 to 3700 kDa) that resides at the end of the thick filament (Granzier

et al., 2007). Titin is thought to generate passive force when muscle is stretched (Trombitas et al., 1998). However, titin's importance to macroscopic passive mechanics is still debated (Lieber and Friden, 2019).

Microstructural Contributions to Muscle Function

How muscles actively contract has long been an interest to scientists. After all, the active generation of force is the process by which muscles move our limbs. As stated above, the contractile components of muscle are contained within the muscle fibers. Muscle fibers are elongated and multinucleated rods of varying diameter (Sweeney and Hammers, 2018). The collection of muscle fibers innervated by a single motor neuron is a motor unit (Purves, 2018). The number of muscle fibers in a motor unit can vary across and within muscles (Buchthal and Schmalbruch, 1980). The activation of these motor units is coordinated across all the fibers contained within a muscle to produce a contraction. Through neural drive, the activation and deactivation of muscles is coordinated to maintain postural stability and voluntarily complete tasks (Grillner, 1972). Unfortunately, this high interest in active muscle has resulted in less research of the passive muscle properties. While we are aware of the significance of active contraction, this dissertation instead will focus on the importance of muscle's passive properties.

Both the ECM and muscle fibers contribute to the passive mechanics of muscle. However, the relative contributions of each has yet to be agreed upon (Brynnel et al., 2018; Gillies and Lieber, 2011; Gindre et al., 2013; Sleboda and Roberts, 2017). Passive stiffness has been linked to three main components: 1) the ECM (Fomovsky et al., 2010; Gillies and Lieber, 2011; Huijing, 1999; Kjaer, 2004); 2) titin within muscle fibers (Brynnel et al., 2018; Heidlauf et al., 2017; Li et al., 2016; Prado et al., 2005); and 3) incompressible fluid in the muscle (Jenkyn et al., 2002;

Sleboda and Roberts, 2017; Takaza et al., 2013b). Researchers have argued that these elements independently constitute the majority of passive stiffness, while others support the proposition that a combination of them together provide the passive stiffness (Bleiler et al., 2019; Gindre et al., 2013). Unfortunately, due to limitations in our knowledge of muscle mechanics and ability to isolate components of muscle for testing, a consensus on which structures contribute most to passive muscle stiffness has yet to be reached. In Chapter 3, we attempt to address this limitation by identifying a method in which the ECM can be isolated for testing. Additionally, we supply evidence towards the notion that ECM is a major contributor of passive stiffness.

The ECM provides a mechanical scaffold to support muscle fibers, transmit force, and contribute to passive stiffness. The ECM, as stated previously, at rest is composed of slack collagen fibers of varying lengths (Gillies et al., 2017). During extension of the muscle, these collagen fibers nonuniformly elongate until they become taut (Munster et al., 2013; Roeder et al., 2002). This unequal loading of the ECM is thought to give muscle its nonlinear passive stiffness (Fratzl et al., 1998; Meyer and Lieber, 2011; Sopher et al., 2018). This nonlinearity aids muscle by preventing damage to the muscle fibers. Under increased load, the ECM provides more resistance to muscle elongation. Unfortunately, there seems to be a narrow range of ECM stiffness that is physiological and healthy. In individuals with Duchenne muscular dystrophy, there is an influx of collagenous ECM (Duance et al., 1980; Jones et al., 1983). This results in an increase of the macroscopic stiffness of muscle and a decrease in strength and mobility of the muscle (Klingler et al., 2012). Similarly, in aging muscle, structural and functional changes to the ECM contribute to the alteration of muscle's mechanical properties (Kragstrup et al., 2011; Rosant et al., 2007). Older adults tend to be weaker and more susceptible to musculoskeletal injuries (Brooks and Faulkner, 1994). Therefore, identifying changes to the underlying muscle structure that influence function

are important to disease diagnosis, treatment, and rehabilitation. How these microstructural changes due to pathology are potentially measured in muscle with SWE is covered later in this introduction as well as detailed further in Chapter 4.

Macro- and Microscopic Stiffness of Skeletal Muscle

Skeletal muscle stiffness is a fundamental property that contributes to the body's ability to move (Ettema and Huijing, 1994; Grillner, 1972). Stiffness is a material's resistance to deformation in response to an applied load. Changes in external load and composition of the microstructure can influence stiffness and the muscle's ability to function appropriately (Handorf et al., 2015). While there have been great strides in measuring the Young's modulus of active muscle (Brozovich et al., 1988; Ettema and Huijing, 1994; Joyce and Rack, 1969; Joyce et al., 1969; Lieber, 2018; Rack and Westbury, 1974), as it is most relevant to voluntary movement, this has come at the neglect of understanding the passive properties. The passive stiffness of the muscle plays a central role in how muscle resists joint motion and transmits forces internally through muscle (Grillner, 1972; Handorf et al., 2015). These functions stem from both shear and longitudinal loads on the muscle, which are influenced by shear and Young's modulus, respectively. Understanding how the shear and Young's modulus of muscle, and its constitutive parts, is paramount to better knowing how changes to these properties influence muscle mechanics. With more knowledge of muscle's material properties, we can provide further insight and care for people with musculoskeletal conditions.

The shear modulus of muscle, a quantification of resistance to shear deformations, is thought to be the primary regulator of force transmission between muscle fibers and the ECM and between the tendon and muscle (Huijing, 1999). Shearing forces in muscle are produced by injury,

physiologically through the transference of forces, and between adjacent muscles (Huijing, 1999; Jarvinen et al., 2013). These forces can result in three-dimensional deformations of muscle. In muscle, shear forces are applied in three functionally relevant directions with respect to the muscle's architecture: 1) parallel, 2) perpendicular, and 3) across muscle fibers. These directions encompass the anisotropic properties of muscle, the physiological loading directions, and those that may occur with injury. Despite the importance of shear modulus in 3D, only one study has directly measured the shear modulus in muscle. Morrow et al. (2010) used a novel apparatus to measure the shear modulus of the whole muscle through direct mechanical testing. Unfortunately, they only characterized the muscle when subjected to shear deformations parallel to the muscle fiber orientation. Therefore, the shear modulus perpendicular and across muscle fibers remains unknown. Additionally, there have been many reports of shear modulus measured from ultrasound elastography, but again these are usually restricted to one direction (Eby et al., 2013; Koo et al., 2013; Maisetti et al., 2012). Without measures of shear modulus in all three directions, we will continue to limit our understanding of how the directionally specific stiffness of muscle influences function. In Chapter 2, we address this gap in knowledge by directly quantifying the shear modulus of whole muscle in three functionally-relevant degrees of freedom.

In tension, skeletal muscle passively deforms longitudinally as the structure is elongated from antagonistic muscle contraction. The resistance in response to this force is quantified as the Young's modulus. During passive extension of the muscle, the tendon pulls the muscle transferring forces through the tendinous aponeurosis throughout muscle's ECM and fibers. As previously stated, there are three factors (ECM, titin, and intramuscular fluid) that may influence muscle's resistance to these passive forces. Previous research has elucidated some of the mechanical properties of ECM through manipulation of whole muscles, fiber bundles, and single fibers (Meyer

and Lieber, 2011). Additionally, researchers have used knowledge of single collagen fibers and arrangement of ECM to model the deformations of the ECM structure (Bleiler et al., 2019; Roeder et al., 2002). These studies suggest that ECM is the dominating factor contributing to the Young's modulus of passive muscle. However, these studies have not been validated by direct measurements. This is because such measurements require the isolation of intact ECM from the muscle. In Chapter 3, we address this gap by quantifying the efficiency of three decellularization methods on removing muscle cells from skeletal muscle and to determine their effects on the remaining ECM.

Methods to Measure Stiffness

There are many ways to measure the material properties of muscle. However, the scale and parameter of interest aids in the selection of which is most appropriate. The material properties of muscle have been measured on scales as small as single cells and as large as entire muscles. Scientists have used atomic force microscopy (AFM)(Defranchi et al., 2005; Friedrichs et al., 2010; Mathur et al., 2001; Oberhauser et al., 2002; Wenger et al., 2007), uniaxial tensile testing (Donahue et al., 2001; Meyer and Lieber, 2018; Meyer and Lieber, 2011; Morrow et al., 2010; Smith et al., 2011; Takaza et al., 2013a), and rheology (Aimedieu et al., 2003; Chen et al., 2010; Chotard-Ghodsnia and Verdier, 2007; van Turnhout et al., 2005) to obtain most of the available measures of muscle.

The devices to measure material properties can be variable in their resolution and accuracy depending on the configuration of the machine. AFM has the highest resolution and is typically used to measure the smallest components of a material. AFM uses a laser to detect the deflection of a cantilever with a nanometer sized tip. When the cantilever and tip contact a material, the

cantilever will deflect more in a stiff material and less in a soft one. In muscle research, AFM has been used to measure the viscoelastic properties of single muscle cells (Mathur et al., 2001), the adhesion force between cells and ECM (Friedrichs et al., 2010), and the Young's modulus of collagen fibers (Wenger et al., 2007), to name a few. Commercially available uniaxial tensile testers are by far the most commonly used method to test the macroscopic properties of muscle. Uniaxial tensile testers can apply a controlled elongation on a material and measure the resulting tensile force. These measures are often used to identify the forces at which a material fails or to compute the Young's modulus. These machines, unless configured for detailed measurements, have the lowest resolution. However, this is a trade off with a higher load capacity. This is why tensile testers are commonly used for whole muscle measurement. They have been used to measure the anisotropic tensile properties of whole muscle (Morrow et al., 2010), the viscoelastic and failure load of tendon under cyclic loads (Donahue et al., 2001), and the anisotropic deformation of muscle under large strains (Takaza et al., 2013a). Custom built tensile testers, while less common, provide scientists with a unique opportunity to tailor a machine specifically for their needs. For example, this has been done to measure the transverse mechanical properties of single muscle fibers and fiber bundles (Smith et al., 2011), to compare fiber mechanics between species (Meyer and Lieber, 2018), and to indirectly elucidate the nonlinear mechanics of ECM (Meyer and Lieber, 2011). Finally, rheometers sit between the resolution of AFM and tensile testers. Rheometers use two parallel plates to compress or torsional shear a material under a controlled cyclic force or displacement. These machines are often used to study the viscoelastic characteristics of a material, yet its functionality is far from optimal. Rheometers are limited in the physical size of a sample it can accept on both the small and large end (Mackay, 1998). Despite this limitation, its utility still exists and is important to material characterization in general, and of

muscle. It has been used to measure the compression characteristics (Aimedieu et al., 2003) and the effects of temperature on the passive transverse properties of muscle biopsies (van Turnhout et al., 2005).

In Chapter 2 and 3 of this dissertation, we use a uniaxial tensile tester to measure the material properties of ECM in tension and whole muscle in shear. In Chapter 2, due to the size and properties of the muscle we were interested in (shear modulus), we substituted the standard pincher clamps for custom manufactured one. This substitution is elaborated in more detail within that section, but it is worth reiterating that we made no adverse changes to the machine that would compromise our measures. With our custom clamps, we moved from a force generated at the ends of our sample to ones at the faces. This simple shift allowed our uniaxial tensile tester to switch from longitudinal to shear deformations. In Chapter 3, we used the commercially supplied clamps of our tensile tester to measure the Young's modulus of whole muscle ECM.

Clinical Assessment of Muscle Stiffness

The musculoskeletal system is one of the major organ systems in the human body. This organ system is primarily responsible for force generation, postural control, and movement. Skeletal muscles, one of three types of muscle groups, accounts for 30 to 40% of total mass of an adult (Janssen et al., 2000). Unfortunately, this means when a muscle becomes impacted by disease or injury, localizing the change can be rather difficult.

Musculoskeletal disease can often negatively impact muscle or joint stiffness. Current clinical evaluation of muscle and joint stiffness is done with palpation, joint resistance examination, or tissue biopsies (Howell et al., 1993). In palpation and joint resistance evaluations, clinicians are qualitatively discerning the stiffness of a person's muscle or joint. These methods

are usually subjective and based on the experience of the clinician performing the examination. Additionally, palpation, while moderately specific in nature, is only able to identify changes that occur in superficial muscles. Joint resistance is even less specific, giving a global view of changes that occur about a joint. Of the three commonly used methods, tissue biopsies may provide the most specific information in regard to disease diagnosis. Using histology, biopsies are capable of visualizing the biological microstructure of the sampled tissue (Alnaqeeb et al., 1984; Duance et al., 1980; Goebel et al.). This information allows clinicians to precisely identify compositional changes to the microstructure that are synonymous with diseases like muscular dystrophy. However, biopsies are invasive, provide no quantitative measure of stiffness, and may inflict damage to the tissue. Therefore, to aid healthcare professionals, noninvasive diagnostic tools are needed to quantify and identify the changes in microstructure involved in disease.

In recent years, ultrasound shear wave elastography (SWE) has presented itself as a possible means through which the Young's modulus of a material can be measured. In homogeneous tissues, like breast and liver, it has been commonly used to identify tumors (Cosgrove et al., 2012; Frulio and Trillaud, 2013; Sebag et al., 2010). Similar to mechanical testing, SWE measures a tissue's deformation in response to an applied stress or force. In SWE, this force is produced through an acoustic radiation pressure within the material (Brandenburg et al., 2014; Gennisson et al., 2013). This radiating force causes shear waves to propagate in the tissue that have a velocity related to the stiffness in which they are traveling (Gennisson et al., 2013). A stiffer material will result in a faster wave propagation, and vice versa. In the case of homogeneous isotropic materials, the relationship between shear wave speed and shear modulus, which can be used to calculate Young's modulus, is widely accepted. However, the validity of this relationship

in skeletal muscle, a heterogeneous anisotropic material, remains to be seen as direct comparisons to quantitative measures of shear modulus have not been made.

Muscle stiffness measures from SWE are complicated by the material and the environment in which they are obtained. Shear wave propagation has been shown to be impacted by the anisotropy properties of muscle (Gennisson et al., 2010b), active and passive state of muscle (Wang et al., 2019), and tension applied to the muscle (Bernabei et al., 2020). Furthermore, how much compression of the probe on the material that is applied by the sonographer may influence the imaging contrast and amount of noise (Li and Cao, 2017). Unfortunately, these variables, and possibly more, make comparing measures between clinicians and experiments difficult.

Despite the challenge in making SWE measures in muscle, researchers have continued to use this tool to correlate changes in muscle stiffness to disease (Lacourpaille et al., 2015; Simon et al., 2016; Zhou et al., 2018). These diseases, as previously stated, are typically associated with a change in microstructural stiffness or composition. However, our ability to decipher measures of shear wave speed into diagnostically useful measures of microstructural stiffness is nonexistent. We do not yet know the sensitivity of shear wave propagation to changes in microstructure, or simply how shear waves traverse through the muscle microstructure. Many studies have made significant contributions towards the validation of SWE in muscle at a macroscopic level, but few have probed at the microstructural scale. The measurements in Chapters 2 and 3 work toward advancing the understanding of macro- and microstructural properties which are useful for SWE. In Chapter 4, we further describe and discuss our current understanding of shear wave propagation in muscle and how microstructure may influence these measures.

Statement of Objectives

The aim of this dissertation was to measure the material properties of skeletal muscle and lay the foundation needed to better understand and model skeletal muscle mechanics. There is much we have yet to quantify in muscle as it is a functionally and architecturally complex material. In Chapter 2, we quantify the shear moduli of skeletal muscle in the three degrees of freedom relevant to the function of whole muscle. Using a custom designed and manufactured clamp, we determined if the orientation of muscle significantly affected shear moduli in a manner similar to the transversely isotropic Young's modulus. We also evaluated the significance of differing muscular architecture on the values of shear moduli. In Chapter 3, we pursued a finer level of detail in muscle by critically evaluating methods through which ECM can be isolated and mechanically tested. We used two commonly used decellularization techniques and one proposed to be superior in muscle to establish a method to isolate ECM. We determined the efficiency of cellular removal and effects on the remaining tissue. Finally, in Chapter 4, we reviewed the scientific literature on shear wave elastography's sensitivity to microstructural muscle properties. We discussed the potential influences of architectural arrangement of muscle and changes to microstructural composition and stiffness on shear wave propagation. We also note the experimental challenges of these measures and propose questions associated with relating shear wave propagation to informative, quantitative measures of muscle. Together, these studies further our understanding of the material properties of muscle. Furthermore, quantifying the macroscopic and microscopic properties of muscle opens the way to be able to more accurately validate and model shear wave propagation. This more detailed knowledge of muscle mechanical properties will aid in the transition of ultrasound shear wave elastography of muscle to a more clinically valuable diagnostic tool.

Chapter 2: Multidirectional measures of shear modulus in skeletal muscle

This work was completed under the mentorship of Eric Perreault, PhD. I would also like to acknowledge Daniel Ludvig, PhD for his helpful contributions to the data analysis.

This study was funded by the National Institutes of Health (R01AR071162 and T32HD07418).

Abstract:

Skeletal muscle stiffness is a fundamental property that contributes to the body's ability to locomote and complete everyday tasks. Understanding healthy skeletal muscle stiffness and evaluating changes to stiffness can facilitate better clinical evaluation of muscle pathologies. While recent studies have evaluated stiffness in tension, there remains a void in understanding muscle's anisotropic shear properties. Shear modulus aids in the resistance to injury and physiologically with the transmission of forces within muscle. The objective of this study was to quantify the shear moduli of skeletal muscle in the three degrees of freedom relevant to the function of whole muscles. We collected data from the extensor digitorum longus, tibialis anterior, and soleus harvested from both hindlimbs of 12 rats. These muscles were chosen to further evaluate the consistency of shear moduli across muscles with different architectures. We calculated the shear modulus from muscles oriented in three directions: parallel, perpendicular, and across with respect to muscle fiber alignment. Results showed that the shear modulus measured perpendicular to fibers was greater than in any other direction, but only significantly different from the modulus measured across fibers. At the estimated maximum physiological strain, shear modulus was 6 ±1, 7 ±1, and 4 ±1 kPa when measured parallel, perpendicular, and across muscle fibers, respectively. Despite architectural differences between muscles, in our paradigm we did not find an effect of muscle type on shear modulus. However, this does not exclude the possibility that muscle type may be significant in another species. Finally, shear modulus increased linearly with increasing strain,

indicative of a nonlinear elastic material. Our results show that in rat, muscles' shear moduli are similar when measured parallel and perpendicular to fibers and are not influenced by architectural differences in muscles.

Introduction:

The shear modulus, a value quantifying a material's resistance to shear deformation, is thought to be the primary factor in load transfer within muscle (Huijing, 1999). These loads can be internal from active or passive muscle function or external from injury (Huijing, 1999; Jarvinen et al., 2013). Most of muscle research has been on the active properties of muscle, as they are most relevant to voluntary movement. However, the passive properties of muscle play a central role in how muscle resists joint motion, transmits forces internally, and repairs (Herbert and Gandevia, 2019). Passive forces on muscle can be parallel, perpendicular, or across muscle fibers. This can result in purely shear or tensile deformation, or a combination of the two. While recent studies have begun to investigate passive stiffness in tension (Bosboom et al., 2001; Lieber and Friden, 2019; Morrow et al., 2010), there remains a void in understanding muscle's anisotropic shear properties. Therefore, it is necessary to quantify the three-dimensional (3D) shear modulus of muscle. This will allow us to better interpret the anisotropic function of muscle and its resistance to shearing forces.

Muscle has often been described as a transversely isotropic material based on the geometric arrangement of its fibers (Blemker and Delp, 2005). Material properties parallel to the fibers are typically considered to differ from those in the plane of symmetry perpendicular to the fibers. In tension, muscle has two primary directions: 1) longitudinal (parallel) and 2) transverse (perpendicular) to muscle fibers. Any measurement taken perpendicular to muscle fibers will result

in the same Young's modulus. However, in shear, where forces are applied in planes, the muscle should have three defining directions: 1) parallel, 2) perpendicular, and 3) across muscle fibers. These correspond to forces oriented in the 1) z-axis laying on the xz- or yz-planes, 2) x- or y-axis laying on the xy-plane, and 3) y-axis laying on the xz- or yz-planes (Fig. 2.1). For continuum modeling, measuring the shear modulus in these three directions would allow us to describe muscle under purely shear strain or stress. Additionally, these directions encompass the physiological loading directions and those that may occur with injury, such as blunt force trauma. Without these multidirectional measures of shear, we limit our understanding of muscle to forces oriented parallel to fibers, thereby excluding the potential for simulating injuries, or shear wave propagation, with shearing forces in other directions. Furthermore, combining 3D measures of shear modulus with measures of Young's modulus and Poisson ratio we gain the ability to model muscle under any stress or strain. Currently, to our knowledge, direct measures of a muscle's shear modulus have been limited to a single dimension. Previous work by Morrow et al. (2010) used a novel apparatus to directly quantify Young's modulus in two dimensions and shear modulus in one dimension. They made measurements in longitudinal extension, transverse extension, and lateral shear of whole muscle. They concluded that the Young's modulus in tension was higher in the fiber direction (parallel) than in the cross-fiber (perpendicular) direction. However, as they only measured one direction of shear, the 3D characterization and anisotropy of the shear modulus remains to be determined.

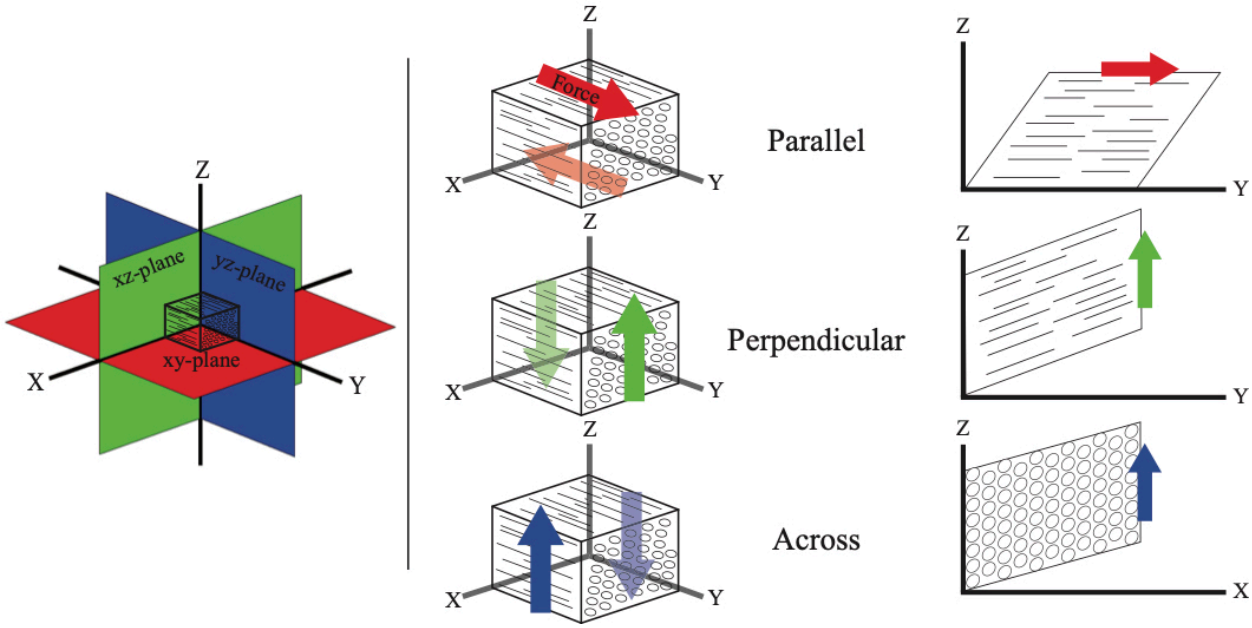

Figure 2.1 Three-dimensional representation of shearing muscle in the parallel (xy-plane), perpendicular (xz-plane), and across (yz-plane).
Solid arrows indicate direction of force and displacement, while transparent arrows indicate stationary resistant force.

Furthermore, it is unknown how differences in muscle architecture alter the shear modulus of muscle. Muscles differ in architectural features like length, cross-sectional area, fiber packing and muscle fiber arrangement (Gans, 1982; Lieber and Friden, 2000). These architectural differences change the amount of excursion and how passive load is distributed through the muscle (Burkholder et al., 1994; Gans, 1982). One of the most striking differences in muscle can be pennation angle, a measure of fiber orientation in reference to the longitudinal axis of muscle. In rat hindlimbs, the pennation angle of muscles can range from around 0 to 20 degrees (Eng et al., 2008). These differences in fiber orientation can result in varying levels of force generation (Lieber and Friden, 2000) and transmission (Huijing, 1999). It has been proposed that for a given change in fiber length, more resistance will be incurred as the pennation angle increases (Huijing, 1999). Therefore, it is important to evaluate the consistency of shear modulus measures across muscles

with differing architectures. This will provide further clarity into the potential relationship between shear modulus and muscle architecture.

Indirect testing using ultrasound elastography has shown great promise in measuring the shear modulus in muscle. However, there remains uncertainty in its measures of heterogeneous materials making direct material measurements the most reliable. Despite this concern with heterogeneity, the shear modulus of muscle derived from measures of shear wave speed have been reported. These reported measures are usually of one direction (Koo et al., 2013; Maisetti et al., 2012). While these studies report shear moduli values with confidence, we are unaware of direct comparisons between direct measures of shear modulus and estimates from elastography. Most studies use elastography to measure Young's modulus under the assumption that shear and Young's moduli are related (Bercoff et al., 2004). In the case of unstressed homogenous isotropic materials, such as breast and liver, Young's and shear moduli have been shown to directly relate to shear wave speed (Cosgrove et al., 2012; Frulio and Trillaud, 2013). However, in muscle, this relationship may differ from what is expected in other soft tissue (Eby et al., 2013). Therefore, not only are direct mechanical measurements of skeletal muscle shear modulus needed for a general understanding of muscle mechanics, but they are necessary towards the validation of the measures in elastography.

The objective of this study was to quantify the shear moduli of skeletal muscle in the three degrees of freedom relevant to the function of whole muscles. We measured the shear modulus in the extensor digitorum longus (EDL), tibialis anterior (TA), and soleus from rat hindlimbs to evaluate the consistency of shear modulus across muscle with differing architectures. We also estimated the shear wave speed from our measures of shear modulus to compare against previous studies of ultrasound elastography. Our results are the first to quantify the multidirectional shear

modulus of skeletal muscle that can be used in three-dimensional modeling. This is an important step towards evaluating shearing forces in muscle and validating the measures of ultrasound elastography.

Materials and Methods:

All data were collected from healthy Sprague-Dawley rats obtained through the Northwestern University tissue sharing program. A total of 12 rats were used. We evaluated three muscles with differing architectures (EDL, TA, and soleus) to determine if shear modulus was consistent across muscles. The typical pennation angle of these muscles in rat are 9.0 ±1.1 degrees, 12.8 ±1.2 degrees, and 3.9 ±2.4 degrees for the EDL, TA, and soleus, respectively (Eng et al., 2008).

Tissue Preparation

The EDL, TA, and soleus muscles were harvested from both hindlimbs immediately following termination and placed in chilled phosphate-buffered saline to stem the effects of rigor (Tuttle et al., 2014). Muscle samples had their aponeuroses dissected away using a surgical scalpel to ensure measurements were made only on muscle tissue, similar in procedure to Morrow et al. (2010). Before mechanical testing, muscles were sectioned into rectangular cubes (~9 x 9 x 4 mm) aligned with the muscle fibers. Shear measurements were made with the cubes oriented in one of three directions: parallel, perpendicular, or across muscle fibers, allowing us to obtain 3D measures of the shear modulus (Fig. 2.1). Data were collected from 106 total samples. Samples (24 total) were eliminated if they showed separation from our testing apparatus during testing or artifacts (drops and rises) were observed in the raw data. These methods resulted in approximately 9

samples for each of the three muscles and each of the three directions. The length, width, and thickness of each sample was measured prior to testing. These physical properties were used in the calculation of stress and strain.

Mechanical Testing

Shear modulus was measured using an Instron mechanical tester (Instron 5942; Instron Corp., Canton, MA). An offset aluminum bracket with acrylic inserts was mounted into the uniaxial tensile tester, similar in design to Morrow et al. (2010) (Fig. 2.2A). Aluminum brackets were milled in unison to ensure that surfaces were parallel with one another. Acrylic inserts were used to promote adhesion of the tissue and to easily exchange the testing surface between samples. The harvested muscle samples were fixed to the acrylic plates using cyanoacrylate glue. The plates were then screwed onto the aluminum brackets to form a rigid clamp. Specimens were positioned in the center of the testing apparatus to ensure that forces were uniformly applied to the tissue faces and that measurements were in line with the load cell. The use of cyanoacrylate glue bonded tissue to the fixture beyond muscle failure, as seen by rupture within samples as opposed to separation from our mounting plates.

Muscle samples were tested within 12 hours of harvesting. Data were collected at a strain rate of 5% per minute until failure, as indicated by a sudden drop in force and tearing of the muscle.

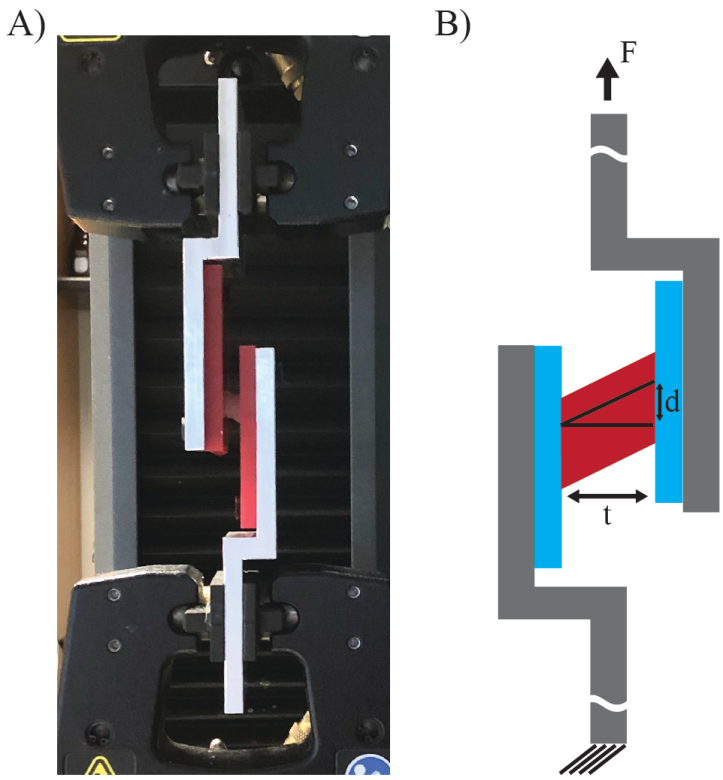

Figure 2.2 Shear testing apparatus A) photograph and B) schematic.
Exaggerated representations of the thickness (t), displacement (d), and force (F) are shown in the schematic.

Data Analysis

Shear modulus was calculated from measures of shear stress and shear strain. Tissue shear stress, specifically the second Piola-Kirchhoff stress, was calculated as the applied force (F) divided by the initial cross-sectional area (Fig. 2.2B). The second Piola-Kirchhoff stress is used as it references the undeformed state of a material with a constant cross-section. Our cubic samples, to the best of our abilities, have a constant cross-section and our adhered surface encompasses the entire face of the sample. Tissue shear strain, specifically the Green shear strain, was calculated as the inverse tangent of displacement (d) divided by initial thickness (t) (Fig. 2.2B). Green shear strain was used because of the small deformations in length. Representative stress-strain data are shown in Fig. 2.3A. Instantaneous shear modulus was computed as the slope of the stress-strain

curve (Fig. 2.3B). We report values at regular strain intervals of 0.1, within the predicted physiological range of 0 to 0.4 (Blemker et al., 2005).

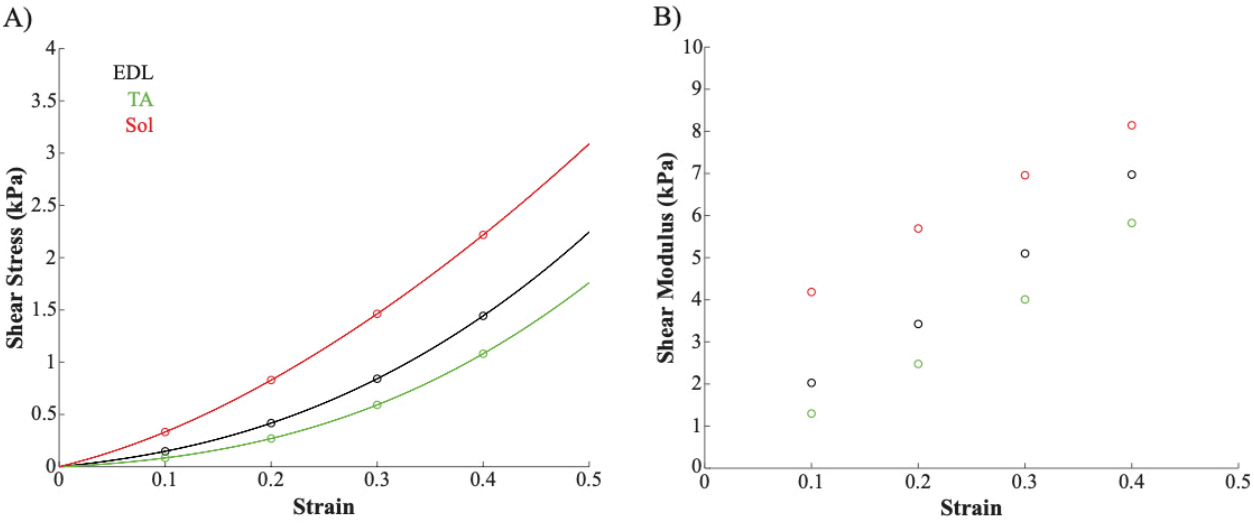

Figure 2.3 Representative data for A) shear stress and B) shear modulus versus strain from each of the three tested muscles types (EDL, TA, and Soleus) measured parallel to muscle fibers.
Open circles indicate the strain values selected within the physiological strain limit for shear modulus calculation.

Shear wave elastography provides an alternative method for measuring the shear modulus of muscle, but we are unaware of direct comparisons between direct measures of shear modulus and estimates from elastography. We used our measures of shear modulus to estimate the speed with which shear waves would have propagated in our tissue samples. Shear wave speed was estimated using Eq. 1, which has been validated for homogenous materials (Yamakoshi et al., 1990) but not for muscle.

$$Shear\ wave\ speed = \sqrt{shear\ modulus / density} \qquad (1)$$

We used an approximation of 1000 kg/m^3 for muscle density (Segal et al., 1986). Magnitude comparisons were made to previously published data in cats (Bernabei et al., 2020) and humans (Wang et al., 2019).

Statistical Analyses

We compared the shear modulus across the three different orientations using the statistical tests in Matlab (Mathworks, Natick, MA). Shear moduli were analyzed with a linear mixed effects model. Shear modulus was the dependent variable, modeled as a linear function of strain. Strain was modeled with interactions due to muscle and orientation. Strain was down-sampled to points within the physiological range of 0 to 0.4 (Blemker et al., 2005), and modeled as a nominal variable to reduce unnecessary high degrees of freedom and correlation within the model. Samples were treated as a random factor. The orientation and muscle were both categorical variables. We tested the model estimates with an analysis of variance to determine significance between the various fixed factors and correlation terms (significance of muscle type). Bonferroni corrections were used to account for multiple comparisons. There were 3 planned comparisons associated with testing between orientations, resulting in a significance level of $\alpha=0.05/3$.

Results:

There was no significant effect on shear modulus due to muscle type in our linear mixed effects model ($p=0.21$). Furthermore, we found no significant effect in the interactions of muscle type with any combination of orientation and strain or between orientation and strain (all $p>0.13$). We therefore simplified our model to exclude the muscle type and interaction terms. All further analyses are based on this reduced model.

The effect of muscle orientation on the shear modulus was significant ($p=0.007$). At the estimated maximum physiological strain, shear modulus was 6 ±1 kPa (mean ± 95% confidence interval), 7 ±1 kPa, and 4 ±1 kPa when measured parallel, perpendicular, and across muscle fibers, respectively. Using multiple comparisons, we found only the shear modulus perpendicular to

muscle fibers was significantly different (p=0.002), and greater, than the shear modulus in the across direction (Fig. 2.4). There was no significant difference in shear modulus between perpendicular and parallel (p=0.15) or between across and parallel directions (p=0.06). This can be seen in Fig. 2.4, where the shear modulus measured parallel to fibers lays between the predicted values of moduli measured in the perpendicular and across directions. The average percent difference of shear modulus between the parallel and perpendicular direction was 27 ±7 % (mean ± standard deviation). The average percent difference of shear modulus between the parallel and across direction was 33 ±9 %. Whereas in the significantly different directions, the average percent difference of shear modulus between the perpendicular and across direction was 47 ±10 %.

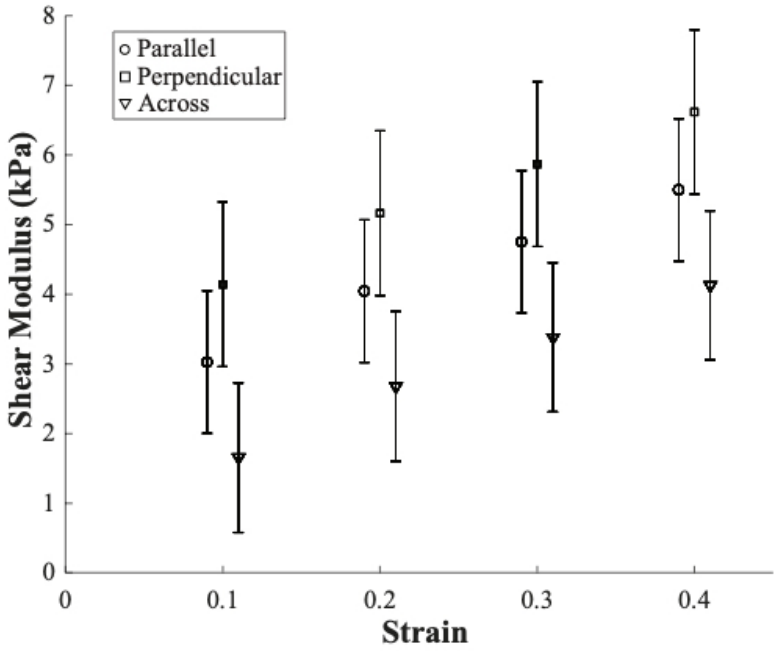

Figure 2.4 Shear modulus as a function of strain for the three orientations (parallel, perpendicular, and across). Predicted shear moduli and 95% confidence intervals are from the estimated linear mixed effects model. The samples oriented in the perpendicular direction were significantly different (p=0.002), and stiffer, than the across. There was no significant difference between parallel and the other two directions (p>0.05).

The effect of strain on shear modulus was significant ($p<0.0001$). The shear modulus increased linearly with increasing strain, indicative of a nonlinear elastic material (Fig. 2.4). We excluded strain's interaction with orientation in our model, as stated above, because it was not significant. Therefore, the rate of increase in shear modulus was the same for all directions. The predicted rate of increase in shear modulus between a strain of 0.1 and 0.4 was 8 ±1 kPa (mean ± 95% CI).

As reported above, we did not see a muscle-specific effect on shear modulus. However, it is important to note that these measures were difficult to acquire, with a fair bit of variability (Fig. 2.5). For example, at a strain of 0.1, the shear modulus in the across direction was 1.7 ±1.2 kPa (mean ± STD), 2.4 ±1.0 kPa, and 1.9 ±0.9 kPa for the EDL, TA, and soleus respectively. The shear modulus in the parallel direction was 3.3 ±2.6 kPa, 2.3 ±2.1 kPa, and 3.5 ±2.5 kPa for the EDL, TA, and soleus respectively. The shear modulus in the perpendicular direction was 6.2 ±4.5 kPa, 3.0 ±2.6 kPa, and 4.7 ±3.0 kPa for the EDL, TA, and soleus respectively. Though we did not observe statistically significant differences between muscles, there were some interesting trends (Fig. 2.6). The soleus has the largest shear modulus in the parallel and perpendicular direction, whereas the TA has the largest shear modulus in the across direction (Fig. 2.6). At the physiological limit, the largest mean difference across muscles was observed in the across orientation, where the TA had a shear modulus that was approximately 50% greater than the EDL. All other observed differences were closer to 20%.

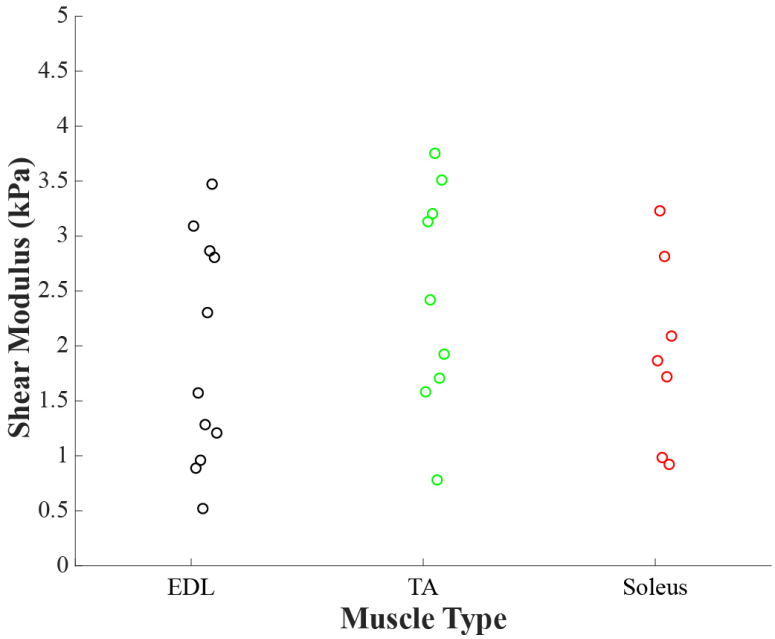

Figure 2.5 Shear modulus measured across muscle fibers of the EDL, TA, and Soleus at a strain of 0.1. There was no statistically significant difference between muscles. However, there was a large amount of variability in the measurements from each muscle type.

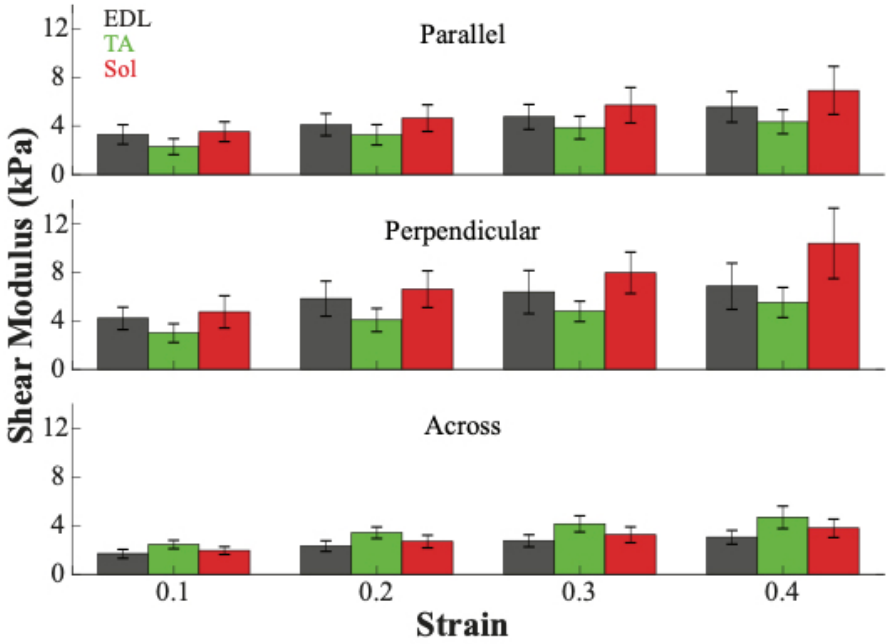

Figure 2.6 Average shear modulus versus strain for each of the three muscle types (EDL, TA, and Soleus) and orientations (parallel, perpendicular, and across). There was no significant difference due to muscle, but the average shear modulus measured in the parallel and perpendicular direction showed a trend between muscles. In these directions, the soleus was most stiff, followed by the EDL, and finally TA. However, the shear modulus measured in the across direction of the TA was stiffest, followed by soleus, and finally EDL.

Discussion:

The objective of this study was to quantify the shear moduli of skeletal muscle in the three degrees of freedom relevant to the function of whole muscles. We performed direct mechanical testing on tissue samples from three muscles of differing architecture in the rat hindlimb. We found no statistically significant effect due to muscle type on shear modulus. However, we did find the effect of strain on shear modulus was significant. The shear modulus increased linearly with increasing strain. Additionally, we found that the shear modulus when measured perpendicular to fibers was greatest. Within the physiological strain range, the average perpendicular shear modulus was 27 ±7 % greater than the parallel and 47 ±10 % greater than across. These results support the notion that muscle can be described as anisotropic in shear, but the transverse symmetry plane may not be as readily evident as it is in tension.

The shear modulus increased linearly with increasing strain. Muscle has been shown to exhibit a nonlinear stress-strain response when subjected to longitudinal extensions (Morrow et al., 2010). We found a similar response to shear deformations (Fig. 2.3), which resulted in a linear shear modulus-strain relationship (Fig. 2.4). This relationship is perhaps due to the nonlinear mechanics of the extracellular matrix. In longitudinal extension, muscle fibers and fiber bundles had a linear Young's modulus-strain relationship, while the inclusion of extracellular matrix made it nonlinear (Meyer and Lieber, 2011). The extracellular matrix is composed of many wavy collagen fibers (Gillies and Lieber, 2011; Trotter and Purslow, 1992). Therefore, the nonlinear shear modulus for muscle, which increases linearly with strain over the full range of physiological values, may be a result of unequal straightening of the extracellular matrix's collagenous structure (Munster et al., 2013; Sopher et al., 2018). Lengthening of the extracellular matrix due to shearing

decreases the number of slack collagen fibers. The addition of more load bearing collagen fibers at greater shear strains may correspond to the increase in shear modulus we observed.

The shear modulus measured perpendicular to fibers was significantly greater than the shear modulus measured across fibers. Whereas the shear modulus measured perpendicular and parallel to fibers were not significantly different. This difference could be due to muscle's directionally-dependent composition (Gans, 1982; Lieber and Friden, 2000). Muscle is composed of two macroscopic structures, muscle fibers and the extracellular matrix, both of which have unique orientations in muscle (Eng et al., 2008; Purslow and Trotter, 1994; Trotter and Purslow, 1992). It is possible that the muscle fibers have a greater shear modulus than the surrounding extracellular matrix. Therefore, shearing perpendicular to fibers could result in a larger shear modulus because of the resistance caused by the extracellular matrix and muscle fibers, whereas shearing in the parallel and across directions may only have resistance due to the extracellular matrix and transmembrane proteins. This difference could also be in response to how the muscle is physiologically loaded. Under normal physiological conditions, the body does not commonly experience shearing forces across the face of muscle fibers (Blemker et al., 2005; Purslow, 2002). One possible exception to this is blunt trauma where the muscle may be sheared in all three directions (Best, 1997; Loerakker et al., 2013; Woodhouse and McNally, 2011). However, for normal force transmission the structural arrangement of muscle doesn't provide, or necessitate, a large shear stiffness in the across direction. Speculating at a scale beyond what was measured here, the similarity in perpendicular and parallel directions could be due to negligible stiffness of the transmembrane proteins at the scale we measured. It could also be that the stiffness of the extracellular matrix dominates the total passive muscle stiffness, as alluded to by indirect measures (Meyer and Lieber, 2011). Contrary to what we first assumed with our hypothesis, one could argue

that muscle fibers simply glide past each other when subjected to shear forces and the interwoven extracellular matrix resists shearing. Without separating and testing these elements independently, we cannot confirm what component of muscle dominates the passive shear modulus.

Despite using muscles with different architectures, we did not find evidence that muscle type significantly influenced shear moduli. One potential reason is rats have a short life span, ranging from 2.5 – 3.5 years (Sengupta, 2013). In humans, the pennation angle, muscle volume, and fascicle length is reduced with age (Narici et al., 2003; Thom et al., 2007). Additionally, in aging human muscle, there are reductions in fiber size (Lexell, 1995; Lexell et al., 1988; Trappe, 2009) and increases in collagen and fat content (Kragstrup et al., 2011). These age-related architecture and composition changes result in reduced force generation and transmission (Bemben et al., 1991; Lieber and Friden, 2000; Thom et al., 2007). This reduction in force transmission seen in older humans could be a result of changes to the shear modulus that resist it (Huijing, 1999; Kragstrup et al., 2011). These increases in shear modulus may be incurred as a way to influence muscle function by providing greater resistance to potentially injury causing shear loads (Kjaer, 2004). Therefore, a rat's short life span may not provide sufficient time in which they can have changes to muscle architecture and composition. In an experiment that evaluated the effect of aging on the shear modulus of various muscles, we may have found a significant effect. Furthermore, examining the shear modulus between muscles within a species that has a longer lifespan, like humans, may show a significance due to muscle type. While not significant in our experiment, we did observe a trend in the shear moduli of the muscles we tested. In the parallel and perpendicular orientations, the average modulus of soleus was highest followed by EDL then TA. This was not the case when measured across fibers, where the TA was stiffest followed by the soleus then EDL.

Therefore, under a longitudinal (time) study, there may be a slight difference due to architectural differences in rat muscles.

The estimated shear wave speed was extrapolated back to zero strain to correspond to shear wave elastography measures made in passive, non-tensioned muscle (Fig. 2.7). At zero strain, the predicted shear wave speed was 1.5 ±0.3 m/s (mean ± CI), 1.8 ±0.3 m/s, and 1.0 ±0.3 m/s in the parallel, perpendicular, and across directions respectively. Under maximum passive strain, the highest predicated shear wave speed was 2.6 ±0.2 m/s measured perpendicular to fibers. The shear wave speed, in all cases, increased with strain. In general, shear wave speed calculated from the passive muscle increased by 1 m/s between a strain of 0.1 up to the physiological range limit 0.4. These estimates from direct shear moduli measures produced results near those directly measured with elastography in passive muscle. In the study by Bernabei et al. (2020), cats exhibited a shear wave speed of approximately 3 m/s. Similarly, in the study by Wang et al. (2019), human participants showed a shear wave speed of approximately 2.5 m/s at a neutral elbow angle of 80 degrees. Species-specific differences may contribute to some of the variability in muscle, but the estimates calculated here fall within these direct measurements. It is important to note that this conformity does not confirm that shear wave speed only relies on shear modulus in muscle, rather that shear modulus is a major component of that potentially complicated relationship. Our results suggest that shear wave speed may be useful for estimating shear modulus of non-tensioned tissue. Therefore, elastography could be used to measure the shear modulus in a variety of species and muscles to further our understanding of species and muscle architecture differences.

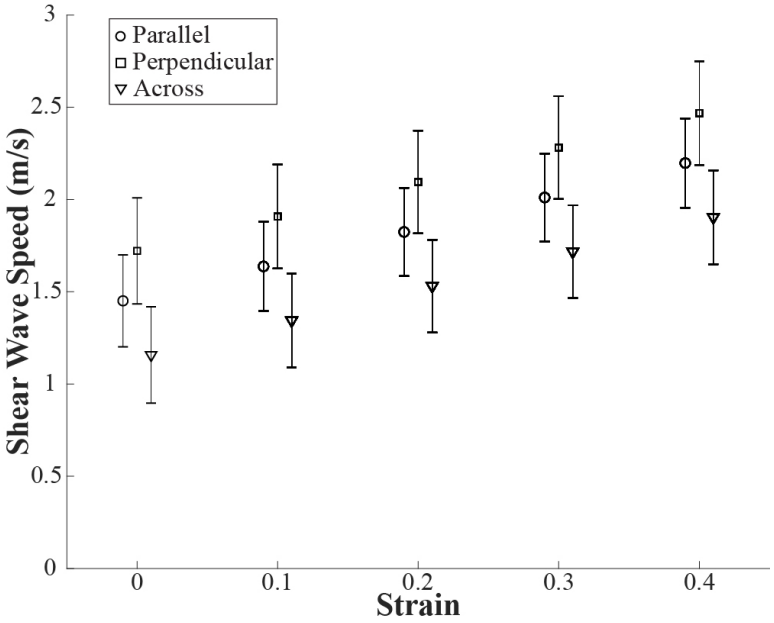

Figure 2.7 Estimated shear wave speed for the three orientations (parallel, perpendicular, and across). Estimates and 95% confidence intervals are from the estimated linear mixed effects model. The shear wave speed estimates showed a slight upwards trajectory with increasing strain from 1 to 3 m/s. This is consistent with directly measured shear wave speed for passive muscle in both cats and humans.

Limitations

The results presented here generalize muscle as one uniform material with anisotropic properties. However, muscle is a complex heterogeneous material. The shear moduli we measured are of total muscle which include the combination of extracellular matrix and muscle fiber properties. Without investigating these materials separately, one cannot decipher the individual contributions of these elements. Additionally, we selected a slow rate of extension to eliminate the viscoelastic effects of muscle from our measures. The rate used is most likely below typical physiological speeds where viscoelastic properties may be important for normal muscle function. Studies at higher rates, capable of measuring the viscoelastic properties, may supplement the measures collected here. Finally, samples were cut into cubes by hand, which may introduce slight variations in shape. The utmost care was taken in being consistent, but slight undercuts not easily

visible by eye may produce measurement variability. This was mitigated to the best of our ability by taking dimensional measures before testing and using a large sample size. Despite these limitations, the values reported here provide new insight into muscle anisotropy and useful parameters to simulate shear wave propagation.

Conclusions:

Our results are the first direct measures of three-dimensional shear moduli in skeletal muscle. These results show that the shear modulus measured perpendicular to fibers was greater than any other direction, but only significantly different from the moduli measured across fibers. Additionally, the shear modulus increased linearly with increasing strain, indicative of a nonlinear elastic material. Despite architectural differences between muscles, we did not find the shear modulus of the rat muscles we tested to be different. The estimated shear wave speed is consistent with those directly measured in cats and humans. This suggests that shear wave speed can be used to estimate shear modulus, and vice versa, in passive non-tensioned muscle. Finally, for continuum models, the quantitative measures reported here can be used to describe the mechanical properties of muscle in shear. In combination with 3D measures of Young's modulus and Poisson ratio, any deformation within the muscle can be determined.

Chapter 3: Efficiency of skeletal muscle decellularization methods and their effects on the extracellular matrix

This chapter consists of a manuscript published in the Journal of Biomechanics:
Reyna, W. E., Pichika, R., Ludvig, D., Perreault, E. J. (2020).
"Efficiency of skeletal muscle decellularization methods and their effects on the extracellular matrix." J Biomech

This study was funded by the National Institutes of Health (R01AR071162 and T32HD07418). We would like to acknowledge Dr. Richard Lieber for his technical support and comments during the formative stages of this project.

Abstract:

Extracellular matrix (ECM) is widely considered to be integral to the function of skeletal muscle, providing mechanical support, transmitting force, and contributing to passive stiffness. Many functions and dysfunctions attributed to ECM are thought to stem from its mechanical properties, yet there are few data describing the mechanics of intact ECM. Such measurements require isolating intact ECM from the muscle cells it surrounds. The objectives of this study were to quantify the efficiency of three techniques for this purpose: Triton, Triton with sodium dodecyl sulfate, and latrunculin B; and to determine their impact on properties of the remaining ECM. Efficiency was quantified by DNA content and evaluation of western blot intensities for myosin and actin. The properties of ECM were quantified by collagen content and uniaxial tensile testing. We found that latrunculin B was the most efficient method for removing skeletal muscle cells, reducing DNA content to less than 10% of that seen in control muscles, and substantially reducing the myosin and actin to 15% and 23%, respectively; these changes were larger than for the competing methods. Collagen content after decellularization was not significantly different from control muscles for all methods. Only the stiffness of the muscles decellularized with latrunculin B differed significantly from control, having a Young's modulus reduced by 47% compared to the other methods at matched stresses. Our results suggest that latrunculin B is the most efficient

method for decellularizing skeletal muscle and that the remaining ECM accounts for approximately half of the stiffness in passive muscle.

Introduction:

The extracellular matrix (ECM) is widely considered integral to the function of skeletal muscle, providing mechanical support to muscle fibers, transmitting force from fibers to tendon, and contributing to passive stiffness. The importance of ECM is underscored by the disabilities accompanying changes in ECM structure resulting from age, injury, or disease (Alnaqeeb et al., 1984; Handorf et al., 2015; Lieber et al., 2003; Woolf and Pfleger, 2003). Many of the functions and dysfunctions attributed to ECM stem from its mechanical properties (Gillies and Lieber, 2011), yet there are few data quantifying them.

Many studies of ECM have considered the mechanics of single collagen fibers, or indirect measures of whole ECM stiffness. The beautiful images from Trotter and Purslow (1992), showed that ECM is hierarchical in structure, containing endo-, peri-, and epimysium layers surrounding muscle fibers. The collagen fibers within these layers create a reinforced structure that stiffens upon stretching (Huijing, 1999). Indirect measures of ECM have been made by looking at changes in mechanical properties of fiber bundles with and without ECM. These results suggested that ECM is the dominant factor contributing to the Young's modulus of muscle (Gillies et al., 2017; Meyer and Lieber, 2011). However, a quantitative assessment of ECM properties was not obtained. Modeling has also been used to predict the mechanical properties of ECM from knowledge of collagen fiber mechanics and the structure of their arrangement in ECM (Bleiler et al., 2019; Roeder et al., 2002), but these predictions have not been validated by direct measurements. Such measurements require isolating intact ECM from the muscle cells it surrounds. Though there are

many approaches for skeletal muscle decellularization, their efficiency for removing cellular material from intact muscles and their influence on whole muscle ECM has yet to be quantified.

The focus of this study work was on decellularization as a tool for assessing the role of ECM in muscle mechanics. Many decellularization processes were developed for applications in tissue transplantation and regeneration, for which a primary concern is the elimination of antigenic components that could cause an immune response inhibiting recellularization (Crapo et al., 2011; Gilbert et al., 2009; Soto-Gutierrez et al., 2011). While we draw on some of the techniques developed for regeneration applications, we limit our evaluations to metrics of muscle cell removal and ECM integrity specific to our application. Still, our results may serve as a starting point for choosing a decellularization process suitable for muscle transplantation by providing measures of scaffold stiffness and removal efficiency, as recent work has shown the importance of scaffold stiffness on facilitating cellular differentiation and migration (Breuls et al., 2008).

Many techniques use harsh chemicals and physical disruptions to lyse cells and wash out cellular components, processes that may also disrupt ECM composition (Crapo et al., 2011; Gilbert et al., 2006). Gillies and colleagues (2011) proposed a novel method for decellularizing skeletal muscle using latrunculin B to disrupt actin, and additional washes to induce cell lysis, disrupt titin, depolymerize myosin, and remove DNA. The proposed benefits were an efficient removal of muscle cells with a preservation of ECM structure. This method was shown to reduce more than 90% of the cellular DNA, nearly all of the full chain myosin, and to partially degrade actin. However, comparisons to alternative methods were not made. Two common alternatives use Triton X-100 alone or in combination with sodium dodecyl sulfate (SDS) (Caralt et al., 2015). Triton X-100 lyses cells by disrupting the lipid-lipid and lipid-protein interactions, SDS solubilizes cytoplasmic and nuclear cellular membranes. The reported actions of these chemicals do not

include degradation of collagen, a proxy for ECM integrity (Crapo et al., 2011). Thus, it remains unknown how the use of latrunculin B, a method that is proposed to be more effective, compares to these alternatives with respect to the efficacy of decellularization and the corresponding impact on the properties of the remaining ECM structure.

The objectives of this study were to quantify the efficiency of three decellularization methods on removing muscle cells from skeletal muscle and to determine their effects on the remaining ECM. Decellularization efficiency was quantified by measures of DNA content and evaluation of western blot intensities for myosin and actin. The characteristics of the resulting ECM were quantified by measures of collagen content. We also performed uniaxial tensile testing to quantify the mechanical properties of the remaining ECM structure. All measures were made in the flexor digitorum profundus muscle of fresh chicken. Our results are the first to comparatively evaluate decellularization methods for skeletal muscle using mechanical measures of whole muscle ECM. This is an important step towards characterizing the mechanical properties of intact skeletal muscle ECM so as to understand its contribution to whole muscle mechanics during passive and active conditions.

Materials and Methods:

Decellularization was evaluated using two criteria: 1) content of cellular DNA, myosin, and actin, and 2) properties of ECM. All data were collected from the chicken flexor digitorum profundus muscle obtained from a local butcher; a total of 212 fresh muscles were harvested. Muscles were tested within a week of death, a period in which mechanics, collagen, and myosin heavy chain (MHC) are unaffected by post-mortem time (Tuttle et al., 2014). The interface

between tendon and muscle was marked immediately after dissection, and the length of the muscle excluding the tendon was used as a reference for all future measurements.

The length, mass, and volume of each sample was measured before and after decellularization but prior to tensile testing to track changes in these physical properties at each stage of the experiment. Volume was measured using the water suspension method (Hughes, 2005).

Decellularization Procedures

Muscles were randomly assigned to one of four treatment groups: 1) untreated Control, 2) 1.0% Triton X-100 only decellularization, 3) 1.0% Triton X-100 and 0.1% SDS decellularization, and 4) 50 nM latrunculin B with 0.6 M potassium chloride and 1.0 M potassium iodide washing. Control muscles were tested immediately following harvest. We also completed a control that followed the times, temperatures, and washes in the decellularization processes but these outcome measures did not differ from the untreated control and therefore are not presented for conciseness. The decellularization procedures followed those detailed by Gillies et al. (2011) and Caralt et al. (2015). In short, each group went through 3-6 solution changes to perform decellularization. Washes were completed by placing each muscle in a 50mL vial and covering with 25 mL of solution. Vials were agitated on a vertical and horizontal orbital shaker (Belly Dancer Shaker, IbI Scientific, Dubuque, IA) at approximately 80 rpm.

Thirty-eight samples from each treatment group were used for biochemistry to evaluate decellularization efficiency. The remaining 15 samples were used for tensile testing to evaluate the mechanical consequences of decellularization.

Biochemical Analysis

Samples from each group allocated for biochemistry underwent one of three tests: 1) DNA content (n=15), 2) myosin and actin western blot (n=8), and 3) collagen content (n=15). DNA content has previously been used as the main metric to evaluate decellularization (Crapo et al., 2011; Gilbert et al., 2009; Soto-Gutierrez et al., 2011). We also considered myosin and actin due to their roles in muscle contraction. ECM is composed primarily of collagen (Purslow, 1999, 2008; Trotter and Purslow, 1992), which we used as a quantitative metric of ECM integrity; a substantial reduction in collagen content would indicate damage to the ECM.

DNA was isolated from whole muscle using the PureGene Cell and Tissue Kit protocol (Qiagen, Valencia, CA). DNA content per total pre-decellularization wet weight was quantified using the Eppendorf Bio-Spectrometer Basic (Eppendorf, Hamburg, Germany) at an absorbance value of 260nm. Values with a 260/280 absorbance ratio outside of 1.7-2.0 were thrown out due to potential contaminants (Ahn et al., 1996; Sambrook et al., 1989).

Myosin and actin were measured relative to the control using the intensity of the western blot bands. The eight samples allocated for western blot analysis were split into two equal groups, one for myosin and one for actin. Muscles in their entirety from each group, including control, were freeze dried and pulverized. Pulverized samples were reconstituted with equal volume to produce a consistent dilution across groups. Myosin samples were further purified using the MHC protocol detailed by Minamoto and colleagues (2015). Aliquots from the homogenate were plated to measure total protein content using the Pierce™ BCA protein assay kit (Pierce Biotechnology, Rockford, IL). This measurement was used to determine the most concentrated sample, the control, and least concentrated, latrunculin B. Balancing these total protein values, so as not to saturate the gel or miss protein, we loaded 25 μL of tissue homogenate from each sample into wells of a

NuPAGE 4-12% Bis-Tris gradient gel to separate proteins based on molecular weight. Once separated, protein was transferred using the Bio-Rad Trans-Blot SD semi-dry transfer cell to a Nitrocellulose membrane and checked using the water soluble Ponceau S stain. Membranes were blocked overnight at 4°C with 5% Bovine Serum Albumin (BSA) in Tris Buffered Saline-TWEEN 20 (TBST). Membranes were incubated with the primary antibody myosin skeletal muscle monoclonal antibody (Mouse MAb (MYSN02) (NeoMarkers, Fremont, CA) and actin monoclonal antibody (ACTN05(C4)) (ThermoFisher Scientific, Rockford, CA) for 1 hr at room temperature. Membranes were washed with 4 changes of TBST every 20 min. The secondary antibody (Goat Anti-Mouse IgG HRP Conjugate (H+L), used for Myosin and Actin) (EMD Millipore Corp, Billerica, MA) was incubated on the membrane for 1 hr at room temperature followed by a 2-hr wash with TBST. The membrane was developed with a 50:50 mixture of detection reagent from the Pierce™ ECL Western kit (Pierce Biotechnology, Rockford, IL) for 7 min. Membranes were imaged using a Syngene PX*i* imager (Syngene, Frederick, MD). Bio-Rad's Precision Plus Protein™ Standard was used to identify the molecular weights of actin and myosin based on previous measures made in chicken skeletal muscle (Rosser et al., 1996; Soglia et al., 2016). Post processing densitometry was made using ImageJ (NIH), to determine the intensity of bands and the subsequent percent difference from control.

Collagen content was quantified from the entire muscle using the hydroxyproline protocol (Edwards and O'Brien, 1980). Briefly, whole muscle tissue was hydrolyzed with 6 N hydrochloric acid for 22 hrs or until no particles of tissue could be seen. The hydrolysate was dried, then dissolved in 3 ml of water to create samples of equal volume. Ten to twenty-five microliters of the hydrolysate were oxidized with chloramine-T followed by p-dimethylaminobenzaldehyde and absorbance was read at 550 nm in triplicates to determine the hydroxyproline content.

Measurements were made using the Synergy|HTX multi-mode plate reader (Bio-Tek Instruments, Inc., Winooski, VT). Collagen content was calculated using the hydroxyproline to collagen conversion multiplication factor of 7.46, determined from mammalian and avian experiments (Neuman and Logan, 1950).

Mechanical Testing

Uniaxial testing was used to determine elastic tensile properties of the tissue along the direction most relevant to muscle structure and function (Lloyd LF Plus; Amatek Inc, Lloyd Instruments, Leicester, UK). Samples were hydrated in phosphate-buffered saline, then rigidly anchored using two vertically aligned metal wedge clamps at the interface between tendon and muscle. Data were collected at a strain rate of 5% per min until failure.

Tissue stress was calculated by dividing the applied load by the cross-sectional area, estimated for each sample as the volume divided by length using the pre-decellularization measures. Tissue strain was calculated by dividing the extension of the tissue by the pre-decellularization sample length. Pre-decellularized dimensions were used to reduce normalization errors induced by sample swelling associated with the decellularization processes. Instantaneous Young's modulus was computed as the slope of the stress-strain curve.

Statistical Analyses

Statistical tests were performed in Matlab (Mathworks, Natick, MA). Physical properties were analyzed using a paired t-test between pre-decellularized and post-decellularized observations. DNA and Collagen content were analyzed using a one-way ANOVA. Post-hoc comparisons between treatment groups were made using the Tukey-Kramer method at a

significance level of p=0.05. Biochemical and physical data results are presented as means ± standard error.

We modeled Young's modulus as a function of stress to determine how it was influenced by the different treatment groups. Linear mixed effects models were used for this analysis. Young's modulus was the dependent variable, modeled as a linear function of stress. Samples were treated as a random factor to account for the correlation of repeated measurements within each sample. The preparation for each treatment group was modeled as a fixed factor. We compared the slopes and intercepts of the fitted models to determine how the different treatments influenced mechanical properties. Bonferroni corrections were made to account for multiple comparisons. There were 12 planned comparisons, resulting in a significance level of p=0.05/12 for reference.

Results:

Decellularization Efficiency

Latrunculin B and Triton/SDS reduced DNA content more than Triton alone. Triton/SDS and latrunculin B decreased DNA content to 8 ± 1 ng/mg and 7 ± 1 ng/mg, respectively, a significant difference from the control samples (78 ± 5 ng/mg; $p<0.0001$). There was no significant difference between the Triton/SDS and latrunculin B treatment groups ($p>0.9$; Figure 3.1). Triton without SDS also significantly decreased DNA content relative to control (25 ± 3 ng/mg; $p<0.0001$), though not as effectively as latrunculin B or Triton SDS (both $p<0.0001$).

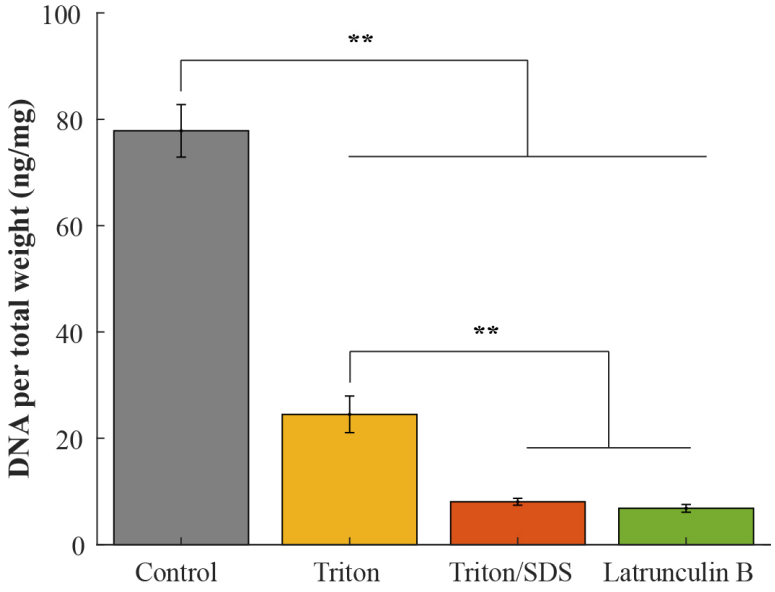

Figure 3.1 Average DNA content per total pre-decellularization wet weight from 15 samples in each treatment group.
There were significant differences (** denotes $p < 0.0001$) between control and treatment groups and Triton to other treatments. Error bars indicate standard errors.

Latrunculin B removed more actin and myosin than the two Triton based methods. Densitometry of the western blots showed latrunculin B on average was able to reduce myosin by 85 ± 7 % and actin by 77 ± 10 % (Figure 3.2, bar graphs). Whereas Triton and Triton/SDS reduced the myosin content by 26 ± 15 % and 16 ± 14 % and actin by 14 ± 9 % and 29 ± 11 %, respectively. This is also shown by visual inspection of the western blots for all groups (Figure 3.2, blots). Myosin content was nearly eliminated by latrunculin B, as noticed by its near absence in the western blot. There was no noticeable difference in the Triton and Triton/SDS groups compared to each other, or to the control. The removal of actin varied across treatment groups. Latrunculin B had the lowest content followed by smaller reductions in the Triton and Triton/SDS groups relative to the control.

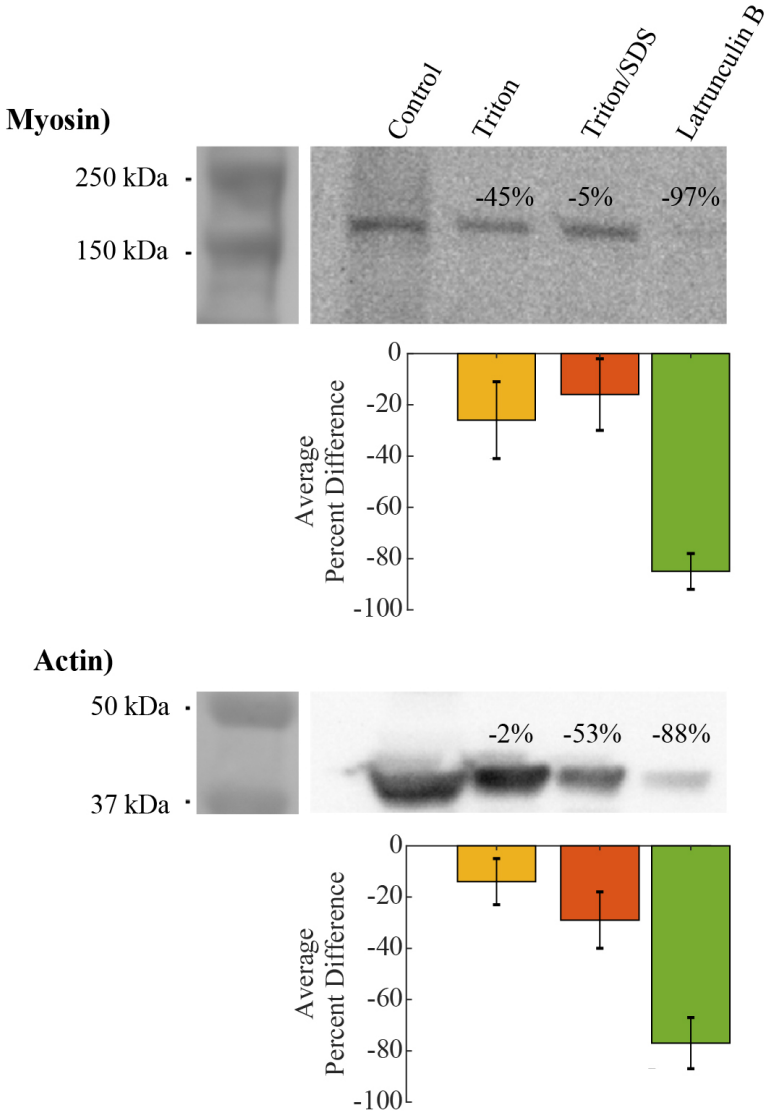

Figure 3.2 Representative western blots and average percent difference from control of full chain myosin and actin for each of the treatment groups.
Both proteins were reduced substantially by the latrunculin B treatment. Left Bar of western blot represents protein standard for protein density identification. Error bars indicate standard errors.

None of the decellularization methods altered collagen content relative to control (Figure 3.3). The control tissue had a collagen concentration of 155 ± 10 ug/mg. All other treatment groups did not differ significantly from this value ($F(3,56)=0.76$, $p>0.5$).

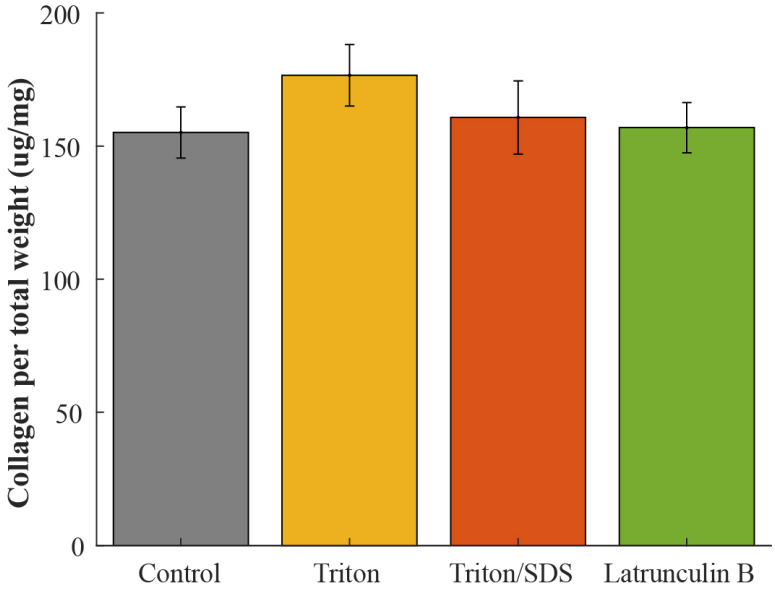

Figure 3.3 Average collagen content from 15 samples in each treatment group.
There were no significant differences between groups. Error bars indicate standard errors.

Mechanical Effects

All decellularization methods caused swelling of the tissue samples, which must be considered when evaluating mechanical properties. This swelling caused small decreases in length (Figure 3.4A) that reached statistical significance in the latrunculin B group ($p<0.0001$). It also led to increases in mass for all treatment groups (Figure 3.4B; Triton and latrunculin B $p<0.005$, Triton/SDS $p<0.0001$).

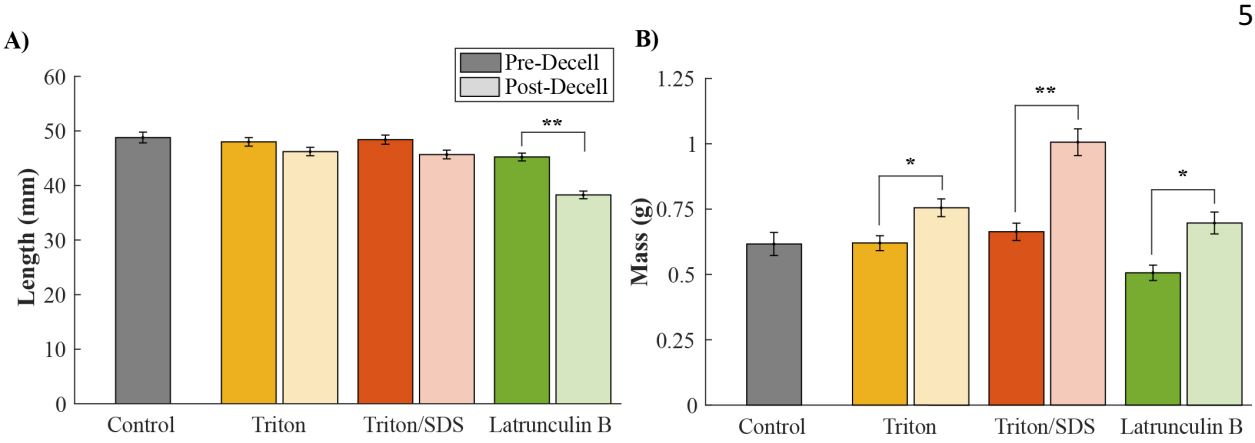

Figure 3.4 Physical properties, A) length and B) mass, of 15 samples per treatment group.
Measurement obtained pre- and post-decellularized show signs of swelling in decelluarize samples. There was a significant difference between latrunculin B lengths. Additionally, all treatment groups had significantly different masses after decellularization. Error bars indicate standard errors. * denotes significant difference of $p < 0.005$ and ** of $p < 0.0001$.

The shortened length in the decellularized samples relative to their pre-decellularized length caused force to increase above zero at lengths shorter than the control samples. Similar results were shown by Sleboda and Roberts (2017), who demonstrated that swelling shifts the onset of passive force development in muscle. This shift can be observed in the average stress-strain curves for each treatment group (Figure 3.5). Analyzing further, the Young's modulus versus strain (Figure 3.6A) shows that the unaligned strain makes comparisons impossible. Without accounting for the swelling, comparable points cannot be identified. We accounted for this shift by examining Young's modulus as a function of stress rather than the more commonly used strain, which eliminates effects due to a shift in the length at which passive force development begins (Figure 3.6B; see Supplementary Material for rationale).

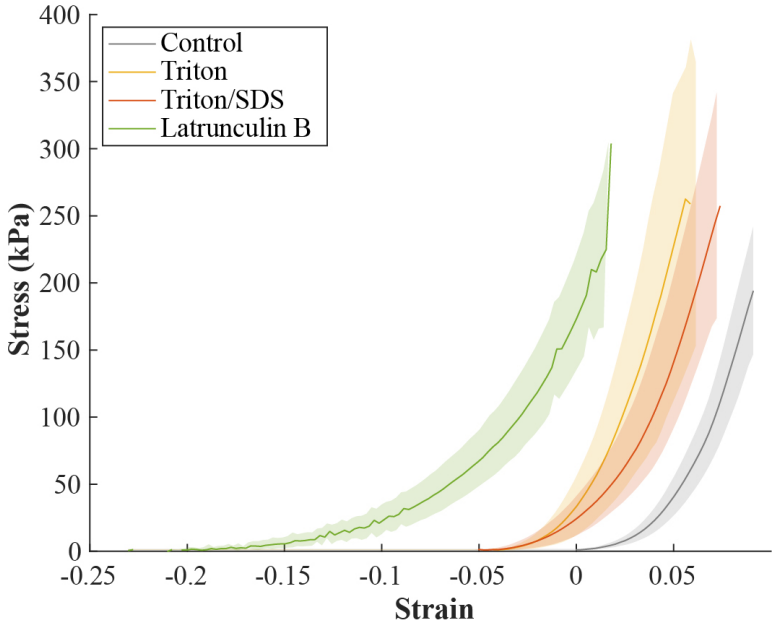

Figure 3.5 Average stress versus strain relative to the original starting length of each muscle.
All treatment groups show lateral shifts in decellularized samples due to swelling. Shaded regions represent standard deviations.

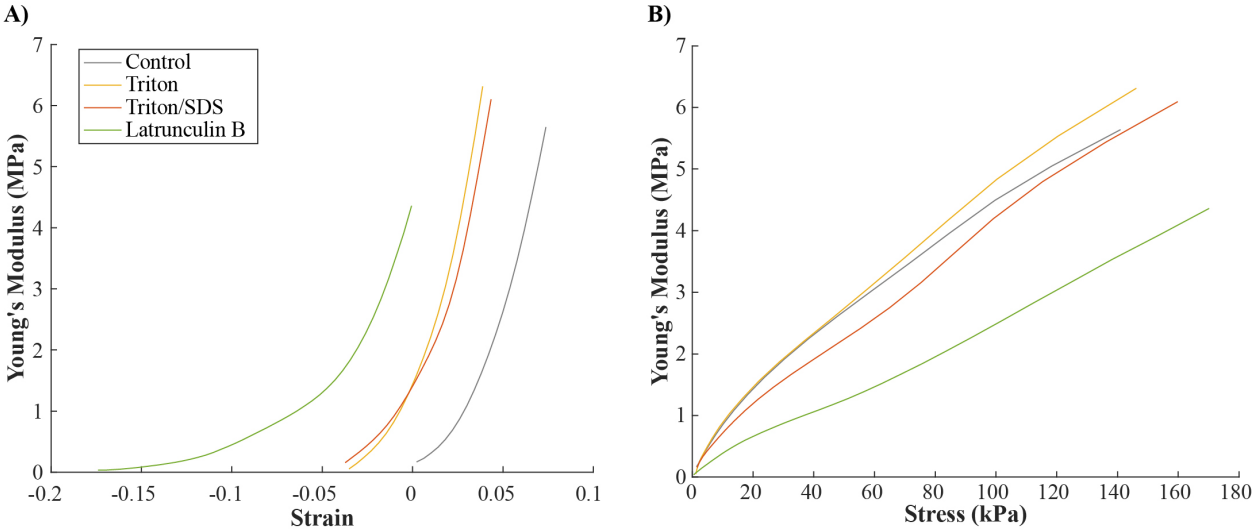

Figure 3.6 Representative data for Young's modulus versus A) strain and B) stress from each of the four treatment groups.
All treatment groups exhibited a lateral shift in strain due to swelling that prevents comparisons across samples. Whereas Young's modulus visualized against stress does not have these limitations, as a result of its invariance to swelling

The relationship between Young's modulus and stress was different for latrunculin B than for all other treatment groups. The linear mixed-effects model describing this relationship for all treatment groups had an R^2=0.92 and a log-likelihood of -1923 (Figure 3.7). The control group had a slope and intercept of 32 ± 2 and 0.43 ± 0.05 MPa, respectively. Only the slope for latrunculin B (17 ± 3) differed significantly ($p<0.0001$) from the control group. There were no significant differences in the intercept for any decellularization group compared to control. However, the intercepts for latrunculin B (0.23 ± 0.07 MPa) and Triton (0.55 ± 0.05 MPa) differed significantly ($p=0.0003$), as did the intercepts between Triton and Triton/SDS (0.33 ± 0.05; $p=0.002$). The stiffness for the latrunculin B group was significantly lower than the other treatment groups over nearly the entire measurement range (Figure 3.7). There was also a smaller but significant difference between Triton/SDS and the control and Triton groups at low stresses.

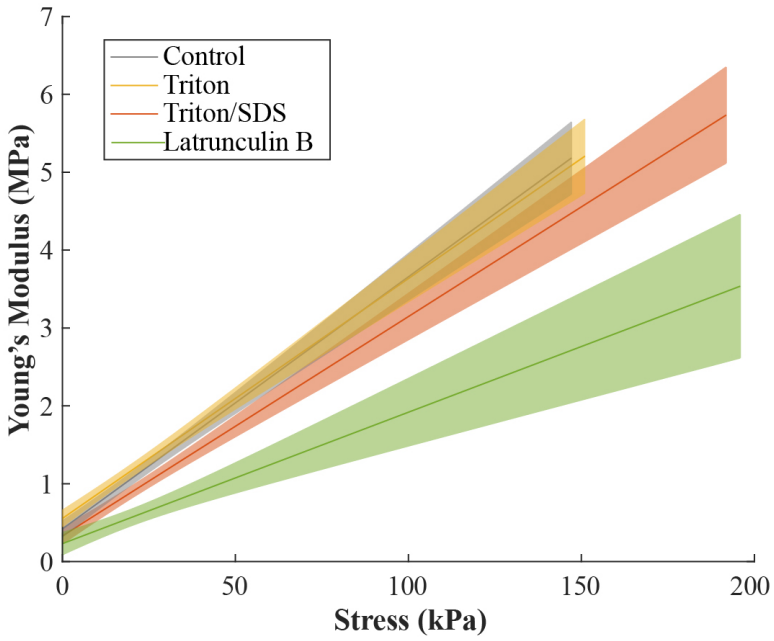

Figure 3.7 Young's modulus as a function of stress for the four treatment groups.
Lines and 95% confidence intervals are from the estimated linear mixed effects model. Latrunculin B is significantly less stiff than control. Triton/SDS is also significantly different from control at low stresses.

Discussion:

The objectives of this study were to quantify the efficiency of three decellularization methods on removing muscle cells from skeletal muscle and to determine their effects on the remaining ECM. Biological and mechanical tests were performed to quantify the efficacy of decellularization and their influence on stiffness, respectively. We found that latrunculin B and Triton/SDS reduced DNA content by approximately 90%. However, latrunculin B was the only method to show substantial decreases in myosin and actin, suggesting that it was the most effective method for removing the cellular content of skeletal muscle from the surrounding ECM. None of the tested methods altered the content of ECM, as was expected from previous results (Caralt et al., 2015; Gillies et al., 2011). Together, these results suggest that latrunculin B is the most effective of the tested methods for decellularizing skeletal muscle. The latrunculin B treatment group was also the only one that had a Young's modulus significantly different from the control group. It had a stress-dependent increase in stiffness that was approximately 50% of the control group, suggesting that nearly half of the passive stiffness in our muscle samples can be attributed to ECM remaining after decellularization.

Decellularization Efficiency

Decellularization is common in tissue transplantation and regenerative engineering research, where the main concern is removing cellular-DNA to eliminate an immune response in the recipient. When the goal is to isolate ECM from skeletal muscle, it is important to remove as much of the cellular content as possible, especially the load bearing proteins. Gillies et. al. (2011) proposed a method involving latrunculin B that was designed to remove all cellular content and preserve ECM integrity. It was stated that this method was advantageous in comparison to others

though experimental assessments were not published. We found that latrunculin B led to a decellularization efficiency similar to what was reported by Gillies et al. We observed a decrease in DNA to about 10% of control values, slightly larger than the 4% reported in the earlier study. We also found myosin was reduced to about 15% and actin to about 23%, as seen before. The differences in DNA content could be attributed to species differences or simply muscle size. The volume of the mouse tibialis anterior has been reported to be ~50 mm^3 (Zhang et al., 2008) whereas the average volume of the chicken flexor digitorum profundus muscles used in our study was (530 ± 130 mm^3).

Triton and Triton/SDS were also effective at removing DNA but not the actin and myosin proteins essential for muscle contraction. Similar reductions in DNA have been reported when decellularizing organs for regeneration and transplantation applications (Caralt et al., 2015), but we are unaware of previous studies that examined the use of Triton and Triton/SDS for removing actin and myosin from skeletal muscle. Our results suggest that they are not effective for this purpose.

Gillies et al. also suggested that latrunculin B would cause less damage to the ECM. Our measures of collagen content do not support that statement. We found no significant changes in the collagen content across all treatment groups. However, it is important to acknowledge that different procedures (e.g. concentrations, wash durations, …) may lead to different results from the same chemicals.

Decellularization is strongly influenced by the size of the specimen and the composition of the tissue being decellularized. While we expect our results to extend to skeletal muscles with similar cross-sectional areas, the efficacy of the decellularization processes should be carefully quantified if used for other muscles. Freezing tissue for histological staining proved challenging

and unfeasible due to the high liquid content following decellularization, which produced structure-damaging ice crystals. We also attempted to stain the decellularized muscles after fixing with formalin due to its stiffening effects on tissues (Fox et al., 1985). Unfortunately, there was not enough muscle tissue remaining to maintain the shape of the material after decellularization, making it impossible to obtain architecturally intact sections suitable for staining. However, throughout mechanical testing, visual inspection and physical examination of the decellularized tissue did not show exhibit notable signs of degradation leading to disintegration or loss of its general geometric shape. This observation is further substantiated by our collage measures; collagen, our proxy for integrity, did not show a substantial decrease in content. Additionally, while densitometry of western blots has been used to determine the content of imaged proteins, care should be taken with directly reporting these concentration values. Western blots are highly dependent on how loading was controlled, how successful gel to membrane transfer, and how normalization was done. We preformed these experiments according to the suggestions provided in the Aldridge et al. (2008) study and using the entire muscle to eliminate dissecting unequal subsections of the muscle.

Mechanical Effects

The muscles decellularized with latrunculin B were significantly less stiff (~47%) than all other treatment groups. This result coupled with the effectiveness of latrunculin B decellularization suggests that ECM accounts for approximately half of the passive stiffness in the muscles used for this study. This estimate assumes that decellularization did not damage the integrity of the ECM. Collagen content was unaffected relative to our control samples, but we did not examine changes in the microstructure of ECM. If it was damaged, then our estimate could be considered as a lower

bound on the passive force load carried by ECM. Our estimate of the ECM contributions to passive stiffness lies between what has been suggested by other groups. Gillies et al. (2011) concluded that ECM accounts for most of the passive muscle stiffness based on results using the same decellularization method. They also observed a clear separation (~30% difference at 100% strain) in the stiffness of control samples and those decellularized with latrunculin B, but their statistical tests did not reach significance. The difference may be due to the methods of analysis or overall measurement variability. Brynnel et al. (2018) concluded that titin rather than ECM dominates the passive stiffness of muscle. They disrupted titin with KCl/KI washes similar to those used in our study, and observed a much larger decrease in passive stiffness. Those results might arise from species-specific differences in the role of ECM (Meyer and Lieber, 2018) or from the fact that they referenced stiffness to sarcomere lengths prior to decellularization, which may make it difficult to compare across treatment conditions (Figure 3.5).

There were challenges measuring the mechanical properties of muscle after decellularization due to swelling. Treatment groups showed various amounts of swelling. This likely arises from osmotic differences caused by the chemical agents used in decellularization. This swelling may have been exacerbated by the loss of muscle fibers, which normally generate a transverse force restricting volume changes (Smith et al., 2011), which could explain the increased swelling in the latrunculin B samples. This swelling made it impossible to compare measured mechanical properties using lengths, such as slack length or the optimal force length, identified prior to decellularization (Figure 3.6A). Swelling caused a treatment-dependent shift to shorter slack lengths after decellularization. Similar shifts were observed by Sleboda and Roberts (2017), who examined the effects of swelling on passive muscle mechanics. They concluded that swelling influences slack length but not the form of the passive force-length curves. Assuming that swelling

has the same effect on decellularized tissue, we compensated for changes in slack length by comparing our treatment groups at matched stresses (Figure 3.6B) rather than matched strains since changes in stress are invariant to changes in slack length (see Supplementary Material).

Conclusions:

Our results suggest that latrunculin B is an effective method for decellularizing skeletal muscle, outperforming Triton and Triton/SDS methods that are common in other applications. While all tested methods had no measured effect on the quantity of ECM, latrunculin B was more effective at removing cellular DNA, myosin, and actin. The efficacy of this method allowed us to measure the Young's modulus of the remaining ECM structure. It increased linearly with the applied stress and remained at approximately 50% of the value measured in control samples. These results suggest that ECM carries approximately half of the passive load in the chicken flexor digitorum profundus muscle used in this study.

Supplementary material:

This supplementary material provides an explanation for why evaluating Young's modulus as a function of strain rather than stress provides an analysis that is invariant with respect to shifts in the strain at which stress becomes nonzero, such as those that occur with muscle swelling (Sleboda and Roberts, 2017).

A typical plot of muscle's stress-strain response is shown (Figure 3.8A), where stress (σ) is assumed to increase for strain (ε) greater than zero. Swelling has been shown to change the strain at which stress rises above zero, shifting it to a lower value (ε_0) (Sleboda and Roberts, 2017). Assuming that there is only a lateral shift in the stress-strain curve after swelling, the relationship between the stress of the swelled material and the original material is given by:

$$\sigma_{swell} = \sigma(\varepsilon + \varepsilon_0)$$

Instantaneous Young's modulus (E) is calculated by taking the derivative of the stress-strain equation:

$$E = \frac{d\sigma}{d\varepsilon} = \frac{d\sigma(\varepsilon)}{d\varepsilon}$$

which in the case of swelling is:

$$E_{swell} = \frac{d\sigma_{swell}}{d\varepsilon} = \frac{d\sigma(\varepsilon + \varepsilon_0)}{d\varepsilon}$$

It is traditional to evaluate how Young's modulus changes as a function of strain but such analyses are sensitive to swelling-induced changes in where stress begins to rise above zero (Figure 3.8B). Changes in the amount of swelling and therefore the value of ε_0 can make it challenging to compare across samples or treatment groups. These difficulties can be eliminated by evaluating how Young's modulus changes as a function of stress rather than strain (Figure 3.8C). This is because plotting E_{swell} as a function of σ_{swell} is identical to plotting E as a function of σ, as there

is a consistent change of variables ($\varepsilon \rightarrow \varepsilon + \varepsilon_0$) mapping the original to the swelled values of interest.

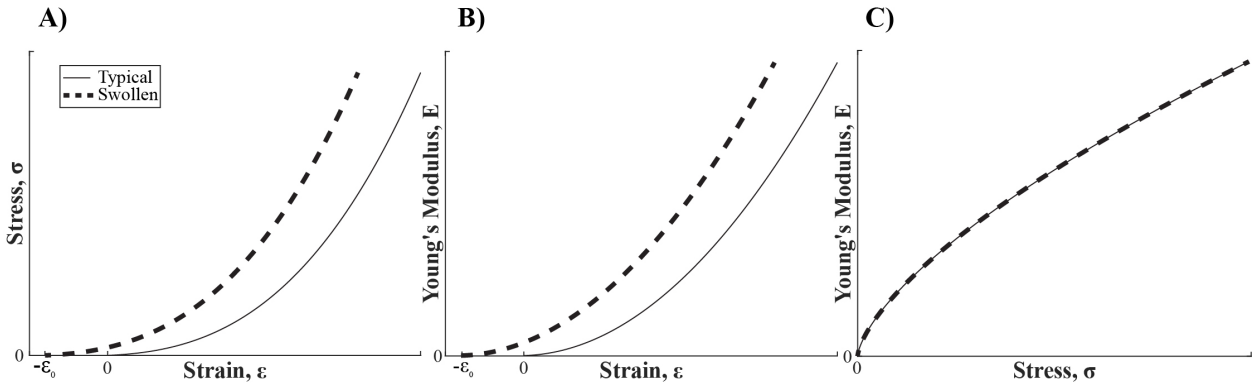

Figure 3.8 Characteristic representation of muscle's A) Stress versus strain, B) Young's modulus versus strain, and C) Young's modulus versus stress response in a typical and swollen state.
Assessment versus stress is invariant to swelling, unlike those that are reliant on strain.

Chapter 4: Influence of muscle's structure on ultrasound shear wave propagation

This work was completed under the mentorship of Eric Perreault, PhD.

This study was funded by the National Institutes of Health (T32HD07418).

Abstract:

There is great potential in the diagnostic value of ultrasound shear wave elastography. In muscle, it has been proposed as a noninvasive quantitative way to measures stiffness. However, muscle's underlying structure, which contributes to the macroscopic properties, complicates how we relate measures from elastography to stiffness and disease. The goal of this review was to describe and discuss how the structure of muscle influences shear wave propagation. The basic assumptions of ultrasound wave propagation in materials, specifically of biological tissue, used to transpose propagation speed to stiffness is summarized. The potential implications of structural arrangement of muscle on shear wave propagation, with an emphasis on resolution and scale, is described. Physical properties of muscle that are thought to be important for shear wave propagation that have not yet been measured are identified. Lastly, the current and future use of phantoms and computational simulations are explored. We found that studies reporting macroscopic stiffness of muscle do not account for muscle's heterogeneous structure. The compositional changes and intricacies of muscle structure are not well understood in the current elastography measures. We propose that quantitative material property measures of muscle's constituents, specifically the extracellular matrix and muscle fibers, and macroscopic properties will facilitate a better understanding of wave propagation, disease identification, muscle-mimicking phantoms, and computation simulation validation. Through further research of general muscle mechanics and simultaneous material property and shear wave measures, we will yield results that will propel the use of SWE into the clinic for musculoskeletal diagnosis.

Introduction

Skeletal muscles are the means by which we move and physically interact with the world on a daily basis. Muscles do this by working in concert with each other to create actions about a joint. The ability of muscles to elongate and compress to complete these tasks is greatly influenced by the mechanical properties of the underlying structure of muscle, specifically the extracellular matrix (ECM) and muscle fibers (Figure 4.1) (Huijing, 1999). Consequently, our muscles' abilities are inhibited by pathological changes to the mechanical properties of the muscle structure, such as changes in stiffness, as we succumb to injuries, aging, or disease (Alnaqeeb et al., 1984; Handorf et al., 2015; Lieber et al., 2003). One in four adults in developed countries report musculoskeletal impairments resulting in a variety of mild to severely debilitating symptoms, including pain, stiffness, and reduced range of motion (White and Harth, 1999; Woolf and Akesson, 2001). These symptoms often result in costly and sometimes ineffective medical care and treatment in our attempt to reduce suffering and disability (Woolf and Pfleger, 2003; Woolf and Akesson, 2001). Clinical evaluations of muscle stiffness-related impairments can be expensive, invasive, and in many cases, not sufficient in detail to identify the specific muscle structures involved in impairment (Simons and Mense, 1998). This lack of specificity unfortunately impedes clinicians' ability to identify, treat, and monitor the structures of muscle responsible for debilitation.

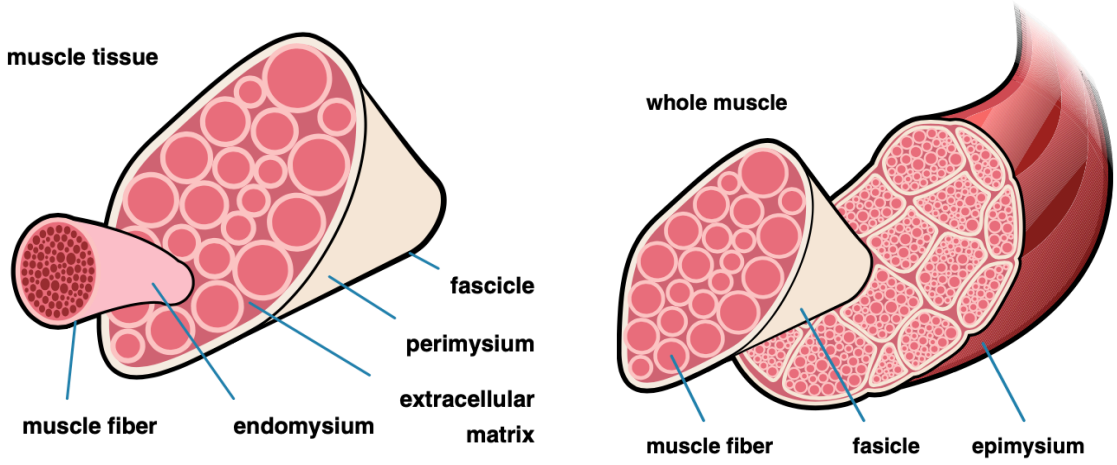

Figure 4.1 Graphic of muscle scaling.
A) Muscle fibers are encapsulated circumferentially by endomysium which form a fascicle. Fascicles are a bundle of muscle fibers and their endomysium which are surrounded by the perimysium. B) Bundles of fascicles are contained within the epimysium to form the whole muscle. The components of the extracellular matrix are: endomysium, perimysium, and epimysium. Images from Wisdom et al. (2015)

Ultrasound shear wave elastography has presented itself as a promising tool that may overcome these clinical hurdles, but few have considered elastography to quantify the mechanics of muscles underlying structure. This noninvasive method induces shear waves in a tissue and measures the speed of propagation. In homogeneous isotropic materials, measures of shear wave speed can be used to estimate Young's modulus (Berg et al., 2012; Cosgrove et al., 2012; Frulio and Trillaud, 2013; Tanter et al., 2008). In muscle, a heterogeneous and transversely isotropic material, changes to the underlying structure that occur as a result of aging or disease, can change the macroscopic properties (Campbell, 1995; Duance et al., 1980; Jones et al., 1983; Klingler et al., 2012; Lieber and Friden, 2019). For example, in patients who exhibit increased muscle stiffness as a result of Duchenne muscular dystrophy, there is an increase in extracellular matrix and intramuscular fat (Duance et al., 1980; Jones et al., 1983; Klingler et al., 2012). Similarly, with human aging we find structural muscle changes, as well as functional changes to the extracellular matrix which can contribute to the degradation of muscle's mechanical properties and increased

stiffness (Kragstrup et al., 2011; Rosant et al., 2007). The macroscopic disease related changes have been correlated to changes in the measured shear wave speed (Lacourpaille et al., 2015; Simon et al., 2016; Zhou et al., 2018). Our ability, however, to perform the inverse clinical analysis is nonexistent, thereby thwarting efforts to diagnose the underlying muscle constituent changes from elastography measures. These obstacles exist in large part because we do not fully understand the effects of muscle structure on shear wave propagation. Some of the important structural components of muscle that influence macroscopic function, and are also likely to influence shear wave propagation, are the muscle fibers and extracellular matrix (ECM). Many studies have made significant progress in developing ultrasound elastography for muscle, yet few have probed the sensitivity of these results to muscle structure. Therefore, the goal of this review is to describe and discuss our current understanding of shear wave propagation in muscle and how muscle structure may influence these measures. This information will aid in our pursuit of understanding the measures of shear wave elastography for the diagnosis of musculoskeletal disease.

This goal will be accomplished by reviewing studies related to four key themes, all focused on helping us understand how the structure of muscle influences shear wave propagation. First, we will review the basic assumptions of ultrasound shear wave propagation in materials, specifically of biological tissue, used to infer stiffness from propagation speed. Second, we will discuss the potential implications of the structural constituents of muscle on shear wave propagation, with an emphasis on resolution and scale. Third, we will identify the physical properties of muscle that are thought to be important for shear wave propagation, and identify those that have not yet been measured. Lastly, we will discuss how phantoms and computational simulations can be used to investigate the effects of structural changes on shear wave propagation. Throughout will be a discussion of previous studies that have used ultrasound elastography in muscle and the influence

of structure on those measures. In the collection of relevant studies, we will discuss the bridge between the underlying structure and shear wave propagation, as well as note the challenges and questions associated with relating shear wave propagation speed to informative measures of muscle. These aspects will inform future researchers and direct focus to propel the use of ultrasound elastography for skeletal muscle diagnostics into the clinic.

Methods

We performed a literature search on 8/5/2020 in PubMed to identify manuscripts relevant to the use of elastography in muscle. Our search terms, including derivations, were mechanical (elastic modulus, stiffness, modulus), skeletal muscle, and elastography (shear wave propagation, elasticity imaging techniques, acoustic microscopy). Four hundred and thirty-six articles were identified from this search (Figure 4.2). Articles were included if they met all of the following criteria: 1) published within 1990 to 2020; 2) used or modeled an elastography technique (ultrasound or magnetic resonance); 3) measured skeletal muscle; 4) provided quantitative measures of material properties; and 5) published in English. Articles were excluded if they 1) were abstracts or non-peer reviewed, or 2) did not report shear wave speed, Young's modulus, or shear modulus. This resulted in one hundred and eighty-two articles that were further categorized into four groups: 1) ultrasound elastography (110 articles); 2) magnetic resonance elastography (40 articles); 3) computational simulations (17 articles); and 4) reviews (15 articles). A majority of these articles were used to formulate this review; some with overlapping concepts were excluded. In addition to these primary sources on muscle elastography, we incorporated some texts and manuscripts describing the fundamental principles of elastography in materials other than muscle (13 articles).

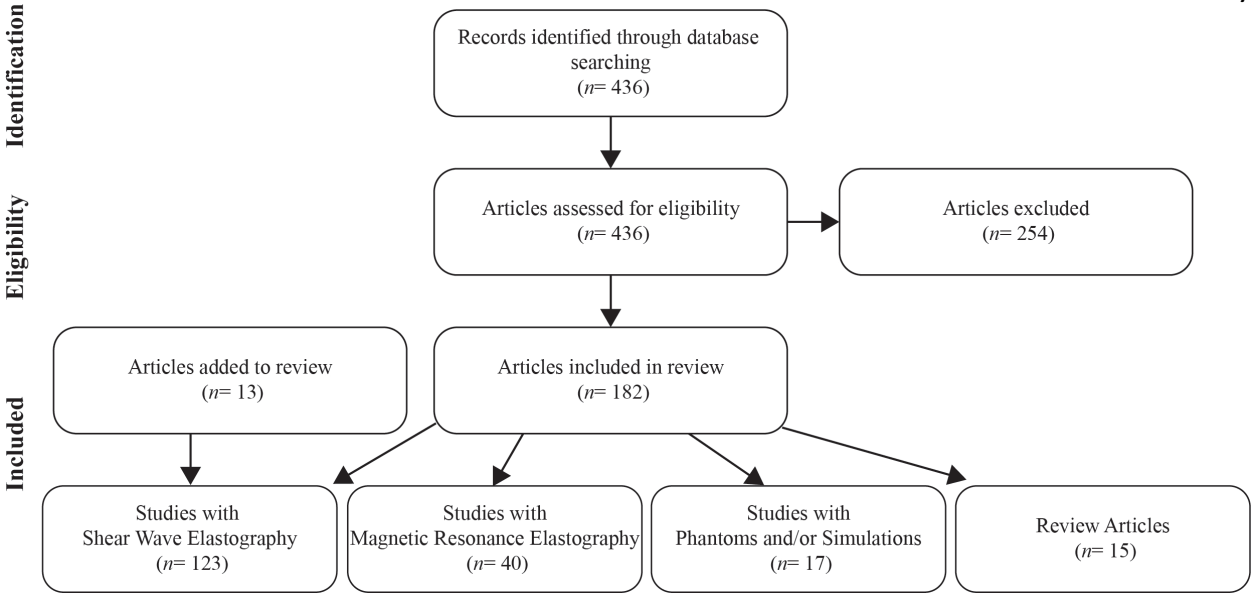

Figure 4.2 Adapted PRISMA diagram.

Ultrasound elastography: assumptions about a material

Elastic Wave Equation Assumptions

Ultrasound shear wave elastography, developed in the 1990's as one potential replacement for palpation, measures the speed of a propagating shear wave in a material to estimate the Young's modulus (O'Donnell et al., 1994; Ophir et al., 1991; Sarvazyan et al., 1995; Yamakoshi et al., 1990). A history of the principles and functions of ultrasound elastography can be found in the review by Gennisson et al. (2013). Briefly, much of what we know about shear wave propagation in biological tissue is based on the elastic equations of wave motion, where shear wave speed (V) is directly linked to shear modulus (μ) and density (ρ) (Eq. 1)(Graff, 1991).

$$V = \sqrt{\mu/\rho} \quad (1)$$

In nearly incompressible (Poisson Ratio (ν) ≈0.5) homogeneous isotropic linear elastic materials, there is a direct relationship between shear and Young's modulus (E) (Eq. 2).

$$E = 2\mu(1+\upsilon) \approx 3\mu \quad (2)$$

An increase in stiffness results in an increase in wave speed, this direct relationship allows measures of shear wave speed to be used to estimate Young's modulus. Clinically, this relationship was used to identify tumors in soft tissue, such as breast and liver, where stiff inclusions in an otherwise soft homogenous material is able to be localized (Figure 4.3)(Cosgrove et al., 2012; Frulio and Trillaud, 2013). These assumptions have often been applied to muscle.

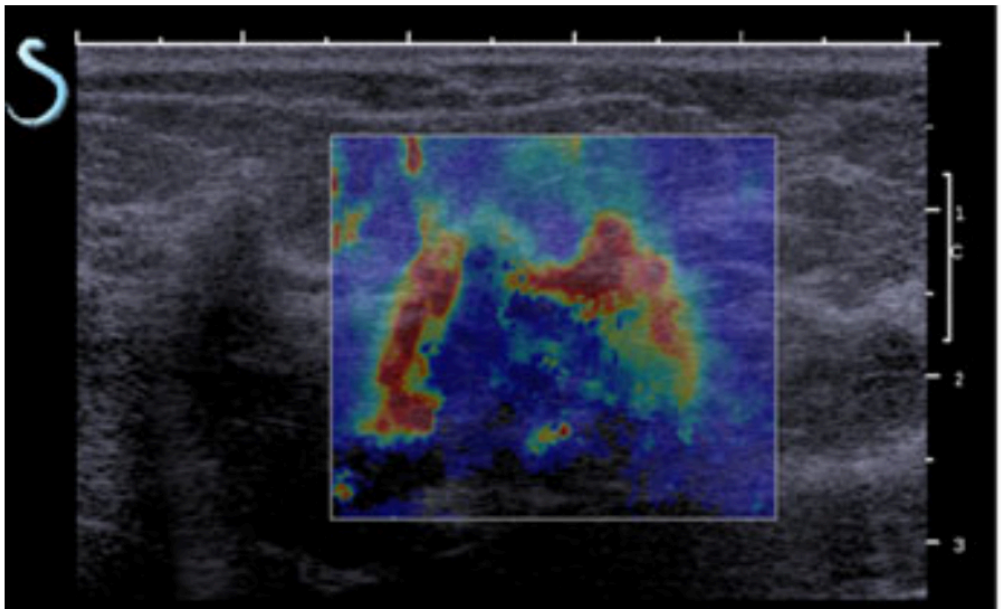

Figure 4.3 Shear wave elastography image of breast cancer with color elasticity map overlay.
Red represents highest stiffness and blue lowest. Image from Cosgrove et al. (2012)

In the case of muscle, which is neither homogeneous nor isotropic, the assumptions of wave propagations used in other soft tissues are not satisfied. Much of the initial elastography work in muscle took similar assumptions from other soft tissues (Bilston and Tan, 2015; Brandenburg et al., 2014; Deffieux et al., 2008; Drakonaki et al., 2012; Gennisson et al., 2010a; Miyamoto et al., 2015). In these studies, muscle is assumed to be homogeneous, isotropic, unstressed, and linear elastic. It has become increasingly evident that these assumptions do not hold, since shear wave velocity measures may be effected by stress (Bernabei et al., 2020; Sandercock et al., 2018),

anisotropy (Gennisson et al., 2003; Gennisson et al., 2010a; Li and Lee, 2017; Qin et al., 2014), and homogeneity (Guidetti and Royston, 2018; Klatt et al., 2010; Magin, 2010; Palnitkar et al., 2019). Despite this evidence, the basic assumptions for muscle which are imposed by the elastic wave equations have persisted over time. Recently, in materials that exhibit axial loads, there has been a new-found interest in the Timoshenko beam model (Graff, 1991; Mei and Mace, 2005) and the inclusion of stress (σ) in the relationship between propagation speed and stiffness (Eq. 3) (Martin et al., 2018).

$$V = \sqrt{\frac{\mu+\sigma}{\rho}} \quad (3)$$

Variations in the Timoshenko beam equation (Eq. 3) can lead to changes in how wave speed approximates Young's modulus. Physiologically, the inclusion of stress is more akin to muscle's *in vivo* state, where it is under passive or active load and rarely truly unstressed, unlike the breast or liver. While it may be beneficial and perhaps more accurate to include stress, measuring the isolated stress on muscle does pose a new technical and device requirement for measurements in the clinic.

Timoshenko Beam Equation Assumptions:

The Timoshenko beam equation assumes a tissue is homogenous, isotropic, and abides by the fundamental laws of continuum mechanics (Graff, 1991). Muscle is not homogeneous. While previous studies have ignored this fact, there remains a large area of doubt in the validity of using elastography to measure muscle stiffness. In continuum mechanics, bulk modulus, shear modulus, Young's modulus, and Poisson ratio are linked with each other; thus, when given any two parameters the other two can be calculated. The Timoshenko beam, as well as much of the

mechanics of the body, fall within fundamental laws of continuum mechanics. However, there are materials that do not obey the laws of continuum mechanics and some of these have properties analogous to muscle. For example, work by van Oosten et al. (2016) on biopolymer networks, which show similarities to muscle's extracellular matrix, would suggest that muscle at a macroscopic level may not abide by continuum mechanic rules. van Oosten and colleagues formed biopolymer networks from intracellular and extracellular proteins to measure the axial and shear stress when subjected to uniaxial and shear strains. In these experiments, it was found that shear and Young's moduli were not proportional, as expected by the rules of continuum mechanics. This experiment also showed a difference in biopolymer network compression versus extension. Unfortunately, van Oosten and colleagues did not determine if this result was due to the composite nature of the material, but did suggest a possible mechanism for compression and extension differences were a result of undulations and buckling of individual fibers, which are similar to the collagen fibers within the ECM (Gillies et al., 2017; Purslow and Trotter, 1994; Trotter and Purslow, 1992). They proposed that it is easier to compress or buckle a fiber, which does not contribute to the stiffness of the network, than it is to remove undulations. Therefore, without more direct measures of muscle we cannot determine if shear and Young's moduli are related in some other way. Perhaps the individual components of muscle structure (ECM and muscle fibers) may act as expected, but collectively produce a complicated mechanical response. ECM is known to be made up of wavy collagen fibers (Gillies et al., 2017) that unequally elongate with strain (Munster et al., 2013; Roeder et al., 2002), with different arrangement depending on scale (endo-, peri-, or epimysium) (Purslow and Trotter, 1994; Trotter and Purslow, 1992). Surprisingly, there is not much work looking at directly measured shear modulus in muscle, which perhaps perpetuated our assumption that Young's and shear moduli were inherently linked. There is also a lack of data

describing how the mechanical properties scale in muscle, which not only inhibits our ability to understand elastography but also muscle stiffness. In summary, given evidence that muscle is not homogenous, isotropic, or unstressed we should be wary of the Young's moduli calculated from shear wave speed using the wave equations or Timoshenko beam model in muscle.

Relevant scale and arrangement of muscle structure

Size of Shear Waves and Resolution

Ultrasound elastography induces micron sized displacements within a tissue, which are thought to be entirely shear in nature (Gennisson et al., 2013; Graff, 1991; Royer and Dieulesaint, 2000). However, muscle being isovolumetric and nearly incompressible, with a Poisson ratio near 0.5 (Takaza et al., 2013a; Van Loocke et al., 2006) cannot have a purely unidirectional deformation. A displacement perpendicular to fibers, like those generated by shear waves, would theoretically require compensatory displacements parallel to fibers. Additionally, the collagen fibers in ECM are not unidirectional organized or distributed (Neuman and Logan, 1950). Some portion of shear wave induced displacement will cause elongation of the ECM. Furthermore, muscle is known to transmit active and passive force through transmembrane protein linkages (Buck and Horwitz, 1987; Friedrichs et al., 2010; Ingber, 2003; Juliano and Haskill, 1993) between ECM and muscle fibers. Therefore, shear forces that deform tissue should be dispersed through the ECM, muscle fibers, and proteins in directions that may lay outside our expected orientation.

The spatial resolution of ultrasound elastography is dependent on vibration frequency and the shear wavelength through a material (Righetti et al., 2002). Experimental results by Zemzemi et al. (2020) showed an axial B-mode imaging resolution between 140 and 50 μm, but elastography resolution was limited by post-processing down to 1/45 of the shear wavelength (400 μm) when a

constant central shear wavelength of 18mm was used. While simulations by Righetti et al. (2002) with a central acoustic wavelength showed that at low frequency (<10MHz) axial resolution could be as high as 600 μm, but at high frequency (>60MHz) the resolution could be 50 μm. This would suggest, depending on measurement parameters, there is some spatial averaging of muscle fibers which can range from 20 to 100 μm in diameter and a up to 12 cm long (Cooper, 2000; Feher, 2017). However, there would remain clear separation between fascicles which are approximately 1 to 10 mm in diameter (Jensen et al., 2004) and the perimysium, the middle layer of ECM, which surrounds fascicles up to approximately 3cm long and 300 μm thick (Passerieux et al., 2006; Passerieux et al., 2007; Sleboda et al., 2020). Therefore, as the resolution is smaller than fascicles and within a few 100 μm of single fibers and ECM thickness it is possible that muscle's underlying structure can influence the travelling dynamics of waves.

Changes to Muscle Constituents

The variation in stiffness between muscle constituents may cause waves to travel faster in one element than they do through the other depending on the state of the muscle (active or passive). Physiologically, we know that changes to muscle stiffness, commonly associated with musculoskeletal impairment, are a result of compositional changes (Handorf et al., 2015). These changes include disturbances to activation dynamics and the loss, or addition, of muscle fibers and/or ECM (Alnaqeeb et al., 1984; Janssen et al., 2000; Kragstrup et al., 2011; Lexell, 1995). For example, post-stroke patients exhibit muscle contracture as a result of muscle fibers activation and subsequent stiffening. The prevalence of musculoskeletal impairments is high with a majority resulting in clinical visits. Unfortunately, current clinical evaluation is limited in specificity, or invasive, which can cause unnecessary damage. The most widely accepted and used technique to

identify changes in stiffness is palpation. Palpation about a joint of suspected impairment gives clinicians a qualitative measure of joint and muscle stiffness. This method is highly reliant on the skill of the clinician and gives only a superficial "view" of muscle with low specificity. Changes to the macroscopic stiffness can be identified using ultrasound shear wave elastography when compared to the non-paretic side, or healthy controls (Figure 4.4) (Jakubowski et al., 2017; Lee et al., 2015; Rasool et al., 2016; Rasool et al., 2018; Wu et al., 2017). However, these comparative studies rely on prior diagnosis, with the current macroscopic measures from ultrasound shear wave elastography we cannot do the inverse and diagnose diseases. Perhaps with the addition of machine learning, and a large dataset in which to compare to, these measures may serve better diagnostic purpose. As categorizing by age, sex, and activity level which have been shown to affect the stiffness of muscle's constituents (Alnaqeeb et al., 1984; Bonnans et al., 2014; Ettema and Huijing, 1994; Grillner, 1972; Howell et al., 1993; Kragstrup et al., 2011; Rosant et al., 2007) will all undoubtedly impact classification. All of these aspects change the macroscopic stiffness, it's in the interpretation of the underlying muscle structure that we gain the ability to specify where the change stems from. Using the phase velocity curves fit to a Voigt model may be a way to separate the components of a tissue (Dai et al., 2015; Qiang et al., 2015; Royston et al., 2011; Sack et al., 2013). In the lung and brain, both of which are heterogeneous tissues like muscle, phase velocity curves were fit with fractional Voigt models to separate the viscous and elastic components of their underlying structure (Dai et al., 2015; Sack et al., 2013). In muscle, a Voigt model from phase velocity was shown to distinguish between active and passive force generation where it was speculated that fibers dominate in the active state and ECM in the passive (Wang et al., 2019). However, this is a new area of research and whether the quantitative parameters from a Voigt model represent the individual mechanical properties of muscle remains to be determined.

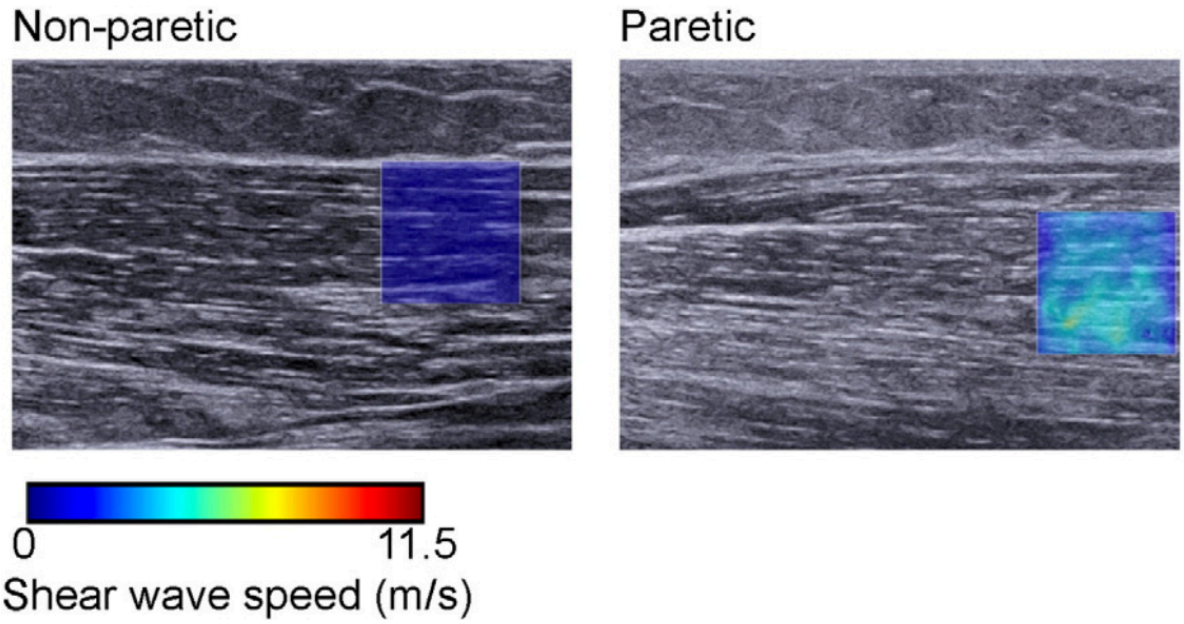

Figure 4.4 Shear wave elastography image of the biceps brachii muscle in a human show differences in shear wave speed between non-paretic and paretic sides.
Non-paretic side shows a slower (mean = 2.5 m/s) shear wave speed than the paretic side (mean = 4.7 m/s). Images from Lee et al. (2015)

Muscle Architecture

Despite muscle being heterogeneous, many studies continue to use the direct relationship between shear wave speed and stiffness derived for homogenous materials (Ballyns et al., 2012; Chan et al., 2012; Chen et al., 2016; Koo and Hug, 2015). These studies typically use shear wave elastography to report total muscle stiffness to correlate disease with changes in measured properties. Of the studies that populated under a search for skeletal muscle elastography, few critically evaluated ultrasound elastography's validity against direct mechanical measures. However, even at the macroscopic scale contradictions to our accepted assumptions about shear wave propagation came up. It was found that muscle's anisotropic material properties significantly affected propagation speed (Aubry et al., 2017; Gennisson et al., 2010a; Li and Cao, 2017) and arrangement of muscle fibers could act as wave guides (Brum et al., 2014; Guidetti et al., 2019;

Palnitkar et al., 2019). It has been proposed that materials with parallel arranged fibers could focus and constrain how waves traversed (Li and Cao, 2017; Romano et al., 2005). It was further speculated that waves travelling parallel with fibers had less damping and scattering than those travelling perpendicular (Ballyns et al., 2012; Palnitkar et al., 2019). In an attempt to simplify the ultrasound elastography technique future studies were recommended to restrict measures to the axis parallel with fibers (Ballyns et al., 2012; Brandenburg et al., 2014). This is a reasonable request, but it is also not entirely achievable. Muscles can vary in architecture. One of the most striking differences can be pennation angle, a measure of fiber orientation with respect to the longitudinal axis of muscle (Gans, 1982). In small, pennate, muscles the ultrasound probe can be larger than the tissue, in which case there will inevitably be some portion of the region of interest that is angled from fibers. This can be compensated by selecting a smaller region of interest, but in doing so decreases the sample size. Unfortunately, there is not a unified method in which to perform shear wave elastography. Therefore, it is worthwhile to further investigate the cause of shear waves' sensitivity to fiber arrangement by implementing faster data acquisition frame rates. Additionally, we should provide a comprehensive method for acquiring reliable measures to facilitate cross-study comparisons.

The difficulty in connecting measures of shear wave propagation speed to meaningful estimates of muscle mechanics, commonly termed the inverse problem, has been hampered by a lack of knowledge about the material properties of muscle. Skeletal muscle is an architecturally complex composite material made up of two primary components, the extracellular matrix (ECM) and muscle fibers. The arrangement of these two produce the characteristic transversely isotropic material properties and mechanics seen at the macroscopic level (Fung, 1993; Gindre et al., 2013; Meyer and Lieber, 2011; Yucesoy et al., 2002). Muscle fibers are arranged in parallel surrounded

by the ECM, growing in scale from single fibers and endomysium, to fiber bundles and perimysium, and finally total muscle and epimysium. These two are connected with transmembrane proteins that assist in force transmission (Elosegui-Artola et al., 2018; Ingber, 2003). Collectively, these give muscle its unique functions and specificity in the line of action it is able to move in. While there is a wealth of knowledge on muscle fibers, there is little direct material property measures of ECM and the transmembrane proteins that connect ECM and fibers together. In recent years, ECM's importance has become a hot topic of discussion, some of which is outlined by the review presented by Gillies and Lieber (2011). However, much of the available work on ECM at the time was done indirectly or based on simulations and consequently remains a serious concern in the ability to translate microscopic to macroscopic mechanical properties. This lack in quantitative knowledge inhibits our ability to solve the inverse problem in elastography because we do not know how the underlying mechanical properties influence shear wave propagation.

Muscle mechanics is further complicated by its loading states, passive and active. Material property recordings can, and have been, done in both passive and active conditions at the whole muscle and single fiber level (Friedman and Goldman, 1996; Fung, 1993; Morrow et al., 2010; Munster et al., 2013; Oberhauser et al., 2002; Rack and Westbury, 1974; Roeder et al., 2002; van Turnhout et al., 2005; Wenger et al., 2007). However, we lack a sufficiently detailed understanding of ECM and transmembrane proteins to determine their contributions to whole muscle mechanics. We know a great deal about ECM's geometry, thanks to the iconic images (Figure 4.5) by Purslow and Trotter (1994) and (1992). These images have been used to inform our perception of fiber attachment and arrangement. However, we know very little about ECM's mechanical properties. This has been primarily due to the difficulty in isolating ECM from the muscle fibers that it

surrounds. Recent work has proposed a method to separate and directly measure ECM (Gillies et al., 2011; Reyna et al., 2020), but there remains much to be learned. In particular, how ECM behaves *in vivo* and at its smaller levels of scale (endo-, peri-, and epimysium). Increasing our understanding of ECM with quantitative material measures could be used in combination with material measures of muscle fibers to determine how these elements impact shear wave propagation. This knowledge would allow us to simulate shear wave propagation through a precisely controlled muscle structure which in turn would lead us to solving the inverse problem. Translating measures of shear wave speed to the individual stiffness of muscle's constituents.

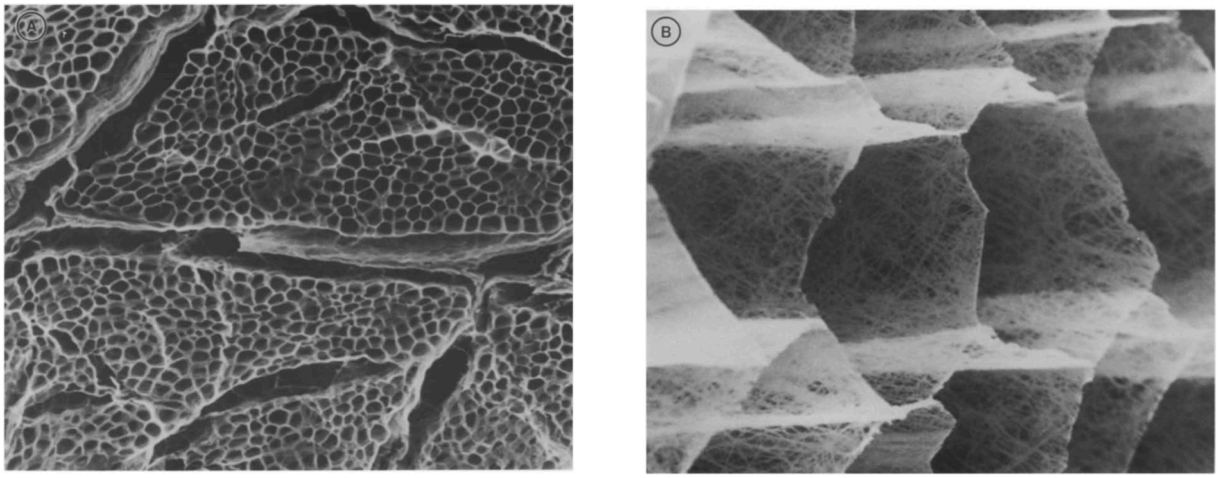

Figure 4.5 Scanning electron micrographs from bovine sternomandibularis muscle after sodium hydroxide digestion of muscle fibers.
A) Low magnification of the collagenous endomysium, within fascicles, and perimysium, separating fascicles, connective tissue. B) High magnification of the endomysium showing the individual collagen fibers. Images from Purslow and Trotter (1994)

Validating elastography with material properties of muscle constituents

As stated previously, much of the work in measuring muscle mechanics has been focused on the muscle fibers, active contraction, or at a scale well below the measurable range of ultrasound shear wave elastography (titin, actin and myosin cross-bridge, etc). It is in our favor to fully understand passive muscle mechanics and the implementation of ultrasound elastography in

passive tissue. This will eliminate confounding factors that may arise from active muscle contraction and give us a basis on which to expand upon. Additionally, direct measures of shear and Young's moduli will give us values in which to compare estimates from elastography against. This premise has been done in active tissue, where direct measures of muscle's short range stiffness, a proxy for Young's modulus, were correlated with shear wave speed (Bernabei et al., 2020; Sandercock et al., 2018). However, this has not been done in passive tissue or while directly measuring shear modulus. The challenge, and perhaps the reason it hasn't been done, is the space required to do so. Short range stiffness can be measured by measuring the force and displacement when anchored to the tendon which does not encroach on the ultrasound probe. This is unlike measuring shear modulus, where an apparatus such as the one used by Morrow et al. (2010) requires attachment to two surfaces on the muscle (Figure 4.6). This may be feasible in excised tissue where anchoring can be done on the planes of interest, but not *in vivo*. Indention probing, similar in design to the cantilever beam used in atomic force microscopy, could give direct measures of shear modulus. However, the speed and scale at which this can be done needs to be established.

Figure 4.6 Testing apparatus, arranged for longitudinal shear, for direct measurement of shear modulus.
Image from Morrow et al. (2010)

Furthermore, towards validating and investigating the sensitivity of shear wave speed to changes in muscle constituents we should collect accurate measures of the shear and Young's moduli of muscle. The muscle fibers, ECM, tendinous aponeurosis, and transmembrane proteins are all at a scale relevant to disease and some are near the current 50 - 600 μm shear wave elastography resolution. Of these components, we know the Young's modulus of muscle fibers (Defranchi et al., 2005; Friedman and Goldman, 1996; Lieber and Friden, 2019; Meyer and Lieber, 2018; Ogneva et al., 2010), tendon (Bennett et al., 1986; Loren and Lieber, 1995), one transmembrane protein (Aaron and Gosline, 1981), and whole muscle ECM (Gillies et al., 2011; Meyer and Lieber, 2011; Reyna et al., 2020). These measures are typically made in line with the tendon, or axis of load, which is physiologically relevant and important to the understanding of normal muscle functions. These longitudinal measures are also useful in formulating how tension on muscle influences the macroscopic mechanics which can be used to inform our measures of shear wave propagation speed. Unfortunately, we lack a measure of shear modulus in whole muscle, in addition to most of the underlying muscle components making comparisons to elastography measures nonexistent and simulations of the propagation dynamics unreliable. Additionally, as stated previously, the continuum mechanics relationships between shear and Young's moduli may not hold in muscle. We need to make big strides in this field to better compare how estimates of shear moduli from ultrasound shear wave elastography stack up to direct measures. This should be followed up by simulations that probe the effects of changing stiffness and composition, in order to elucidate a relationship capable of distinguishing where changes in propagation speed arise from.

Phantoms and Computational simulations of elastography

Phantoms

Phantoms have been used to represent the heterogeneous anisotropic properties of muscle to have control over the minutia of physical properties. Ultrasound phantoms are not a new construct; in fact, they are used in the calibration of ultrasound systems. However, of the 11 studies that have implemented muscle structure-mimicking phantoms in elastography (Ariji et al., 2016; Aubry et al., 2017; Chakouch et al., 2015; Chatelin et al., 2014; Guidetti et al., 2019; Maccabi et al., 2016; Nightingale et al., 2001; Palnitkar et al., 2019; Qin et al., 2013; Ruby et al., 2019; Urban et al., 2015) none have copied the physical scale of muscle constituents or their relevant stiffness properties. This is primarily due to technical limitations. There are two main aspects of a phantom that need to be considered: the first, and perhaps the most important of all, it must be made of a material which can be imaged by ultrasound and the second, is that it must represent the target materials physical properties (transverse isotropy, shear moduli, and Young's moduli). The study by Nightingale et al. (2001) accomplished the first criterion by including additives (graphite) into the base matrix. This additive allowed an otherwise water based matrix to provide reflections back to the ultrasound probe. However, as you change the chemical concentration of additives the stiffness of the material will change. Therefore, care should be taken in balancing the tradeoffs of imaging ease with the targeted material properties. The second criteria, producing a phantom that represents muscle's transverse isotropy with a scale similar to single fibers, was pursued by Guidetti et al. (2019) with the aid of 3D printing (Figure 4.7). Physiologically muscle fibers run unidirectional through muscle. In Guidetti's experiments, the phantom was printed with gelatin fibers 200 μm in diameter embedded into a soft matrix. Unfortunately, due to 3D printing limitations Guidetti and colleagues had to implement a cross pattern to support higher layers. This

meant they no longer were able to satisfy the transverse isotropic arrangement of muscle. Despite this limitation, they were able to generate a phantom with anisotropic properties by imbedding high stiffness fibers into a low stiffness matrix. Unfortunately, they did not take direct measures of the total material stiffness following creation. Thus, it remains to be seen, and should be pursued, if a phantom representing muscle's unique geometric structure and stiffness can be generated and appropriately imaged with ultrasound elastography. Results of course should be verified against the genuine article. Independent measures of muscle fibers exist, as does the method through which ECM can be isolated and measured (Reyna et al., 2020). Researchers should finish the characterization of ECM and continue pursuit of mimicking these materials in phantoms. Phantoms will give us better control of the relative amount and stiffness of muscle's components. This control will provide a basis through which healthy and eventually diseased tissue can be tuned

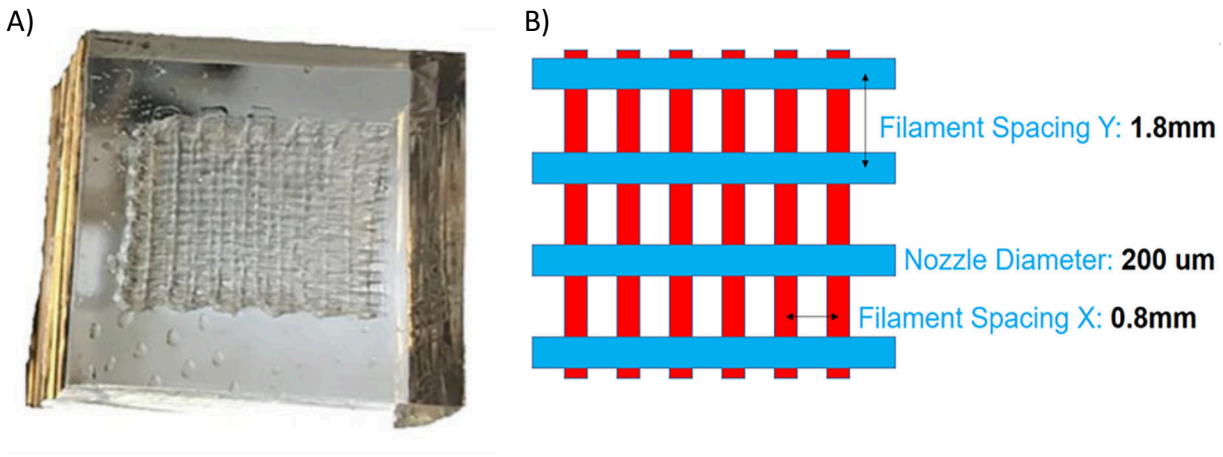

and imaged.

Figure 4.7 Gelatinous 3D printed anisotropic phantom.
A) One representative anisotropic phantom. B) Two layers of the phantom viewed from the top down. Blue filaments sit on the first layer and red filaments sit on the second. Images from Guidetti et al. (2019)

Computational Simulations

Beyond these laboratory experiments exist finite element analysis (FEA), a computational means to evaluating mechanical systems. Many simulations exist that demonstrate the loading attributes of muscle ranging in scale from single fibers (Marcucci et al., 2017; Zhang and Gao, 2012) all the way to strain mapping within whole muscle (Bleiler et al., 2019; Blemker et al., 2005; Gindre et al., 2013; Johansson et al., 2000). Unfortunately, much of these previous studies implemented gross approximations of tissue material properties or find clever ways to avoid them entirely through convoluted relationships. In doing so they avoid the underlying scaling mechanics that describes how muscles structure contributes to the macroscopic properties. Regardless, in many cases these simulations produce a result consistent with strain behavior recorded in laboratory experiments. Although, without well-defined material parameters of the underlying constituents of muscle, we cannot conclude how changes may affect the macroscopic properties or the results of simulations. This is not to say that simulations are not useful, or that these studies failed in some way, but rather without experimental data these results should not be solely used to inform our understanding of muscle's microstructural contributions. How these underlying elements of muscle interact with each other and how much stiffness they contribute remains to be seen.

Using FEA simulations will allow us to exclude confounding factors (activation amount, temperature,…) and control the individual material properties and tension on a material. FEA simulations have been used to simulate shear wave propagation through isotropic and anisotropic materials (Chen et al., 2005; Gennisson et al., 2003; Guidetti et al., 2019; Guidetti and Royston, 2018; Li and Lee, 2017; Palmeri et al., 2005; Palnitkar et al., 2019). For example, the work by Chen et al. (2005) systematically examined the effect of material properties, excitation frequency,

boundary conditions, and applied tension on shear wave propagation through a homogeneous phantom. They found "good agreement" between their simulation and magnetic resonance elastography (MRE) measures, concluding that FEA is capable of simulating shear waves. Work by Guidetti et al. (2019) developed and simulated an anisotropic phantom. They showed that FEA could generate the same elliptical shaped wavefronts seen in experimental measures. Similarly concluding that FEA simulations can provide insight into the proper interpretation of experimental measures of anisotropic materials, like skeletal muscle. Unfortunately for ultrasound shear wave elastography, most of these simulations are focused on MRE where excitation frequency is externally produced and significantly slower (typically below 200Hz; (Glaser et al., 2012)) than in ultrasound. As nearly all of these simulations studies suggest, the FEA simulations can be adapted for ultrasound and other tissues.

Despite varying levels of model complexity, the validity of the approximation is dependent on the material properties used (Bleiler et al., 2019; Blemker et al., 2005; Jenkyn et al., 2002; Johansson et al., 2000). In the case of skeletal muscle, there is a great deal we still lack. As stated previously, we have an incomplete set of material parameters, particularly of non-parallel to fiber measures. It has long been concluded that muscle is transversely isotropic based on geometry at the macroscopic level, but it has only been in the last decade that anyone confirmed this with direct mechanical measures (Morrow et al., 2010). Models can provide, and have provided, a fantastic purpose, but extreme care and vigilance should be taken in the use of material properties. Our simulations are only as good as the parameters we use to make them. As it currently stands, far too many assumptions must be made about muscle's constitutive properties to appropriately simulate shear wave propagation. Despite this reservation, a handful of studies have implemented finite element modeling to investigate the effects of material properties, boundary conditions, and

applied tension on shear wave propagation (Chen et al., 2005; Dao et al., 2014; Deffieux et al., 2012; Guidetti and Royston, 2018). Most simulation studies validate against experimental measures - as they should. However, this validation is not always quantitative or definitive. For example, in the study by Chen et al. (2005), while they validated their simulations against laboratory measures they concluding "good agreement" between the two. In their defense, there are many variables in experimental measures that are ignored in simulations making quantitative validation difficult. Additionally, while some models may be flawed in the selection of material properties, they still conclude, as argued throughout this review, that elastography is not solely a measure of shear modulus. Rather it is a collective measure of many muscular variables. Quantifying the material properties of muscle's constituents, as suggested in the previous section, will yield more properties that will bolster the validity of models. Additionally, with a more detailed model we will be able to better simulate how shear waves displace and traverse the muscle structure.

Summary and Future Directions

There is great clinical significance, and diagnostic value, of developing ultrasound elastography for the evaluation of muscle mechanics. There are hundreds of studies that have outlined the significance of developing this noninvasive tool for monitoring muscle; These include, but are not limited to monitoring, athletic performance (Akkoc et al., 2018; Bailey et al., 2015; Chino et al., 2018; Souron et al., 2019), effects of static stretching (Akagi and Takahashi, 2014; Andrade et al., 2016; Blain et al., 2019; Caliskan et al., 2019; Freitas et al., 2016; Hirata et al., 2017), muscular dystrophy (Lacourpaille et al., 2017; Lacourpaille et al., 2015; Moore et al., 2018; Pichiecchio et al., 2018; Qin et al., 2014), spasticity from cerebral palsy (Bilgici et al., 2018;

Brandenburg et al., 2016; Ceyhan Bilgici et al., 2018; Eby et al., 2017; Mathevon et al., 2018; Vola et al., 2018; Wu and Wang, 2012), pharmacological interventions (Aşkın et al., 2017; Brandenburg et al., 2018; Mathevon et al., 2015; Park and Kwon, 2012), topical therapy (Eriksson Crommert et al., 2015; Ichikawa et al., 2015; Leow et al., 2017), space flight (Parvin et al., 2017), and injury (Howell et al., 1993; Lv et al., 2012; Miyamoto et al., 2018; Zhou et al., 2018). Despite this list of relevant fields of study and the many associated publications, there is disproportionately few on the validity of shear wave measures. Researchers suggest high reliability and repeatability (Adigozali et al., 2017; Brandenburg et al., 2015; Chen et al., 2019; Chino et al., 2012; Dubois et al., 2015; Gao et al., 2020; Goo et al., 2020), which is interpreted as measuring a relatively consistent stiffness across days or operators. Reliability and repeatability, however, does not necessarily indicate accuracy in measuring the true mechanical stiffness value, but simply that measures are precise with respect to each other when only a single testing method and shear wave speed to shear modulus relationship is considered. Therefore, while comparisons to healthy individuals shows significant differences in shear modulus, the numerical Young's moduli values may only be relative.

Our understanding of the mechanical properties of muscle's underlying structure remains incomplete. Determining the contributions and interactions of muscle's constituents are important in not only understanding the dynamics of shear wave propagation but general muscle function. Until recently we did not have a well-defined method for isolating and directly measuring the stiffness of ECM (Reyna et al., 2020). We should leverage this method and continue to separate ECM into its hierarchal structure, as its geometrical arrangement suggests a difference in stiffness between layers. Furthermore, we should investigate how degenerative diseases influence stiffness changes measured via ultrasound elastography with the use of phantoms and simulations. The

remainder of this section provides a summary of the current gaps and future directions researchers should pursue.

We did not find any report of simultaneously measured shear wave speed, Young's modulus, and shear modulus to verify the continuum mechanic assumptions used in muscle. Therefore, it is paramount we reaffirm our basic understanding of shear wave elastography, the property it measures, and the appropriate relationships to use for muscle. This could be done by taking direct material property and shear wave speed measures within the same tissue. The most robust method to accomplish this would be with simultaneous measures. This would alleviate potential environmental or animal discrepancies that could arise from sequentially made measures. With direct measures of Young's and shear modulus in three-dimensions, this type of study would better identify any relationships that may exist between these parameters.

Few studies have controlled some of the major variables of muscle like activation amount, fatigue, tension, temperature, and composition (fat, ECM, or muscle content). Recent work has concluded shear wave speed is influenced by stiffness independent from changes in tension, suggesting that changes to shear wave speed are not unique to one variable of muscle (Bernabei et al., 2020). It is challenging, and nearly impossible, to have control over all aspects of muscle in the laboratory. Scientists have found clever ways, such as using temperature to adjust stiffness independent from tension. It is through this kind of ingenuity we will continue to find ways to have greater control over the variables of muscle in the laboratory. In isolating and controlling these properties we gain a better understanding of the sensitivity of shear wave propagation in muscle and experimental values to validate computational models against.

Attempts to imitate muscle structure through musculoskeletal mimicking phantoms are in their infancy. They are limited in scale and accuracy to material properties. Muscle is a complex

structure, and the scale at which elements arrange is small, making it difficult to physically model. Novel 3D printing techniques have been developed towards the creation of muscle phantoms, but further work needs to be done. We should continue to innovate new ways to emulate the anisotropic properties of muscle with appropriate stiffness properties in both shear and tension; all the while balancing the need to produce an ultrasound image-able object. In doing so, we will have explicit knowledge of the arrangement and properties of the material, making verification of computational models to experimental results easier and more accurate. This control and knowledge will also facilitate solving the inverse problem and potentially finding how measures of shear wave propagation correspond to the underlying structural stiffness and disease.

In the context of ultrasound shear wave propagation, muscle's arrangement, interactions, and physical linkages between structural elements produce the anisotropic properties of muscle. These anisotropic mechanical and compositional properties make use of homogeneous approximations inappropriate, particularly when measuring between major axes. While some of these elements may be below the measureable scale of ultrasound elastography, they remain an important aspect and limiter to the proper understanding of wave propagation. Any changes in these co-dependent structures will result in a macroscopic change in order to best preserve function. It is important to know fundamentally what is happening in muscle to best predict and measure what is occurring with wave propagation. We should quantify the remaining material properties of muscle constituents, specifically the ECM, to obtain a level of detail necessary for 3D modeling. Then, using muscle models we could simulate how waves propagate through muscle along with the effects of changing structural properties.

Conclusion

There is significant diagnostic value in determining the effects of muscle structure and the changes due to impairment of muscle on the propagation of shear waves. We have discussed the implications of structure on our current measurements and use of shear wave elastography in muscle. Muscle is a heterogeneous material made up of components of various physical size with mechanics that change with injury, age, and disease. Without further investigation, how the compositional changes and intricacies of muscle structure influence the macroscopic measures reported by most elastography studies will remain unknown. Measuring, simulating, and controlling the underlying properties of muscle will better inform and improve our ability to calculate diagnostically meaningful properties, such as stiffness, from measures of shear wave propagation. In doing so, we will provide a more robust and accurate way for clinicians to track, manage, and promote rehabilitation in patients with musculoskeletal ailments.

Chapter 5: Concluding Remarks

Summary of Findings and Future Directions

This dissertation quantified the three-dimensional (3D) shear modulus of skeletal muscle, identified a method to isolate the extracellular matrix (ECM), and described the influence of muscle microstructure on shear wave propagation. This work was motivated by a lack of quantitative material properties of muscle that provide a level of detail useful for 3D modeling stresses and strains in muscle. This work provides a vital piece of information needed to model the macroscopic properties of muscle when subject to shearing, like those produced by blunt force trauma. This work also provides a means to further investigate the microscopic properties of muscle structure necessary for more detailed modelling. The results of the three studies presented in this dissertation are summarized here. This is followed by a discussion on the broader implications of this work and future uses of this research.

In Chapter 2 we quantified the shear modulus of muscle in 3D across muscles of differing architecture. The moduli we measured constituted the three primary directions that a transversely isotropic material can be sheared in. On their own, the parameters presented in Chapter 2 can be used to generate the shear portion of the continuum mechanics stiffness matrix. This completed stiffness matrix will allow future researchers to quantify the macroscopic mechanics of muscle when subjected to shear strains or stresses. In combination with the Young's moduli of rat muscle and the Poisson ratio, any 3D deformation can be determined. However, the three directions we measured does assume muscle's internal cross-section is uniform. Muscle fibers are typically idealized and accepted to be cylindrical rods in 3D modelling (Bleiler et al., 2019; Blemker and Delp, 2005; Blemker et al., 2005). However, light micrographs by Sjostrom et al. (1992) show a nonuniform cross-section of both single fibers and fiber bundles. Future work should further probe

muscle's anisotropy. Taking multiple measurements in different directions may show that muscle is more orthotropic than transversely isotropic.

Furthermore, in Chapter 2 we did not find a significant difference in shear modulus between muscles of different architectures. This result could be due to the short life span of a rat (2.5 – 3.5 years) (Sengupta, 2013), which may not provide sufficient time in which they can have changes to muscle architecture and composition. In humans, aging has been shown to affect muscle architecture (Narici et al., 2003; Thom et al., 2007) and composition (Kragstrup et al., 2011; Lexell, 1995; Lexell et al., 1988; Trappe, 2009). These age-related changes have been associated with increased resistance (shear modulus) to passive force transmission (Bemben et al., 1991; Ettema and Huijing, 1994; Huijing, 1999; Lieber and Friden, 2000). Increases to the shear modulus with aging muscle may be a coping mechanism that is used to provide greater resistance to injury causing shear loads (Kjaer, 2004). Rats short life span may not provide the time needed to see a significant effect. Taking shear moduli measurements across a variety of species and muscles may identify species-specific differences.

In Chapter 3 we critically evaluated and established a method for isolating skeletal muscle ECM. We found that using latrunculin B and osmotic shock was the most efficient method of the three we tested. Isolating skeletal muscle ECM posed a unique problem that typical transplantation decellularization methods did not cover. In transplantation research, scientist commonly use decellularization to remove cellular DNA from an organ (Badylak et al., 2011; Caralt et al., 2015; Crapo et al., 2011; Gilbert et al., 2006). However, isolating skeletal muscle ECM for mechanical testing more importantly required removing the contractile component of muscle. We determined that latrunculin B was superior for muscle specific decellularization. It preserved the collagen content of ECM while simultaneously removing a majority of the actin, myosin, and DNA content

of muscle cells. Using this method, future researchers can isolate and quantify the 3D material properties of whole muscle ECM in tension and shear. Additionally, this decellularization method is a gateway to isolating the hierarchical structure of ECM for analysis. The ECM is composed of three parts: the endomysium, perimysium, and epimysium (Purslow and Trotter, 1994; Trotter and Purslow, 1992). These structures of ECM have their own collagen fiber arrangement that could show differences in material properties (Purslow, 2002; Purslow and Trotter, 1994). Quantification of the material properties of ECM's layers in 3D by future researchers would be instrumental to our understanding of muscle structure. With these measures, we open up a new level of muscle modelling detail that could be used to determine the microscopic to macroscopic scaling of muscle mechanics.

In Chapter 4 we discuss the implications of muscle's structure on obtaining diagnostically useful measures from ultrasound shear wave elastography (SWE). We found a large body of work exists in which researchers have used SWE as their primary method of measuring the Young's modulus of muscle. However, there is a lack of validation studies comparing SWE measures against direct measures of shear and Young's modulus. In Chapter 2, we found similarities between direct and SWE measured shear modulus of passive non-tensioned tissue. The similarity with directly measured values provides confidence in some of the macroscopic measures from SWE, but under active or loaded conditions there still remains uncertainty in the macroscopic stiffness measures obtained from SWE. There is even less confidence in the measure of microstructure and disease diagnosis by SWE. We found a number of publications showed a difference in stiffness between healthy controls and impaired subjects. Unfortunately, the macroscopic stiffness reported does not provide much use in the diagnosis of specific ailments, as it does not identify the source of underlying structural changes. Disease and age can influence the

force generation, transmission, and subsequently stiffness through changes in muscle composition (Gillies and Lieber, 2011; Narici et al., 2003). These unique changes in composition have been associated with nonunique macroscopic stiffness changes (Gans, 1982; Lieber and Friden, 2019). These nonunique changes makes the macroscopic stiffness reported by SWE studies unspecific to the disease or the underlying structures. Without knowing how shear wave propagation can be decomposed into measures of microscopic stiffness, we cannot identify a specific ailment.

With 3D modeling of muscle microstructure, we can begin to better understand shear wave propagation through muscle. Unfortunately, we currently lack the quantitative material properties of ECM's shear and Young's modulus to accomplish this task. Using the decellularization method outlined in Chapter 3, we could make these material property measures. Once isolated, ECM could be dissected into its hierarchical structure (endo-, peri-, and epimysium) providing further insight into muscle microstructural mechanics. Combing these material properties with those reported for muscle fibers (Bensamoun et al., 2006; Meyer and Lieber, 2018; Meyer and Lieber, 2011; Toursel et al., 2002) we could simulate shear wave propagation at a scale on par with the resolution of the SWE (Zemzemi et al., 2020). These simulations would allow us to see the travelling dynamics of shear waves and potentially the decomposition of these measures into the individual muscle constituent stiffnesses.

Broader Implications and Uses

This work makes significant contributions to our understanding of muscle mechanics by providing material properties that can be used to gain better insight into muscle function, impairments, and SWE. We quantified the three-dimensional shear moduli of muscle which can have direct applications in the design of muscle models. Prior models were limited to longitudinal

measured material properties of Young's modulus; we now have the capability to model shear deformations with the inclusion of the shear moduli we measured. Researchers have previously speculated the importance of force transmission in shear (Huijing, 1999). Using our measures, computational simulations can determine how shearing forces propagate through muscle in 3D. These quantitative properties further open the way to investigate the mechanics of injury and passive loading in muscle.

In Chapter 3, we showed a decellularization method capable of isolating ECM for direct mechanical testing. This work bolstered the argument that ECM is a major contributor of passive muscle's Young's modulus (Lieber and Friden, 2019) by showing ~50% of the passive stiffness remained after isolation of the ECM. Using the decellularization method from Chapter 3 will allow us to further investigate the mechanics of ECM independently from muscle fibers. We measured the Young's modulus of ECM in one direction. Future work can directly test and quantify the shear and Young's moduli of the ECM in 3D. The increased level of muscle detail we can achieve with decellularization will facilitate microstructural modeling. This model will also allow characterization of how changes to microstructure, as a result of disease, influences the macrostructural function of muscle.

We also showed evidence that measures of stiffness from SWE are flawed in their current ability to provide quantitative information about the microstructure that is disease specific. Using SWE to target Young's modulus, the measure of interest (Brandenburg et al., 2014; Drakonaki et al., 2012), at a macroscopic and microscopic scale will require more work. The homogeneous assumption we use in muscle to relate shear wave propagation, shear modulus, and Young's modulus is incorrect. Muscle's directionally specific microstructure disproves this assumption (Gans, 1982; Gillies and Lieber, 2011; Lieber and Lieber, 2002). Simultaneous measures of

material properties and shear wave speed will further inform our understanding of their true relationship in muscle. Furthermore, leveraging previous work on muscle fibers and the decellularization method described in this dissertation to measure the material properties of muscle ECM in 3D we can better model how shear waves propagate through the microstructure. These models could possibly relate the measures of shear wave propagation to changes in microstructural stiffness and disease, bringing us one step closer to providing people with quicker diagnosis and, through targeted rehabilitation, a better quality of life.

Remaining Questions

With this dissertation, we scratched the surface of a very large field of study. Our measurements have advanced our understanding of muscle and provided evidence for a technique to isolate muscle's ECM. This work also, as expected, motivates and opens the way to further discovery. The larger logical next steps and questions, some of which are detailed within the chapters of this dissertation, from this work are:

> In non-rodent species, is the shear modulus between architecturally different muscles different? If so, does this difference stem from differences in life style (e.g. activity, injury, …) or life span? With the inclusion of shear modulus in muscle models, do we have a more accurate representation of muscle deformation? Can we use it to determine the dynamics of muscle when subjected to passive loads? Using the decellularization method identified in Chapter 3, what are the 3D shear and Young's moduli of muscle ECM? Are there material property differences between the layers of ECM? With measures of ECM and computational models, how is force transmitted between single fibers and ECM? Simulating shear wave propagation

through a detailed model of muscle, do the differences in microstructure stiffness influence waves? Is there a relationship between changes in ECM or fiber stiffness that are reflected in the measures of shear wave propagation? Using the information from simulations, can we take measures from SWE experiments and predict the corresponding microstructural stiffness and associated disease?

While these are but a few of the remaining questions left to answer, the work completed and presented here have provided a means for assessing the material properties of muscle and its constituents – novel information that promotes future investigation of muscle ECM and 3D musculoskeletal modeling. With this work, we are one step closer to fully understanding skeletal muscle.

References

Aaron, B.B., Gosline, J.M., 1981. Elastin as a random-network elastomer: A mechanical and optical analysis of single elastin fibers. Biopolymers 20, 1247-1260.

Adigozali, H., Shadmehr, A., Ebrahimi, E., Rezasoltani, A., Naderi, F., 2017. Reliability of assessment of upper trapezius morphology, its mechanical properties and blood flow in female patients with myofascial pain syndrome using ultrasonography. J Bodyw Mov Ther 21, 35-40.

Ahn, S.J., Costa, J., Emanuel, J.R., 1996. PicoGreen quantitation of DNA: effective evaluation of samples pre- or post-PCR. Nucleic Acids Res 24, 2623-2625.

Aimedieu, P., Mitton, D., Faure, J.P., Denninger, L., Lavaste, F., 2003. Dynamic stiffness and damping of porcine muscle specimens. Medical Engineering & Physics 25, 795-799.

Akagi, R., Takahashi, H., 2014. Effect of a 5-week static stretching program on hardness of the gastrocnemius muscle. Scand J Med Sci Sports 24, 950-957.

Akkoc, O., Caliskan, E., Bayramoglu, Z., 2018. Effects of passive muscle stiffness measured by Shear Wave Elastography, muscle thickness, and body mass index on athletic performance in adolescent female basketball players. Med Ultrason 20, 170-176.

Aldridge, G.M., Podrebarac, D.M., Greenough, W.T., Weiler, I.J., 2008. The use of total protein stains as loading controls: an alternative to high-abundance single-protein controls in semi-quantitative immunoblotting. J Neurosci Methods 172, 250-254.

Alnaqeeb, M.A., Al Zaid, N.S., Goldspink, G., 1984. Connective tissue changes and physical properties of developing and ageing skeletal muscle. Journal of anatomy 139, 677-689.

Andrade, R.J., Lacourpaille, L., Freitas, S.R., McNair, P.J., Nordez, A., 2016. Effects of hip and head position on ankle range of motion, ankle passive torque, and passive gastrocnemius tension. Scand J Med Sci Sports 26, 41-47.

Ansari, D.M.D.F.A., 2019. Assessment of Chronic Musculoskeletal Pain Management in Elderly Patient at General Hospital in Patna City, India. Journal of Medical Science And clinical Research 7.

Ariji, Y., Nakayama, M., Nishiyama, W., Nozawa, M., Ariji, E., 2016. Shear-wave sonoelastography for assessing masseter muscle hardness in comparison with strain sonoelastography: study with phantoms and healthy volunteers. Dentomaxillofac Radiol 45, 20150251.

Aşkın, A., Kalaycı Ö, T., Bayram, K.B., Tosun, A., Demirdal Ü, S., Atar, E., İnci, M.F., 2017. Strain sonoelastographic evaluation of biceps muscle intrinsic stiffness after botulinum toxin-A injection. Top Stroke Rehabil 24, 12-17.

Aubry, S., Nueffer, J.P., Carrié, M., 2017. Evaluation of the Effect of an Anisotropic Medium on Shear Wave Velocities of Intra-Muscular Gelatinous Inclusions. Ultrasound Med Biol 43, 301-308.

Badylak, S.F., Taylor, D., Uygun, K., 2011. Whole-organ tissue engineering: decellularization and recellularization of three-dimensional matrix scaffolds. Annual review of biomedical engineering 13, 27-53.

Bailey, L.B., Shanley, E., Hawkins, R., Beattie, P.F., Fritz, S., Kwartowitz, D., Thigpen, C.A., 2015. Mechanisms of Shoulder Range of Motion Deficits in Asymptomatic Baseball Players. Am J Sports Med 43, 2783-2793.

Ballyns, J.J., Turo, D., Otto, P., Shah, J.P., Hammond, J., Gebreab, T., Gerber, L.H., Sikdar, S., 2012. Office-based elastographic technique for quantifying mechanical properties of skeletal muscle. J Ultrasound Med 31, 1209-1219.

Bemben, M.G., Massey, B.H., Bemben, D.A., Misner, J.E., Boileau, R.A., 1991. Isometric muscle force production as a function of age in healthy 20- to 74-yr-old men. Med Sci Sports Exerc 23, 1302-1310.

Bennett, M.B., Ker, R.F., Imery, N.J., Alexander, R.M., 1986. Mechanical properties of various mammalian tendons. Journal of Zoology 209, 537-548.

Bensamoun, S., Stevens, L., Fleury, M.J., Bellon, G., Goubel, F., Ho Ba Tho, M.C., 2006. Macroscopic-microscopic characterization of the passive mechanical properties in rat soleus muscle. J Biomech 39, 568-578.

Bercoff, J., Tanter, M., Fink, M., 2004. Supersonic shear imaging: a new technique for soft tissue elasticity mapping. IEEE Transactions on Ultrasonics, Ferroelectrics and Frequency Control 51, 396-409.

Berg, W.A., Cosgrove, D.O., Doré, C.J., Schäfer, F.K.W., Svensson, W.E., Hooley, R.J., Ohlinger, R., Mendelson, E.B., Balu-Maestro, C., Locatelli, M., Tourasse, C., Cavanaugh, B.C., Juhan, V., Stavros, A.T., Tardivon, A., Gay, J., Henry, J.-p., Cohen-Bacrie, C., Investigators, B., 2012. Shear-wave elastography improves the specificity of breast US: the BE1 multinational study of 939 masses. Radiology 262, 435-449.

Bernabei, M., Lee, S.S.M., Perreault, E.J., Sandercock, T.G., 2020. Shear wave velocity is sensitive to changes in muscle stiffness that occur independently from changes in force. J Appl Physiol (1985) 128, 8-16.

Best, T.M., 1997. Soft-Tissue Injuries and Muscle Tears. Clinics in Sports Medicine 16, 419-434.

Bilgici, M.C., Bekci, T., Ulus, Y., Ozyurek, H., Aydin, O.F., Tomak, L., Selcuk, M.B., 2018. Quantitative assessment of muscular stiffness in children with cerebral palsy using acoustic radiation force impulse (ARFI) ultrasound elastography. J Med Ultrason (2001) 45, 295-300.

Bilston, L.E., Tan, K., 2015. Measurement of passive skeletal muscle mechanical properties in vivo: recent progress, clinical applications, and remaining challenges. Ann Biomed Eng 43, 261-273.

Blain, M., Bedretdinova, D., Bellin, M.F., Rocher, L., Gagey, O., Soubeyrand, M., Creze, M., 2019. Influence of thoracolumbar fascia stretching on lumbar back muscle stiffness: A supersonic shear wave elastography approach. Clin Anat 32, 73-80.

Bleiler, C., Ponte Castaneda, P., Rohrle, O., 2019. A microstructurally-based, multi-scale, continuum-mechanical model for the passive behaviour of skeletal muscle tissue. J Mech Behav Biomed Mater 97, 171-186.

Blemker, S.S., Delp, S.L., 2005. Three-dimensional representation of complex muscle architectures and geometries. Ann Biomed Eng 33, 661-673.

Blemker, S.S., Pinsky, P.M., Delp, S.L., 2005. A 3D model of muscle reveals the causes of nonuniform strains in the biceps brachii. Journal of Biomechanics 38, 657-665.

Bonnans, C., Chou, J., Werb, Z., 2014. Remodelling the extracellular matrix in development and disease. Nat Rev Mol Cell Biol 15, 786-801.

Bosboom, E.M.H., Hesselink, M.K.C., Oomens, C.W.J., Bouten, C.V.C., Drost, M.R., Baaijens, F.P.T., 2001. Passive transverse mechanical properties of skeletal muscle under in vivo compression. Journal of Biomechanics 34, 1365-1368.

Brandenburg, J.E., Eby, S.F., Song, P., Bamlet, W.R., Sieck, G.C., An, K.N., 2018. Quantifying Effect of Onabotulinum Toxin A on Passive Muscle Stiffness in Children with Cerebral Palsy Using Ultrasound Shear Wave Elastography. Am J Phys Med Rehabil 97, 500-506.

Brandenburg, J.E., Eby, S.F., Song, P., Kingsley-Berg, S., Bamlet, W., Sieck, G.C., An, K.N., 2016. Quantifying passive muscle stiffness in children with and without cerebral palsy using ultrasound shear wave elastography. Dev Med Child Neurol 58, 1288-1294.

Brandenburg, J.E., Eby, S.F., Song, P., Zhao, H., Brault, J.S., Chen, S., An, K.N., 2014. Ultrasound elastography: the new frontier in direct measurement of muscle stiffness. Arch Phys Med Rehabil 95, 2207-2219.

Brandenburg, J.E., Eby, S.F., Song, P., Zhao, H., Landry, B.W., Kingsley-Berg, S., Bamlet, W.R., Chen, S., Sieck, G.C., An, K.N., 2015. Feasibility and reliability of quantifying passive muscle stiffness in young children by using shear wave ultrasound elastography. J Ultrasound Med 34, 663-670.

Breuls, R.G., Jiya, T.U., Smit, T.H., 2008. Scaffold stiffness influences cell behavior: opportunities for skeletal tissue engineering. Open Orthop J 2, 103-109.

Brooks, S.V., Faulkner, J.A., 1994. Skeletal muscle weakness in old age: underlying mechanisms. Med Sci Sports Exerc 26, 432-439.

Brozovich, F.V., Yates, L.D., Gordon, A.M., 1988. Muscle force and stiffness during activation and relaxation. Implications for the actomyosin ATPase. J Gen Physiol 91, 399-420.

Brum, J., Bernal, M., Gennisson, J.L., Tanter, M., 2014. In vivo evaluation of the elastic anisotropy of the human Achilles tendon using shear wave dispersion analysis. Phys Med Biol 59, 505-523.

Brynnel, A., Hernandez, Y., Kiss, B., Lindqvist, J., Adler, M., Kolb, J., van der Pijl, R., Gohlke, J., Strom, J., Smith, J., Ottenheijm, C., Granzier, H.L., 2018. Downsizing the molecular spring of the giant protein titin reveals that skeletal muscle titin determines passive stiffness and drives longitudinal hypertrophy. Elife 7.

Buchthal, F., Schmalbruch, H., 1980. Motor unit of mammalian muscle. Physiol Rev 60, 90-142.

Buck, C.A., Horwitz, A.F., 1987. Cell surface receptors for extracellular matrix molecules. Annu Rev Cell Biol 3, 179-205.

Burkholder, T.J., Fingado, B., Baron, S., Lieber, R.L., 1994. Relationship between Muscle-Fiber Types and Sizes and Muscle Architectural Properties in the Mouse Hindlimb. Journal of Morphology 221, 177-190.

Caliskan, E., Akkoc, O., Bayramoglu, Z., Gozubuyuk, O.B., Kural, D., Azamat, S., Adaletli, I., 2019. Effects of static stretching duration on muscle stiffness and blood flow in the rectus femoris in adolescents. Med Ultrason 21, 136-143.

Campbell, K.P., 1995. Three muscular dystrophies: loss of cytoskeleton-extracellular matrix linkage. Cell 80, 675-679.

Caralt, M., Uzarski, J.S., Iacob, S., Obergfell, K.P., Berg, N., Bijonowski, B.M., Kiefer, K.M., Ward, H.H., Wandinger-Ness, A., Miller, W.M., Zhang, Z.J., Abecassis, M.M., Wertheim, J.A., 2015. Optimization and critical evaluation of decellularization strategies to develop renal extracellular matrix scaffolds as biological templates for organ engineering and transplantation. American journal of transplantation : official journal of the American Society of Transplantation and the American Society of Transplant Surgeons 15, 64-75.

Ceyhan Bilgici, M., Bekci, T., Ulus, Y., Bilgici, A., Tomak, L., Selcuk, M.B., 2018. Quantitative assessment of muscle stiffness with acoustic radiation force impulse elastography after botulinum toxin A injection in children with cerebral palsy. J Med Ultrason (2001) 45, 137-141.

Chakouch, M.K., Charleux, F., Bensamoun, S.F., 2015. Development of a phantom mimicking the functional and structural behaviors of the thigh muscles characterized with magnetic resonance elastography technique. Conf Proc IEEE Eng Med Biol Soc 2015, 6736-6739.

Chan, S.T., Fung, P.K., Ng, N.Y., Ngan, T.L., Chong, M.Y., Tang, C.N., He, J.F., Zheng, Y.P., 2012. Dynamic changes of elasticity, cross-sectional area, and fat infiltration of multifidus at different postures in men with chronic low back pain. Spine J 12, 381-388.

Chatelin, S., Bernal, M., Deffieux, T., Papadacci, C., Flaud, P., Nahas, A., Boccara, C., Gennisson, J.L., Tanter, M., Pernot, M., 2014. Anisotropic polyvinyl alcohol hydrogel phantom for shear wave elastography in fibrous biological soft tissue: a multimodality characterization. Phys Med Biol 59, 6923-6940.

Chen, D.T., Wen, Q., Janmey, P., Crocker, J.C., Yodh, A.G., 2010. Rheology of Soft Materials. Annual Review of Condensed Matter Physics 1, 301-322.

Chen, G., Wu, J., Chen, G., Lu, Y., Ren, W., Xu, W., Xu, X., Wu, Z., Guan, Y., Zheng, Y., Qiu, B., 2019. Reliability of a portable device for quantifying tone and stiffness of quadriceps femoris and patellar tendon at different knee flexion angles. PLoS One 14, e0220521.

Chen, Q., Ringleb, S.I., Manduca, A., Ehman, R.L., An, K.N., 2005. A finite element model for analyzing shear wave propagation observed in magnetic resonance elastography. J Biomech 38, 2198-2203.

Chen, Q., Wang, H.J., Gay, R.E., Thompson, J.M., Manduca, A., An, K.N., Ehman, R.E., Basford, J.R., 2016. Quantification of Myofascial Taut Bands. Arch Phys Med Rehabil 97, 67-73.

Chino, K., Akagi, R., Dohi, M., Fukashiro, S., Takahashi, H., 2012. Reliability and validity of quantifying absolute muscle hardness using ultrasound elastography. PLoS One 7, e45764.

Chino, K., Ohya, T., Kato, E., Suzuki, Y., 2018. Muscle Thickness and Passive Muscle Stiffness in Elite Athletes: Implications of the Effect of Long-Term Daily Training on Skeletal Muscle. Int J Sports Med 39, 218-224.

Chotard-Ghodsnia, R., Verdier, C., 2007. Rheology of living materials, Modeling of biological materials. Modeling and simulation in science, engineering and technology, Birkhauser, pp. 1-31.

Cooper, 2000. The Cell: A Molecular Approach. Sinauer Associates.

Cosgrove, D.O., Berg, W.A., Dore, C.J., Skyba, D.M., Henry, J.P., Gay, J., Cohen-Bacrie, C., Group, B.E.S., 2012. Shear wave elastography for breast masses is highly reproducible. Eur Radiol 22, 1023-1032.

Crapo, P.M., Gilbert, T.W., Badylak, S.F., 2011. An overview of tissue and whole organ decellularization processes. Biomaterials 32, 3233-3243.

Dai, Z., Peng, Y., Mansy, H.A., Sandler, R.H., Royston, T.J., 2015. A model of lung parenchyma stress relaxation using fractional viscoelasticity. Med Eng Phys 37, 752-758.

Dao, T.T., Pouletaut, P., Charleux, F., Tho, M.C., Bensamoun, S., 2014. Analysis of shear wave propagation derived from MR elastography in 3D thigh skeletal muscle using subject specific finite element model. Conf Proc IEEE Eng Med Biol Soc 2014, 4026-4029.

Deffieux, T., Gennisson, J.L., Larrat, B., Fink, M., Tanter, M., 2012. The variance of quantitative estimates in shear wave imaging: theory and experiments. IEEE Trans Ultrason Ferroelectr Freq Control 59, 2390-2410.

Deffieux, T., Gennisson, J.L., Tanter, M., Fink, M., 2008. Assessment of the mechanical properties of the musculoskeletal system using 2-D and 3-D very high frame rate ultrasound. IEEE Trans Ultrason Ferroelectr Freq Control 55, 2177-2190.

Defranchi, E., Bonaccurso, E., Tedesco, M., Canato, M., Pavan, E., Raiteri, R., Reggiani, C., 2005. Imaging and elasticity measurements of the sarcolemma of fully differentiated skeletal muscle fibres. Microsc Res Tech 67, 27-35.

Donahue, T.L., Gregersen, C., Hull, M.L., Howell, S.M., 2001. Comparison of viscoelastic, structural, and material properties of double-looped anterior cruciate ligament grafts made from bovine digital extensor and human hamstring tendons. J Biomech Eng 123, 162-169.

Drakonaki, E.E., Allen, G.M., Wilson, D.J., 2012. Ultrasound elastography for musculoskeletal applications. Br J Radiol 85, 1435-1445.

Duance, V.C., Stephens, H.R., Dunn, M., Bailey, A.J., Dubowitz, V., 1980. A role for collagen in the pathogenesis of muscular dystrophy? Nature 284, 470-472.

Dubois, G., Kheireddine, W., Vergari, C., Bonneau, D., Thoreux, P., Rouch, P., Tanter, M., Gennisson, J.L., Skalli, W., 2015. Reliable protocol for shear wave elastography of lower limb muscles at rest and during passive stretching. Ultrasound Med Biol 41, 2284-2291.

Eby, S.F., Song, P., Chen, S., Chen, Q., Greenleaf, J.F., An, K.N., 2013. Validation of shear wave elastography in skeletal muscle. J Biomech 46, 2381-2387.

Eby, S.F., Zhao, H., Song, P., Vareberg, B.J., Kinnick, R.R., Greenleaf, J.F., An, K.N., Brown, A.W., Chen, S., 2017. Quantifying spasticity in individual muscles using shear wave elastography. Radiol Case Rep 12, 348-352.

Edwards, C.A., O'Brien, W.D., Jr., 1980. Modified assay for determination of hydroxyproline in a tissue hydrolyzate. Clin Chim Acta 104, 161-167.

Elosegui-Artola, A., Trepat, X., Roca-Cusachs, P., 2018. Control of Mechanotransduction by Molecular Clutch Dynamics. Trends in Cell Biology 28, 356-367.

Eng, C.M., Smallwood, L.H., Rainiero, M.P., Lahey, M., Ward, S.R., Lieber, R.L., 2008. Scaling of muscle architecture and fiber types in the rat hindlimb. J Exp Biol 211, 2336-2345.

Eriksson Crommert, M., Lacourpaille, L., Heales, L.J., Tucker, K., Hug, F., 2015. Massage induces an immediate, albeit short-term, reduction in muscle stiffness. Scand J Med Sci Sports 25, e490-496.

Ettema, G.J.C., Huijing, P.A., 1994. Skeletal muscle stiffness in static and dynamic contractions. Journal of Biomechanics 27, 1361-1368.

Feher, J.J., 2017. Quantitative human physiology : an introduction, Second edition. ed. Elsevier/AP, Academic Press is an imprint of Elsevier, Amsterdam ; Boston.

Fomovsky, G.M., Thomopoulos, S., Holmes, J.W., 2010. Contribution of extracellular matrix to the mechanical properties of the heart. J Mol Cell Cardiol 48, 490-496.

Fox, C.H., Johnson, F.B., Whiting, J., Roller, P.P., 1985. Formaldehyde fixation. J Histochem Cytochem 33, 845-853.

Fratzl, P., Misof, K., Zizak, I., Rapp, G., Amenitsch, H., Bernstorff, S., 1998. Fibrillar structure and mechanical properties of collagen. J Struct Biol 122, 119-122.

Freitas, S.R., Andrade, R.J., Nordez, A., Mendes, B., Mil-Homens, P., 2016. Acute muscle and joint mechanical responses following a high-intensity stretching protocol. Eur J Appl Physiol 116, 1519-1526.

Friedman, A.L., Goldman, Y.E., 1996. Mechanical characterization of skeletal muscle myofibrils. Biophys J 71, 2774-2785.

Friedrichs, J., Helenius, J., Muller, D.J., 2010. Quantifying cellular adhesion to extracellular matrix components by single-cell force spectroscopy. Nat Protoc 5, 1353-1361.

Frontera, W.R., Reid, K.F., Phillips, E.M., Krivickas, L.S., Hughes, V.A., Roubenoff, R., Fielding, R.A., 2008. Muscle fiber size and function in elderly humans: a longitudinal study. Journal of applied physiology (Bethesda, Md. : 1985) 105, 637-642.

Frulio, N., Trillaud, H., 2013. Ultrasound elastography in liver. Diagn Interv Imaging 94, 515-534.

Fung, Y.C., 1993. Biomechanics: Mechanical Properties of Living Tissues, 2 ed. Springer, New York, NY.

Gans, C., 1982. Fiber architecture and muscle function. Exerc Sport Sci Rev 10, 160-207.

Gao, J., Caldwell, J., McLin, K., Zhang, M., Park, D., 2020. Ultrasound Shear Wave Elastography to Assess Osteopathic Manipulative Treatment on the Iliocostalis Lumborum Muscle: A Feasibility Study. J Ultrasound Med 39, 157-164.

Gennisson, J.L., Catheline, S., Chaffai, S., Fink, M., 2003. Transient elastography in anisotropic medium: application to the measurement of slow and fast shear wave speeds in muscles. J Acoust Soc Am 114, 536-541.

Gennisson, J.L., Deffieux, T., Fink, M., Tanter, M., 2013. Ultrasound elastography: principles and techniques. Diagn Interv Imaging 94, 487-495.

Gennisson, J.L., Deffieux, T., Macé, E., Montaldo, G., Fink, M., Tanter, M., 2010a. Viscoelastic and anisotropic mechanical properties of in vivo muscle tissue assessed by supersonic shear imaging. Ultrasound Med Biol 36, 789-801.

Gennisson, J.L., Deffieux, T., Macé, E., Montaldo, G., Fink, M., Tanter, M., 2010b. Viscoelastic and anisotropic mechanical properties of in vivo muscle tissue assessed by supersonic shear imaging. Ultrasound in Medicine and Biology 36, 789-801.

Gilbert, T.W., Freund, J.M., Badylak, S.F., 2009. Quantification of DNA in Biologic Scaffold Materials. Journal of Surgical Research 152, 135-139.

Gilbert, T.W., Sellaro, T.L., Badylak, S.F., 2006. Decellularization of tissues and organs. Biomaterials 27, 3675-3683.

Gillies, A.R., Chapman, M.A., Bushong, E.A., Deerinck, T.J., Ellisman, M.H., Lieber, R.L., 2017. High resolution three-dimensional reconstruction of fibrotic skeletal muscle extracellular matrix. Journal of Physiology 595, 1159-1171.

Gillies, A.R., Lieber, R.L., 2011. Structure and function of the skeletal muscle extracellular matrix. Muscle Nerve 44, 318-331.

Gillies, A.R., Smith, L.R., Lieber, R.L., Varghese, S., 2011. Method for Decellularizing Skeletal Muscle Without Detergents or Proteolytic Enzymes. Tissue Engineering Part C: Methods 17, 383-389.

Gindre, J., Takaza, M., Moerman, K.M., Simms, C.K., 2013. A structural model of passive skeletal muscle shows two reinforcement processes in resisting deformation. J Mech Behav Biomed Mater 22, 84-94.

Glaser, K.J., Manduca, A., Ehman, R.L., 2012. Review of MR elastography applications and recent developments. J Magn Reson Imaging 36, 757-774.

Goebel, H.H., Sewry, C.A., Weller, R.O., Muscle disease: pathology and genetics, 2nd Ed. ed. Wiley-Blackwell, London.

Goo, M., Johnston, L.M., Hug, F., Tucker, K., 2020. Systematic Review of Instrumented Measures of Skeletal Muscle Mechanical Properties: Evidence for the Application of Shear Wave Elastography with Children. Ultrasound Med Biol 46, 1831-1840.

Graff, K.F., 1991. Wave motion in elastic solids. Dover Publications, New York.

Granzier, H., Radke, M., Royal, J., Wu, Y., Irving, T.C., Gotthardt, M., Labeit, S., 2007. Functional genomics of chicken, mouse, and human titin supports splice diversity as an important mechanism for regulating biomechanics of striated muscle. Am J Physiol Regul Integr Comp Physiol 293, R557-567.

Grillner, S., 1972. The role of muscle stiffness in meeting the changing postural and locomotor requirements for force development by the ankle extensors. Acta Physiol Scand 86, 92-108.

Guidetti, M., Lorgna, G., Hammersly, M., Lewis, P., Klatt, D., Vena, P., Shah, R., Royston, T.J., 2019. Anisotropic composite material phantom to improve skeletal muscle characterization using magnetic resonance elastography. J Mech Behav Biomed Mater 89, 199-208.

Guidetti, M., Royston, T.J., 2018. Analytical solution for converging elliptic shear wave in a bounded transverse isotropic viscoelastic material with nonhomogeneous outer boundary. J Acoust Soc Am 144, 2312.

Handorf, A.M., Zhou, Y., Halanski, M.A., Li, W.J., 2015. Tissue stiffness dictates development, homeostasis, and disease progression. Organogenesis 11, 1-15.

Heidlauf, T., Klotz, T., Rode, C., Siebert, T., Rohrle, O., 2017. A continuum-mechanical skeletal muscle model including actin-titin interaction predicts stable contractions on the descending limb of the force-length relation. PLoS Comput Biol 13, e1005773.

Herbert, R.D., Gandevia, S.C., 2019. The passive mechanical properties of muscle. J Appl Physiol (1985) 126, 1442-1444.

Hirata, K., Kanehisa, H., Miyamoto, N., 2017. Acute effect of static stretching on passive stiffness of the human gastrocnemius fascicle measured by ultrasound shear wave elastography. Eur J Appl Physiol 117, 493-499.

Holviala, J., Hakkinen, A., Alen, M., Sallinen, J., Kraemer, W., Hakkinen, K., 2014. Effects of prolonged and maintenance strength training on force production, walking, and balance in aging women and men. Scand J Med Sci Sports 24, 224-233.

Howell, J.N., Chleboun, G., Conatser, R., 1993. Muscle stiffness, strength loss, swelling and soreness following exercise-induced injury in humans. The Journal of physiology 464, 183-196.

Hughes, S.W., 2005. Archimedes revisited: a faster, better, cheaper method of accurately measuring the volume of small objects. Physics Education 40, 468-474.

Huijing, P.A., 1999. Muscle as a collagen fiber reinforced composite: a review of force transmission in muscle and whole limb. Journal of Biomechanics 32, 329-345.

Huxley, A.F., 1957. Muscle Structure and Theories of Contraction. Progress in Biophysics and Biophysical Chemistry 7, 255-318.

Huxley, H.E., 1969. The mechanism of muscular contraction. Science 164, 1356-1365.

Ichikawa, K., Takei, H., Usa, H., Mitomo, S., Ogawa, D., 2015. Comparative analysis of ultrasound changes in the vastus lateralis muscle following myofascial release and thermotherapy: a pilot study. J Bodyw Mov Ther 19, 327-336.

Ingber, D.E., 2003. Mechanobiology and diseases of mechanotransduction. Ann Med 35, 564-577.

Jakubowski, K.L., Terman, A., Santana, R.V.C., Lee, S.S.M., 2017. Passive material properties of stroke-impaired plantarflexor and dorsiflexor muscles. Clin Biomech (Bristol, Avon) 49, 48-55.

Janssen, I., Heymsfield, S.B., Wang, Z.M., Ross, R., 2000. Skeletal muscle mass and distribution in 468 men and women aged 18-88 yr. J Appl Physiol (1985) 89, 81-88.

Jarvinen, T.A., Jarvinen, M., Kalimo, H., 2013. Regeneration of injured skeletal muscle after the injury. Muscles Ligaments Tendons J 3, 337-345.

Jenkyn, T.R., Koopman, B., Huijing, P., Lieber, R.L., Kaufman, K.R., 2002. Finite element model of intramuscular pressure during isometric contraction of skeletal muscle. Phys Med Biol 47, 4043-4061.

Jensen, W.K., Devine, C., Dikeman, M., 2004. Encyclopedia of meat sciences. Elsevier, Oxford England.

Johansson, T., Meier, P., Blickhan, R., 2000. A finite-element model for the mechanical analysis of skeletal muscles. J Theor Biol 206, 131-149.

Jones, D.A., Round, J.M., Edwards, R.H., Grindwood, S.R., Tofts, P.S., 1983. Size and composition of the calf and quadriceps muscles in Duchenne muscular dystrophy. A tomographic and histochemical study. J Neurol Sci 60, 307-322.

Joyce, G.C., Rack, P.M., 1969. Isotonic lengthening and shortening movements of cat soleus muscle. J Physiol 204, 475-491.

Joyce, G.C., Rack, P.M., Westbury, D.R., 1969. The mechanical properties of cat soleus muscle during controlled lengthening and shortening movements. J Physiol 204, 461-474.

Juliano, R.L., Haskill, S., 1993. Signal transduction from the extracellular matrix. J Cell Biol 120, 577-585.

Kjaer, M., 2004. Role of extracellular matrix in adaptation of tendon and skeletal muscle to mechanical loading. Physiological reviews 84, 649-698.

Klatt, D., Papazoglou, S., Braun, J., Sack, I., 2010. Viscoelasticity-based MR elastography of skeletal muscle. Phys Med Biol 55, 6445-6459.

Klingler, W., Jurkat-Rott, K., Lehmann-Horn, F., Schleip, R., 2012. The role of fibrosis in Duchenne muscular dystrophy. Acta Myol 31, 184-195.

Koo, T.K., Guo, J.Y., Cohen, J.H., Parker, K.J., 2013. Relationship between shear elastic modulus and passive muscle force: an ex-vivo study. J Biomech 46, 2053-2059.

Koo, T.K., Hug, F., 2015. Factors that influence muscle shear modulus during passive stretch. J Biomech 48, 3539-3542.

Kragstrup, T.W., Kjaer, M., Mackey, A.L., 2011. Structural, biochemical, cellular, and functional changes in skeletal muscle extracellular matrix with aging. Scand J Med Sci Sports 21, 749-757.

Lacourpaille, L., Gross, R., Hug, F., Guével, A., Péréon, Y., Magot, A., Hogrel, J.Y., Nordez, A., 2017. Effects of Duchenne muscular dystrophy on muscle stiffness and response to electrically-induced muscle contraction: A 12-month follow-up. Neuromuscul Disord 27, 214-220.

Lacourpaille, L., Hug, F., Guével, A., Péréon, Y., Magot, A., Hogrel, J.Y., Nordez, A., 2015. Non-invasive assessment of muscle stiffness in patients with Duchenne muscular dystrophy. Muscle Nerve 51, 284-286.

Lee, S.S., Spear, S., Rymer, W.Z., 2015. Quantifying changes in material properties of stroke-impaired muscle. Clin Biomech (Bristol, Avon) 30, 269-275.

Leow, M.Q.H., Cui, S.L., Cao, T., Tay, S.C., Ooi, C.C., 2017. Measuring the effects of acupuncture on muscle stiffness with shear wave elastography. Acupunct Med 35, 304-306.

Lexell, J., 1995. Human aging, muscle mass, and fiber type composition. J Gerontol A Biol Sci Med Sci 50 Spec No, 11-16.

Lexell, J., Taylor, C.C., Sjöström, M., 1988. What is the cause of the ageing atrophy? Journal of the Neurological Sciences 84, 275-294.

Li, G.Y., Cao, Y., 2017. Mechanics of ultrasound elastography. Proc Math Phys Eng Sci 473, 20160841.

Li, H., Lee, W.N., 2017. Effects of tissue mechanical and acoustic anisotropies on the performance of a cross-correlation-based ultrasound strain imaging method. Phys Med Biol 62, 1456-1479.

Li, Y., Lang, P., Linke, W.A., 2016. Titin stiffness modifies the force-generating region of muscle sarcomeres. Sci Rep 6, 24492.

Lieber, R.L., 2018. Biomechanical response of skeletal muscle to eccentric contractions. J Sport Health Sci 7, 294-309.

Lieber, R.L., Friden, J., 2000. Functional and clinical significance of skeletal muscle architecture. Muscle Nerve 23, 1647-1666.

Lieber, R.L., Friden, J., 2019. Muscle contracture and passive mechanics in cerebral palsy. J Appl Physiol (1985) 126, 1492-1501.

Lieber, R.L., Lieber, R.L., 2002. Skeletal muscle structure, function & plasticity : the physiological basis of rehabilitation, 2nd ed. Lippincott Williams & Wilkins, Philadelphia.

Lieber, R.L., Runesson, E., Einarsson, F., Friden, J., 2003. Inferior mechanical properties of spastic muscle bundles due to hypertrophic but compromised extracellular matrix material. Muscle Nerve 28, 464-471.

Loerakker, S., Solis, L.R., Bader, D.L., Baaijens, F.P., Mushahwar, V.K., Oomens, C.W., 2013. How does muscle stiffness affect the internal deformations within the soft tissue layers of the buttocks under constant loading? Comput Methods Biomech Biomed Engin 16, 520-529.

Loren, G.J., Lieber, R.L., 1995. Tendon biomechanical properties enhance human wrist muscle specialization. J Biomech 28, 791-799.

Lv, F., Tang, J., Luo, Y., Ban, Y., Wu, R., Tian, J., Yu, T., Xie, X., Li, T., 2012. Muscle crush injury of extremity: quantitative elastography with supersonic shear imaging. Ultrasound Med Biol 38, 795-802.

Maccabi, A., Taylor, Z., Bajwa, N., Mallen-St Clair, J., St John, M., Sung, S., Grundfest, W., Saddik, G., 2016. An examination of the elastic properties of tissue-mimicking phantoms using vibro-acoustography and a muscle motor system. Rev Sci Instrum 87, 024903.

Mackay, M.E., 1998. Rheological measurements on small samples, in: Collyer, A.A., Clegg, D.W. (Eds.), Rheological Measurement. Springer Netherlands, Dordrecht, pp. 635-665.

Magin, R.L., 2010. Fractional calculus models of complex dynamics in biological tissues. Comput. Math. with Appl. 59, 1586-1593.

Maisetti, O., Hug, F., Bouillard, K., Nordez, A., 2012. Characterization of passive elastic properties of the human medial gastrocnemius muscle belly using supersonic shear imaging. J Biomech 45, 978-984.

Marcucci, L., Reggiani, C., Natali, A.N., Pavan, P.G., 2017. From single muscle fiber to whole muscle mechanics: a finite element model of a muscle bundle with fast and slow fibers. Biomech Model Mechanobiol 16, 1833-1843.

Martin, J.A., Brandon, S.C.E., Keuler, E.M., Hermus, J.R., Ehlers, A.C., Segalman, D.J., Allen, M.S., Thelen, D.G., 2018. Gauging force by tapping tendons. Nature communications 9, 1592.

Mathevon, L., Michel, F., Aubry, S., Testa, R., Lapole, T., Arnaudeau, L.F., Fernandez, B., Parratte, B., Calmels, P., 2018. Two-dimensional and shear wave elastography ultrasound: A reliable method to analyse spastic muscles? Muscle Nerve 57, 222-228.

Mathevon, L., Michel, F., Decavel, P., Fernandez, B., Parratte, B., Calmels, P., 2015. Muscle structure and stiffness assessment after botulinum toxin type A injection. A systematic review. Ann Phys Rehabil Med 58, 343-350.

Mathur, A.B., Collinsworth, A.M., Reichert, W.M., Kraus, W.E., Truskey, G.A., 2001. Endothelial, cardiac muscle and skeletal muscle exhibit different viscous and elastic properties as determined by atomic force microscopy. Journal of biomechanics 34, 1545-1553.

Mei, C., Mace, B.R., 2005. Wave Reflection and Transmission in Timoshenko Beams and Wave Analysis of Timoshenko Beam Structures. Journal of Vibration and Acoustics 127, 382-394.

Meyer, G., Lieber, R.L., 2018. Muscle fibers bear a larger fraction of passive muscle tension in frogs compared with mice. J Exp Biol 221.

Meyer, G.A., Lieber, R.L., 2011. Elucidation of extracellular matrix mechanics from muscle fibers and fiber bundles. Journal of Biomechanics 44, 771-773.

Minamoto, V.B., Suzuki, K.P., Bremner, S.N., Lieber, R.L., Ward, S.R., 2015. Dramatic changes in muscle contractile and structural properties after 2 botulinum toxin injections. Muscle Nerve 52, 649-657.

Miyamoto, N., Hirata, K., Kanehisa, H., Yoshitake, Y., 2015. Validity of measurement of shear modulus by ultrasound shear wave elastography in human pennate muscle. PLoS One 10, e0124311.

Miyamoto, N., Miyamoto-Mikami, E., Hirata, K., Kimura, N., Fuku, N., 2018. Association analysis of the ACTN3 R577X polymorphism with passive muscle stiffness and muscle strain injury. Scand J Med Sci Sports 28, 1209-1214.

Moore, C.J., Caughey, M.C., Meyer, D.O., Emmett, R., Jacobs, C., Chopra, M., Howard, J.F., Jr., Gallippi, C.M., 2018. In Vivo Viscoelastic Response (VisR) Ultrasound for Characterizing Mechanical Anisotropy in Lower-Limb Skeletal Muscles of Boys with and without Duchenne Muscular Dystrophy. Ultrasound Med Biol 44, 2519-2530.

Morrow, D.A., Haut Donahue, T.L., Odegard, G.M., Kaufman, K.R., 2010. Transversely isotropic tensile material properties of skeletal muscle tissue. Journal of the Mechanical Behavior of Biomedical Materials 3, 124-129.

Munster, S., Jawerth, L.M., Leslie, B.A., Weitz, J.I., Fabry, B., Weitz, D.A., 2013. Strain history dependence of the nonlinear stress response of fibrin and collagen networks. Proc Natl Acad Sci U S A 110, 12197-12202.

Narici, M.V., Maganaris, C.N., Reeves, N.D., Capodaglio, P., 2003. Effect of aging on human muscle architecture. J Appl Physiol (1985) 95, 2229-2234.

Narici, M.V., Roi, G.S., Landoni, L., Minetti, A.E., Cerretelli, P., 1989. Changes in force, cross-sectional area and neural activation during strength training and detraining of the human quadriceps. Eur J Appl Physiol Occup Physiol 59, 310-319.

Neuman, R.E., Logan, M.A., 1950. The determination of collagen and elastin in tissues. J Biol Chem 186, 549-556.

Nightingale, K.R., Palmeri, M.L., Nightingale, R.W., Trahey, G.E., 2001. On the feasibility of remote palpation using acoustic radiation force. J Acoust Soc Am 110, 625-634.

O'Donnell, M., Skovoroda, A.R., Shapo, B.M., Emelianov, S.Y., 1994. Internal displacement and strain imaging using ultrasonic speckle tracking. IEEE Transactions on Ultrasonics, Ferroelectrics and Frequency Control 41, 314-325.

Oberhauser, A.F., Badilla-Fernandez, C., Carrion-Vazquez, M., Fernandez, J.M., 2002. The mechanical hierarchies of fibronectin observed with single-molecule AFM. J Mol Biol 319, 433-447.

Ogneva, I.V., Lebedev, D.V., Shenkman, B.S., 2010. Transversal stiffness and Young's modulus of single fibers from rat soleus muscle probed by atomic force microscopy. Biophys J 98, 418-424.

Ophir, J., Cespedes, I., Ponnekanti, H., Yazdi, Y., Li, X., 1991. Elastography: a quantitative method for imaging the elasticity of biological tissues. Ultrason Imaging 13, 111-134.

Palmeri, M.L., Sharma, A.C., Bouchard, R.R., Nightingale, R.W., Nightingale, K.R., 2005. A finite-element method model of soft tissue response to impulsive acoustic radiation force. IEEE Trans Ultrason Ferroelectr Freq Control 52, 1699-1712.

Palnitkar, H., Reiter, R.O., Majumdar, S., Lewis, P., Hammersley, M., Shah, R.N., Royston, T.J., Klatt, D., 2019. An investigation into the relationship between inhomogeneity and wave shapes in phantoms and ex vivo skeletal muscle using Magnetic Resonance Elastography and finite element analysis. J Mech Behav Biomed Mater 98, 108-120.

Park, G.Y., Kwon, D.R., 2012. Sonoelastographic evaluation of medial gastrocnemius muscles intrinsic stiffness after rehabilitation therapy with botulinum toxin a injection in spastic cerebral palsy. Arch Phys Med Rehabil 93, 2085-2089.

Parvin, S., Taghiloo, A., Irani, A., Mirbagheri, M.M., 2017. Therapeutic effects of anti-gravity treadmill (AlterG) training on reflex hyper-excitability, corticospinal tract activities, and muscle stiffness in children with cerebral palsy. IEEE Int Conf Rehabil Robot 2017, 485-490.

Passerieux, E., Rossignol, R., Chopard, A., Carnino, A., Marini, J.F., Letellier, T., Delage, J.P., 2006. Structural organization of the perimysium in bovine skeletal muscle: Junctional plates and associated intracellular subdomains. J Struct Biol 154, 206-216.

Passerieux, E., Rossignol, R., Letellier, T., Delage, J.P., 2007. Physical continuity of the perimysium from myofibers to tendons: involvement in lateral force transmission in skeletal muscle. J Struct Biol 159, 19-28.

Pichiecchio, A., Alessandrino, F., Bortolotto, C., Cerica, A., Rosti, C., Raciti, M.V., Rossi, M., Berardinelli, A., Baranello, G., Bastianello, S., Calliada, F., 2018. Muscle ultrasound elastography and MRI in preschool children with Duchenne muscular dystrophy. Neuromuscul Disord 28, 476-483.

Prado, L.G., Makarenko, I., Andresen, C., Kruger, M., Opitz, C.A., Linke, W.A., 2005. Isoform diversity of giant proteins in relation to passive and active contractile properties of rabbit skeletal muscles. J Gen Physiol 126, 461-480.

Purslow, P.P., 1999. The intramuscular connective tissue matrix and cell-matrix interactions in relation to meat toughness., Proceedings of the 45th International Congress Meat Science and Technology, Yokohama, Japan, pp. 210-219.

Purslow, P.P., 2002. The structure and functional significance of variations in the connective tissue within muscle. Comparative Biochemistry and Physiology Part A: Molecular & Integrative Physiology 133, 947-966.

Purslow, P.P., 2008. The extracellular matrix of skeletal and cardiac muscle, in: Fratzl, P. (Ed.), Collagen: Structure and Mechanics. Springer Science+Business Media, LLC, New York, NY, pp. 325-357.

Purslow, P.P., Trotter, J.A., 1994. The morphology and mechanical properties of endomysium in series-fibred muscles: variations with muscle length. Journal of Muscle Research and Cell Motility 15, 299-308.

Purves, D., 2018. Neuroscience, Sixth edition. ed. Oxford University Press, New York.

Qiang, B., Brigham, J.C., Aristizabal, S., Greenleaf, J.F., Zhang, X., Urban, M.W., 2015. Modeling transversely isotropic, viscoelastic, incompressible tissue-like materials with application in ultrasound shear wave elastography. Phys Med Biol 60, 1289-1306.

Qin, E.C., Jugé, L., Lambert, S.A., Paradis, V., Sinkus, R., Bilston, L.E., 2014. In vivo anisotropic mechanical properties of dystrophic skeletal muscles measured by anisotropic MR elastographic imaging: the mdx mouse model of muscular dystrophy. Radiology 273, 726-735.

Qin, E.C., Sinkus, R., Geng, G., Cheng, S., Green, M., Rae, C.D., Bilston, L.E., 2013. Combining MR elastography and diffusion tensor imaging for the assessment of anisotropic mechanical properties: a phantom study. J Magn Reson Imaging 37, 217-226.

Rack, P.M., Westbury, D.R., 1974. The short range stiffness of active mammalian muscle and its effect on mechanical properties. J Physiol 240, 331-350.

Rasool, G., Wang, A.B., Rymer, W.Z., Lee, S.S., 2016. Altered viscoelastic properties of stroke-affected muscles estimated using ultrasound shear waves - Preliminary data. Conf Proc IEEE Eng Med Biol Soc 2016, 2869-2872.

Rasool, G., Wang, A.B., Rymer, W.Z., Lee, S.S.M., 2018. Shear Waves Reveal Viscoelastic Changes in Skeletal Muscles After Hemispheric Stroke. IEEE Trans Neural Syst Rehabil Eng 26, 2006-2014.

Reyna, W.E., Pichika, R., Ludvig, D., Perreault, E.J., 2020. Efficiency of skeletal muscle decellularization methods and their effects on the extracellular matrix. Journal of Biomechanics 110.

Righetti, R., Ophir, J., Ktonas, P., 2002. Axial resolution in elastography. Ultrasound Med Biol 28, 101-113.

Roeder, B.A., Kokini, K., Sturgis, J.E., Robinson, J.P., Voytik-Harbin, S.L., 2002. Tensile mechanical properties of three-dimensional type I collagen extracellular matrices with varied microstructure. J Biomech Eng 124, 214-222.

Romano, A.J., Abraham, P.B., Rossman, P.J., Bucaro, J.A., Ehman, R.L., 2005. Determination and analysis of guided wave propagation using magnetic resonance elastography. Magn Reson Med 54, 893-900.

Rosant, C., Nagel, M.D., Perot, C., 2007. Aging affects passive stiffness and spindle function of the rat soleus muscle. Exp Gerontol 42, 301-308.

Rosser, B.W., Wick, M., Waldbillig, D.M., Bandman, E., 1996. Heterogeneity of myosin heavy-chain expression in fast-twitch fiber types of mature avian pectoralis muscle. Biochem Cell Biol 74, 715-728.

Royer, D., Dieulesaint, E., 2000. Elastic waves in solids. Springer, Berlin ; New York.

Royston, T.J., Dai, Z., Chaunsali, R., Liu, Y., Peng, Y., Magin, R.L., 2011. Estimating material viscoelastic properties based on surface wave measurements: a comparison of techniques and modeling assumptions. J Acoust Soc Am 130, 4126-4138.

Ruby, L., Mutschler, T., Martini, K., Klingmüller, V., Frauenfelder, T., Rominger, M.B., Sanabria, S.J., 2019. Which Confounders Have the Largest Impact in Shear Wave Elastography of Muscle and How Can They be Minimized? An Elasticity Phantom, Ex Vivo Porcine Muscle and Volunteer Study Using a Commercially Available System. Ultrasound Med Biol 45, 2591-2611.

Sack, I., Jöhrens, K., Würfel, J., Braun, J., 2013. Structure-sensitive elastography: on the viscoelastic powerlaw behavior of in vivo human tissue in health and disease. Soft Matter 9.

Sambrook, J., Fritsch, E.F., Maniatis, T., 1989. Molecular Cloning: A Laboratory Manual, Second ed. Cold Spring Harbour Laboratory Press, Cold Spring Harbor, NY.

Sandercock, T.G., Bernabei, M., Lee, S.S.M., Perreault, E.J., 2018. Temperature Decouple the Effects of Stiffness and Tension on Ultrasound Shear Wave Velocity, International Society of Electrophysiology and Kinesiology, Dublin, Ireland, p. 103.

Sansone, V.A., Ricci, C., Montanari, M., Apolone, G., Rose, M., Meola, G., Group, I.N., 2012. Measuring quality of life impairment in skeletal muscle channelopathies. Eur J Neurol 19, 1470-1476.

Sarvazyan, A.P., Skovoroda, A.R., Emelianov, S.Y., Fowlkes, J.B., Pipe, J.G., Adler, R.S., Buxton, R.B., Carson, P.L., 1995. Biophysical Bases of Elasticity Imaging, in: Jones, J.P. (Ed.), Acoustical Imaging. Springer US, Boston, MA, pp. 223-240.

Sebag, F., Vaillant-Lombard, J., Berbis, J., Griset, V., Henry, J.F., Petit, P., Oliver, C., 2010. Shear wave elastography: A new ultrasound imaging mode for the differential diagnosis of benign and malignant thyroid nodules. Journal of Clinical Endocrinology and Metabolism 95, 5281-5288.

Segal, S.S., White, T.P., Faulkner, J.A., 1986. Architecture, composition, and contractile properties of rat soleus muscle grafts. Am J Physiol 250, C474-479.

Sengupta, P., 2013. The Laboratory Rat: Relating Its Age With Human's. Int J Prev Med 4, 624-630.

Simon, N.G., Noto, Y.I., Zaidman, C.M., 2016. Skeletal muscle imaging in neuromuscular disease. J Clin Neurosci 33, 1-10.

Simons, D.G., Mense, S., 1998. Understanding and measurement of muscle tone as related to clinical muscle pain. Pain 75, 1-17.

Sjostrom, M., Lexell, J., Downham, D.Y., 1992. Differences in fiber number and fiber type proportion within fascicles. A quantitative morphological study of whole vastus lateralis muscle from childhood to old age. Anat Rec 234, 183-189.

Sleboda, D.A., Roberts, T.J., 2017. Incompressible fluid plays a mechanical role in the development of passive muscle tension. Biol Lett 13.

Sleboda, D.A., Stover, K.K., Roberts, T.J., 2020. Diversity of extracellular matrix morphology in vertebrate skeletal muscle. J Morphol 281, 160-169.

Smith, L.R., Fowler-Gerace, L.H., Lieber, R.L., 2011. Muscle extracellular matrix applies a transverse stress on fibers with axial strain. J Biomech 44, 1618-1620.

Soglia, F., Mudalal, S., Babini, E., Di Nunzio, M., Mazzoni, M., Sirri, F., Cavani, C., Petracci, M., 2016. Histology, composition, and quality traits of chicken Pectoralis major muscle affected by wooden breast abnormality. Poult Sci 95, 651-659.

Sopher, R.S., Tokash, H., Natan, S., Sharabi, M., Shelah, O., Tchaicheeyan, O., Lesman, A., 2018. Nonlinear Elasticity of the ECM Fibers Facilitates Efficient Intercellular Communication. Biophysical journal 115, 1357-1370.

Soto-Gutierrez, A., Zhang, L., Medberry, C., Fukumitsu, K., Faulk, D., Jiang, H., Reing, J., Gramignoli, R., Komori, J., Ross, M., Nagaya, M., Lagasse, E., Stolz, D., Strom, S.C., Fox, I.J., Badylak, S.F., 2011. A Whole-Organ Regenerative Medicine Approach for Liver Replacement. Tissue Engineering Part C: Methods 17, 677-686.

Souron, R., Zambelli, A., Espeit, L., Besson, T., Cochrane, D.J., Lapole, T., 2019. Active versus local vibration warm-up effects on knee extensors stiffness and neuromuscular performance of healthy young males. J Sci Med Sport 22, 206-211.

Squire, J.M., Paul, D.M., Morris, E.P., 2017. Myosin and Actin Filaments in Muscle: Structures and Interactions, in: Parry, D.A.D., Squire, J.M. (Eds.), Fibrous Proteins: Structures and Mechanisms. Springer International Publishing, Cham, pp. 319-371.

Sweeney, H.L., Hammers, D.W., 2018. Muscle Contraction. Cold Spring Harb Perspect Biol 10.

Takaza, M., Moerman, K.M., Gindre, J., Lyons, G., Simms, C.K., 2013a. The anisotropic mechanical behaviour of passive skeletal muscle tissue subjected to large tensile strain. J Mech Behav Biomed Mater 17, 209-220.

Takaza, M., Moerman, K.M., Simms, C.K., 2013b. Passive skeletal muscle response to impact loading: experimental testing and inverse modelling. J Mech Behav Biomed Mater 27, 214-225.

Tanter, M., Bercoff, J., Athanasiou, A., Deffieux, T., Gennisson, J.L., Montaldo, G., Muller, M., Tardivon, A., Fink, M., 2008. Quantitative Assessment of Breast Lesion Viscoelasticity: Initial Clinical Results Using Supersonic Shear Imaging. Ultrasound in Medicine and Biology 34, 1373-1386.

Thom, J.M., Morse, C.I., Birch, K.M., Narici, M.V., 2007. Influence of muscle architecture on the torque and power-velocity characteristics of young and elderly men. Eur J Appl Physiol 100, 613-619.

Toursel, T., Stevens, L., Granzier, H., Mounier, Y., 2002. Passive tension of rat skeletal soleus muscle fibers: effects of unloading conditions. J Appl Physiol (1985) 92, 1465-1472.

Trappe, T., 2009. Influence of aging and long-term unloading on the structure and function of human skeletal muscle. Appl Physiol Nutr Metab 34, 459-464.

Trombitas, K., Greaser, M., Labeit, S., Jin, J.P., Kellermayer, M., Helmes, M., Granzier, H., 1998. Titin extensibility in situ: entropic elasticity of permanently folded and permanently unfolded molecular segments. J Cell Biol 140, 853-859.

Trotter, J.A., Purslow, P.P., 1992. Functional morphology of the endomysium in series fibered muscles. Journal of Morphology 212, 109-122.

Tsou, I.Y., Chng, H.H., 2002. The Bone and Joint Decade 2000-2010: for prevention and treatment of musculoskeletal disease. Ann Acad Med Singapore 31, 69-70.

Tuttle, L.J., Alperin, M., Lieber, R.L., 2014. Post-mortem timing of skeletal muscle biochemical and mechanical degradation. Journal of Biomechanics 47, 1506-1509.

Urban, M.W., Lopera, M., Aristizabal, S., Amador, C., Nenadic, I., Kinnick, R.R., Weston, A.D., Qiang, B., Zhang, X., Greenleaf, J.F., 2015. Characterization of transverse isotropy in

compressed tissue-mimicking phantoms. IEEE Trans Ultrason Ferroelectr Freq Control 62, 1036-1046.

Van Loocke, M., Lyons, C.G., Simms, C.K., 2006. A validated model of passive muscle in compression. J Biomech 39, 2999-3009.

van Oosten, A.S., Vahabi, M., Licup, A.J., Sharma, A., Galie, P.A., MacKintosh, F.C., Janmey, P.A., 2016. Uncoupling shear and uniaxial elastic moduli of semiflexible biopolymer networks: compression-softening and stretch-stiffening. Sci Rep 6, 19270.

van Turnhout, M., Peters, G., Stekelenburg, A., Oomens, C., 2005. Passive transverse mechanical properties as a function of temperature of rat skeletal muscle in vitro. Biorheology 42, 193-207.

Vola, E.A., Albano, M., Di Luise, C., Servodidio, V., Sansone, M., Russo, S., Corrado, B., Servodio Iammarrone, C., Caprio, M.G., Vallone, G., 2018. Use of ultrasound shear wave to measure muscle stiffness in children with cerebral palsy. J Ultrasound 21, 241-247.

Wang, A.B., Perreault, E.J., Royston, T.J., Lee, S.S.M., 2019. Changes in shear wave propagation within skeletal muscle during active and passive force generation. J Biomech 94, 115-122.

Wang, K., Ramirez-Mitchell, R., Palter, D., 1984. Titin is an extraordinarily long, flexible, and slender myofibrillar protein. Proc Natl Acad Sci U S A 81, 3685-3689.

Weinstein, S., Yelin, E., 2014. United States Bone and Joint Initiative: The Burden of Musculoskeletal Diseases in the United States (BMUS), Third ed. The Burden of Musculoskeletal Diseases in the United States (BMUS), Rosemont, IL.

Wenger, M.P., Bozec, L., Horton, M.A., Mesquida, P., 2007. Mechanical properties of collagen fibrils. Biophys J 93, 1255-1263.

White, K.P., Harth, M., 1999. The occurrence and impact of generalized pain. Baillieres Best Pract Res Clin Rheumatol 13, 379-389.

Wisdom, K.M., Delp, S.L., Kuhl, E., 2015. Use it or lose it: multiscale skeletal muscle adaptation to mechanical stimuli. Biomech Model Mechanobiol 14, 195-215.

Woodhouse, J.B., McNally, E.G., 2011. Ultrasound of skeletal muscle injury: an update. Semin Ultrasound CT MR 32, 91-100.

Woolf, A., Pfleger, B., 2003. Burden of major musculoskeletal conditions. Bulletin of the World Health Organization 81, 646-656.

Woolf, A.D., Akesson, K., 2001. Understanding the burden of musculoskeletal conditions. The burden is huge and not reflected in national health priorities. BMJ 322, 1079-1080.

Wu, C.H., Ho, Y.C., Hsiao, M.Y., Chen, W.S., Wang, T.G., 2017. Evaluation of Post-Stroke Spastic Muscle Stiffness Using Shear Wave Ultrasound Elastography. Ultrasound Med Biol 43, 1105-1111.

Wu, C.H., Wang, T.G., 2012. Measurement of muscle stiffness in children with spastic cerebral palsy. Radiology 265, 647; author reply 647-648.

Yamakoshi, Y., Sato, J., Sato, T., 1990. Ultrasonic imaging of internal vibration of soft tissue under forced vibration. IEEE Trans Ultrason Ferroelectr Freq Control 37, 45-53.

Yelin, E., 2003. Cost of musculoskeletal diseases: impact of work disability and functional decline. J Rheumatol Suppl 68, 8-11.

Yelin, E., Callahan, L.F., 1995. The economic cost and social and psychological impact of musculoskeletal conditions. National Arthritis Data Work Groups. Arthritis Rheum 38, 1351-1362.

Yelin, E., Weinstein, S., King, T., 2016. The burden of musculoskeletal diseases in the United States. Seminars in Arthritis and Rheumatism 46, 259-260.

Yelin, E., Weinstein, S., King, T., 2019. An update on the burden of musculoskeletal diseases in the U.S. Semin Arthritis Rheum 49, 1-2.

Yucesoy, C.A., Koopman, B.H., Huijing, P.A., Grootenboer, H.J., 2002. Three-dimensional finite element modeling of skeletal muscle using a two-domain approach: linked fiber-matrix mesh model. J Biomech 35, 1253-1262.

Zemzemi, C., Zorgani, A., Daunizeau, L., Belabhar, S., Souchon, R., Catheline, S., 2020. Super-resolution limit of shear-wave elastography. EPL (Europhysics Letters) 129.

Zhang, C., Gao, Y., 2012. Finite element analysis of mechanics of lateral transmission of force in single muscle fiber. J Biomech 45, 2001-2006.

Zhang, J., Zhang, G., Morrison, B., Mori, S., Sheikh, K.A., 2008. Magnetic resonance imaging of mouse skeletal muscle to measure denervation atrophy. Exp Neurol 212, 448-457.

Zhou, X., Wang, C., Qiu, S., Mao, L., Chen, F., Chen, S., 2018. Non-invasive Assessment of Changes in Muscle Injury by Ultrasound Shear Wave Elastography: An Experimental Study in Contusion Model. Ultrasound Med Biol 44, 2759-2767.